Optics for terawatt-scale photovoltaics
review and perspectives

Jäger, Klaus; Aeberhard, Urs; Llado, Esther Alarcon; Bläsi, Benedikt; Burger, Sven; Gordon, Ivan; Isabella, Olindo; Omair, Zunaid; Lizcano, Juan Camilo Ortiz; More Authors

DOI
10.1364/AOP.530556

Publication date
2025

Document Version
Final published version

Published in
Advances in Optics and Photonics

Citation (APA)
Jäger, K., Aeberhard, U., Llado, E. A., Bläsi, B., Burger, S., Gordon, I., Isabella, O., Omair, Z., Lizcano, J. C. O., & More Authors (2025). Optics for terawatt-scale photovoltaics: review and perspectives. *Advances in Optics and Photonics*, *17*(1), 185-294. https://doi.org/10.1364/AOP.530556

Review Vol. 17, No. 1 / March 2025 / Advances in Optics and Photonics 185

Optics for terawatt-scale photovoltaics: review and perspectives

Klaus Jäger,[1,2,*] Urs Aeberhard,[3] Esther Alarcon Llado,[4] Benedikt Bläsi,[5] Sven Burger,[2,6] Bruno Ehrler,[4] Wilfried Favre,[7] Antonín Fejfar,[8] Tristan Gageot,[7] Ivan Gordon,[9,10,11] Henning Helmers,[5] Oliver Höhn,[5,12] Olindo Isabella,[11] Marko Jošt,[13] Martin Ledinský,[8] Jyotirmoy Mandal,[14] Phillip Manley,[2,6] Delfina Muñoz,[7] Zunaid Omair,[15] Juan Camilo Ortiz Lizcano,[11] Ulrich W. Paetzold,[16,17] Aaswath P. Raman,[18] Hitoshi Sai,[19] Rebecca Saive,[20] Martina Schmid,[21] Eli Yablonovitch,[15] and Christiane Becker[1,22,23]

[1]*Department Optics for Solar Energy, Helmholtz-Zentrum Berlin für Materialien und Energie, Kekuléstraße 5, 12489 Berlin, Germany*
[2]*Computational Nano Optics, Zuse Institute Berlin, Takustraße 7, 14195 Berlin, Germany*
[3]*Fluxim AG, Katharina-Sulzer-Platz 2, 8400 Winterthur, Switzerland*
[4]*LMPV-Sustainable Energy Materials Department, AMOLF, Science Park 104, 1098 XG Amsterdam, The Netherlands*
[5]*Fraunhofer Institute for Solar Energy Systems, ISE, Heidenhofstraße 2, 79100 Freiburg, Germany*
[6]*JCMwave GmbH, Bolivarallee 22, 14050 Berlin, Germany*
[7]*Université Grenoble Alpes, CEA, LITEN, Campus INES, 50 avenue du Lac Léman, 73375 Le Bourget-du-Lac, France*
[8]*FZU - Institute of Physics of the Czech Academy of Sciences, Na Slovance 1999/2, 182 00 Prague 8, Czechia*
[9]*IMEC/Energyville, Thor Park 8320, 3600 Genk, Belgium*
[10]*Hasselt University, Martelarenlaan 42, 3500 Hasselt, Belgium*
[11]*Photovoltaic Materials and Devices Laboratory, Delft University of Technology, Mekelweg 4, 2628 CD Delft, The Netherlands*
[12]*Department of Sustainable Systems Engineering (INATECH), University of Freiburg, Emmy-Noether-Str.2, 79110 Freiburg, Germany*
[13]*Faculty of Electrical Engineering, University of Ljubljana Tržaška 25, Ljubljana 1000, Slovenia*
[14]*Department of Civil and Environmental Engineering, Princeton University, E209A Engineering Quadrangle, Princeton, New Jersey 08544, USA*
[15]*Department of Electrical Engineering and Computer Sciences, University of California, Berkeley, California 94720, USA*
[16]*Institute of Microstructure Technology, Karlsruhe Institute of Technology, 76344 Eggenstein-Leopoldshafen, Germany*
[17]*Light Technology Institute, Karlsruhe Institute of Technology, 76131 Karlsruhe, Germany*
[18]*Department of Materials Science and Engineering, University of California, Los Angeles, California 90095, USA*
[19]*National Institute of Advanced Industrial Science and Technology (AIST), Tsukuba, Ibaraki 305-8568, Japan*
[20]*MESA+ Institute for Nanotechnology, Inorganic Materials Science, University of Twente, 7522 NB Enschede, The Netherlands*

Corrected 28 March 2025

[21] Faculty of Physics and Center for Nanointegration Duisburg-Essen (CENIDE), University of Duisburg-Essen, Forsthausweg 2, 47057 Duisburg, Germany
[22] Faculty 1: School of Engineering – Energy and Information, Hochschule für Technik und Wirtschaft Berlin, 10313 Berlin, Germany
[23] christiane.becker@helmholtz-berlin.de
*klaus.jaeger@helmholtz-berlin.de

Received June 6, 2024; revised January 10, 2025; accepted January 16, 2025; published 27 March 2025

Photovoltaics, a mature technology, is set to play a vital role in achieving a carbon-free energy system. This article examines the pivotal role of optics in advancing photovoltaics. We identify key scientific research areas where the optics community can make significant contributions. We are guided by the central question: How can optics facilitate the large-scale deployment of photovoltaics necessary for decarbonizing our societies?

https://doi.org/10.1364/AOP.530556

Optics for terawatt-scale photovoltaics: review and perspectives

Klaus Jäger, Urs Aeberhard, Esther Alarcon Llado, Benedikt Bläsi, Sven Burger, Bruno Ehrler, Wilfried Favre, Antonín Fejfar, Tristan Gageot, Ivan Gordon, Henning Helmers, Oliver Höhn, Olindo Isabella, Marko Jošt, Martin Ledinský, Jyotirmoy Mandal, Phillip Manley, Delfina Muñoz, Zunaid Omair, Juan Camilo Ortiz Lizcano, Ulrich W. Paetzold, Aaswath P. Raman, Hitoshi Sai, Rebecca Saive, Martina Schmid, Eli Yablonovitch, and Christiane Becker

1. INTRODUCTION

C. Becker and K. Jäger

Photovoltaics (PV) installations reached a global capacity of two terawatt (2 TW) by November 2024 [1], and the rates of growth and cost reduction are remarkable [2]. We took these achievements as an opportunity to reflect on how the optics research community can contribute to the further growth of PV, which is crucial for the transition to a carbon-free energy system. We were guided by two questions.

How can optics help to further support the growth of PV?

Which innovations in the field of optics are needed today to overcome current limitations in efficiency, distribution, and social acceptance?

We also identified optical concepts that might not yet be economically viable and where yet not all open questions have been answered, but which are developing very dynamically and have great potential for further pushing PV technology. Figure 1 presents an outline of this article, which is based on the optical challenges derived from the current pressing needs of PV on terawatt scale.

The pivotal Section 2 deals with the current status of *PV on the terawatt scale*. From this section, we derive the topics to which the optics community can contribute to facilitate such a large-scale exploitation. The section summarizes the different PV technologies ranging from crystalline silicon PV and thin-film solar cells to multijunction solar cells. As illustrated in Fig. 1, the following major challenges are identified (colored arrows): sustainable PV production, increasing the power conversion efficiency (PCE) of PV modules, maximizing the energy yield (EY) of PV systems, and the integration of PV in the environment. From these challenges we derive research topics (rectangles) that are discussed in the subsequent sections of this article.

Figure 1

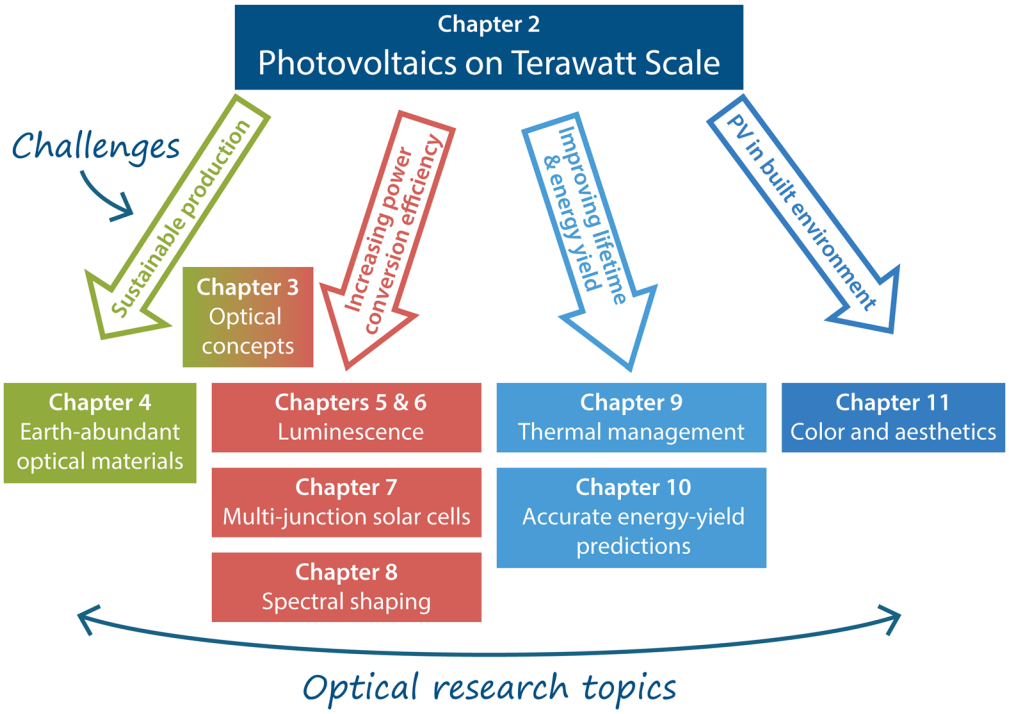

Outline of the article. Optical research topics derived from the current challenges of PV entering the terawatt scale.

Section 3 summarizes important *optical concepts* that have been used in PV in the past. This includes antireflective coatings (ARCs), random and periodic textures for antireflection and light trapping, and concentrated photovoltaics (CPV) systems. Further, illumination conditions different from standard testing conditions are discussed.

Sections 4–11 delve into the research topics outlined in Fig. 1, forming the core of this article. Each section concludes with a summary of the identified *advances required*.

Because the global PV production is growing exponentially, using earth-abundant materials is of utmost importance. However, in state-of-the-art silicon solar modules, large amounts of rare materials such as indium and silver are used. In Section 4, we address the development of alternative optical materials based on earth-abundant elements.

Luminescence of solar cells, discussed in Section 5, has been identified as vivid research area giving insights into both the electrical and optical solar cell properties. With increasing optoelectronic quality of current solar cell absorber materials in terms of photoluminescent quantum yield, the exploration of internal luminescence to increase the voltage in single-junction solar cells, and luminescent coupling in multijunction solar cells is picking up speed. Further, a new perspective on luminescence in solar cells is introduced considering *luminescence as two distinct photon gases present inside every solar cell* in Section 6.

Silicon solar cells have been dominating the PV market with a current share of more than 90%. Silicon technology is already so far developed that it reaches PCEs close to its physical limit. *Multijunction solar cells* are regarded as the most promising concept to surpass the single-junction efficiency limit. Section 7 introduces the general multijunction solar cell concept and summarizes recent multijunction solar cell technologies based on III–V semiconductors, silicon, CIGS, and perovskites. At the

end, we discuss the specific optical challenges and specific scientific and technological questions to be addressed in the future.

While multijunction solar cells are the most promising route to overcome the efficiency limitation of single-junction solar cells, *spectral shaping* aims to convert the solar spectrum into a spectrum that better matches to bandgap of the solar cell, which has a similar effect on the achievable efficiency. Section 8 discusses developments on downconversion of high-energy photons into a larger number of lower-energy photoexcitations, upconversion of below-bandgap photons into a (lower number) of above-bandgap photons, and concentration of the sunlight in luminescent solar concentrators (LSCs).

Thin-film and photonic strategies can increase the front surface emissivity of the cover glass on the module, thereby allowing the module to take better advantage of *thermal management of PV modules* and maintain a lower steady-state temperature. Further, enhancing the reflectance of subbandgap photons can prevent these photons from penetrating into the module and cause parasitic heating. Section 9 discusses, how optimizing both elements in a low-cost and scalable way represents an important opportunity for optics to improve thermal aspects of PV modules.

The performance of PV systems is assessed by a variety of key performance indicators such as levelized cost of electricity (LCOE), energy payback time (EPT), specific CO_2 emissions, or resource efficiency. All these performance indicators require the total amount of energy harvested from the PV installation, taking into consideration seasonal and daily variations in irradiation conditions, spectrum, temperature, as well as all the details of the installation (e.g., module orientation, type of tracking, shadows, and soiling). Therefore, accurately predicting the EY, discussed in Section 10, is pivotal for PV system and device architecture design of solar modules.

Appealing *color and aesthetics of PV modules* have been identified as essential for social acceptance of PV, because stakeholders in rural and urban areas prefer to harmonize the aesthetic appearance of PV modules with their surroundings. The final section (Section 11) summarizes the most commonly used coloring techniques in the production of PV modules.

2. ADVANCING PV TO THE TERAWATT SCALE

I. Gordon and A. Fejfar

In this section, we give an overview of the state-of-the-art of photovoltaics (PV), the main PV technologies currently being produced industrially and in development, and the main technological challenges still remaining for the massive production and deployment of PV technology in the future.

2.1. Global PV Production in 2023

The number of worldwide installed PV systems has grown almost exponentially since 2010, resulting in a cumulative installed PV capacity of roughly 1.5 terawatt peak (TW_p) at the end of 2023 [2], compared with only 39 GW_p installed at the end of 2010 (1 TW_p = 1000 GW_p and W_p denotes the maximum power a PV module can deliver when it is illuminated with the standardized AM1.5 solar spectrum at a module temperature of 25°C). In 2023, around 300 GW_p of PV modules were installed worldwide and it is expected that this yearly installation rate will rapidly increase in the coming decade to 1–3 TW_p per year.

In terms of PV module technology, around 95% of PV modules currently produced are based on crystalline-silicon technology, whereas the remaining 5% are based on thin-film technology. Crystalline-silicon technology uses crystalline silicon wafers with a thickness of 150–180 μm as the absorber material for the incoming light. Thin-film technology, on the other hand, is based on the use of thin layers of a light absorber (mostly CdTe or chalcopyrite materials), grown on a substrate such as glass, a polymer, or a metal sheet. The thin-film absorber thickness is typically in the range of 100 nm to 2 μm.

The rapidly growing PV market is driven by the decreasing cost of PV technology. Figure 2 shows the learning curve for crystalline silicon PV modules from 1976 to 2023 [3]. Prices have fallen by almost 25% with each doubling of installed volume, accelerating to 40% since 2006 due to increased global production. At the end of 2023, the average calculated spot market price for silicon PV modules cost was as low as 0.12 USD per W_p. This cost reduction results from upscaling, manufacturing improvements, and technological innovations in materials and device structure, including optics and light management (Section 3).

In 2023, PV modules for systems over 10 MW_p made up about 1/3 of system costs, with the balance of system (BOS) contributing 2/3 [4]. BOS includes components such as racking, wiring, inverters, and maintenance. The PV module cost share is expected to drop to 20% in the next decade [4]. Higher-efficiency PV modules reduce BOS costs by generating more power per area.

2.2. Main and Upcoming PV Technologies

In this section, we present the various PV technologies and device architectures that are in mass production in 2024, as well as those PV technologies and device structures that are currently being developed and that can be expected to become mass produced relatively soon.

2.2a. Crystalline Silicon PV Technologies

Crystalline silicon PV technology uses crystalline silicon wafers as the active light-absorbing material for the PV devices. Typically, large-area monocrystalline silicon wafers with near-perfect crystal structures are processed into individual solar cells, which are then interconnected and laminated into a solar module [5]. The crystalline silicon solar cells can be classified based on the device architecture that is used.

Figure 2

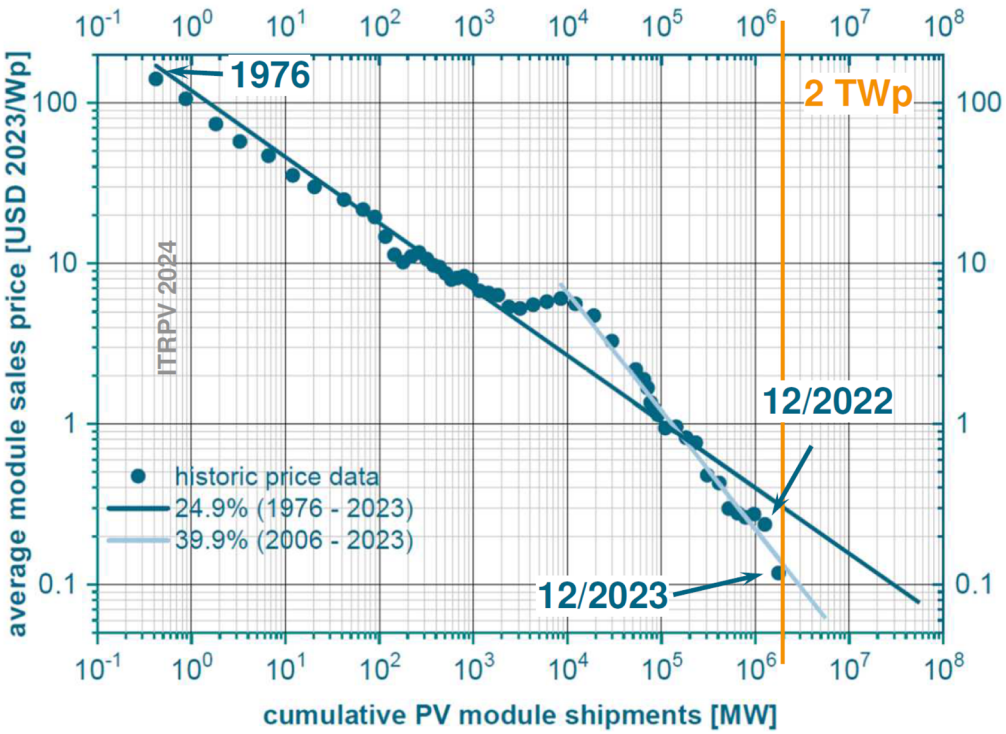

Learning curve for crystalline silicon PV modules. Reprinted from Ref. [3] with permission from VDMA.

Figure 3 shows an overview of the current and anticipated future market shares of the main crystalline-silicon PV cell architectures [3]. The *back surface field* (BSF) cell was the main workhorse of the PV industry until around 2018. In 2023, more than 70% of crystalline silicon solar cells processed worldwide were based on the passivated emitter and rear cell (PERC) device architecture. Upcoming silicon device architectures in industrial production are the *tunnel oxide passivated contacts* (TOPCon) cells and *silicon heterojunction* (SHJ) cells. Finally, *backcontact technology* refers to solar cells where the metal contacts of both polarities are placed at the backside of the solar cell.

Currently, there is a trend in the PV industry to produce more and more bifacial cells and modules (see Fig. 4). In 2023, the market share for bifacial silicon solar cells was around 85% [3]. In bifacial cells, light can enter the solar cell both from the front as well as from the rear side. To make silicon solar cells bifacial, the electrical contacts need to be designed appropriately and the light management and optics of the device need to be adapted. The market share of bifacial solar cells is expected to increase further to 90% within the next decade [3].

PERC. These solar cells have replaced BSF cells in industrial production in recent years because they show much higher energy conversion efficiencies, mainly because of a much better rear surface passivation and a better rear surface light reflection enabling increased carrier densities leading to higher open-circuit voltages (V_{oc}; see Sections 5 and 6). This is achieved using rear surface passivation by dielectric layers and a smaller metal/semiconductor contact area [10]. The insertion of a dielectric passivation layer between metal and silicon also substantially increases the reflection of light at the rear silicon surface. Although the first paper describing a PERC cell architecture (see Fig. 5(a)) already appeared in 1989 [6], it took more than three

Figure 3

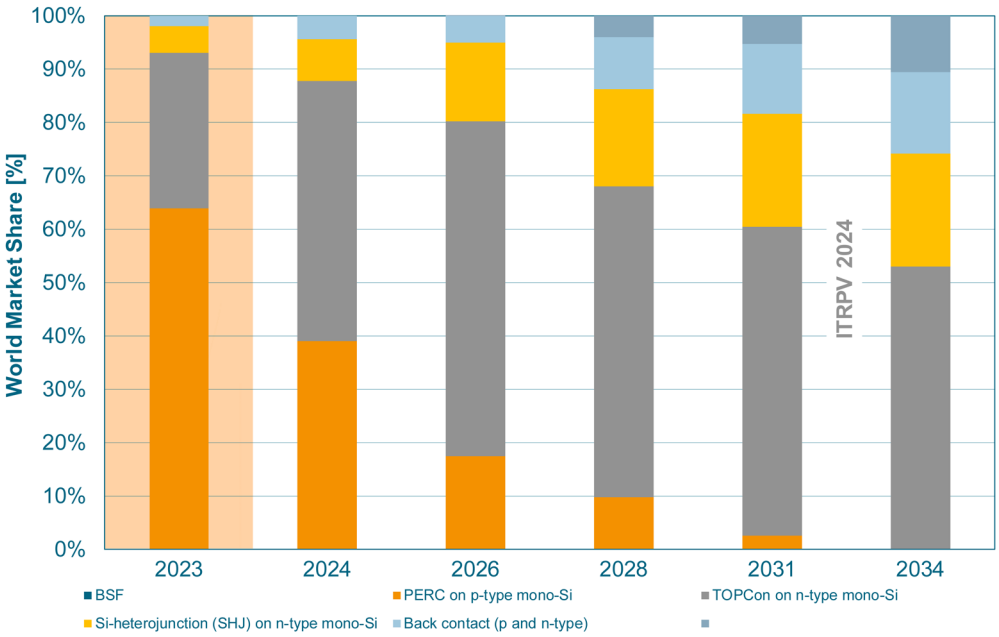

Market shares for different crystalline silicon cell technologies. Reprinted from Ref. [3] with permission from VDMA.

Figure 4

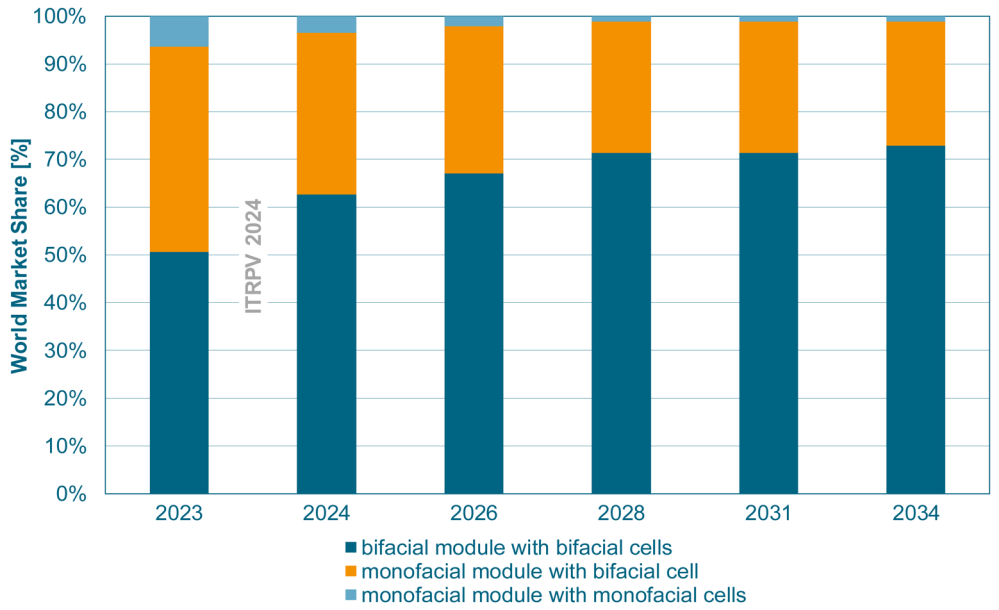

Evolution of the market share for bifacial modules. Reprinted from Ref. [3] with permission from VDMA.

decades before the technology could be industrialized [11]. Typical energy conversion efficiencies at cell level that can be reached by this technology are above 24%.

TOPCon. In 2013, a new silicon solar cell technology called TOPCon was developed by Fraunhofer ISE in Germany [7]. The schematic of the TOPCon solar cell is depicted in Fig. 5(b). In the TOPCon cell architecture, the entire rear surface of the n-type silicon solar cell is passivated by a thin SiO_x layer of around 1–2 nm. In addition, an

Figure 5

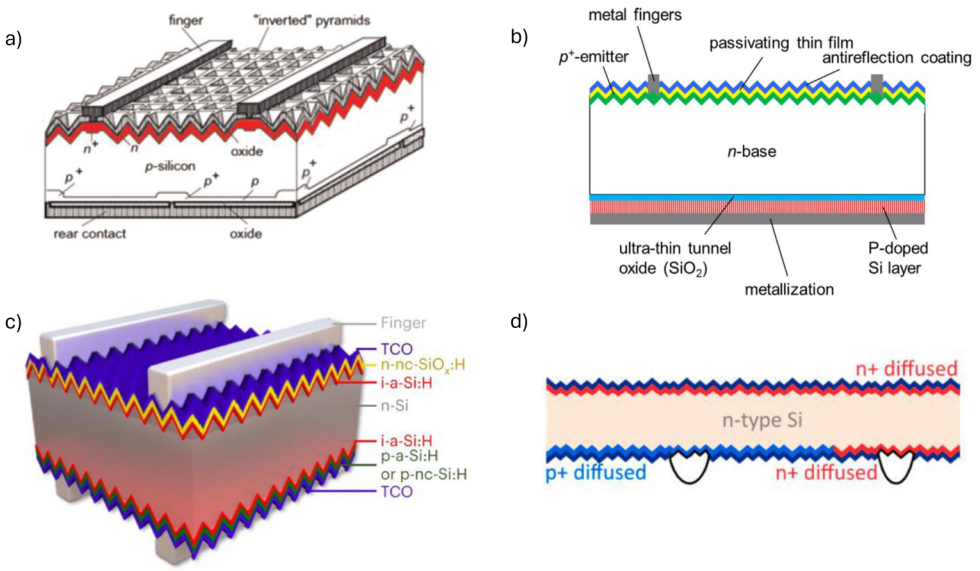

Four of the main silicon solar cell architectures currently in production: (a) PERC solar cell, (b) TOPCon solar cell, (c) bifacial contacted SHJ solar cell, and (d) IBC solar cell. (a) Reprinted with permission from Blakers *et al.*, Appl. Phys. Lett. **55**, 1363–1365 (1989) [6]. Copyright 1989, AIP Publishing LLC. (b) Reprinted from Sol. Energy Mater. Sol. Cells **120**, Feldmann *et al.*, "Passivated rear contacts for high-efficiency n-type Si solar cells providing high interface passivation quality and excellent transport characteristics," 270–274, Copyright 2014, [7], with permission from Elsevier. (c) Reprinted from [8] under a Creative Commons license. (d) Reprinted from [9] under a Creative Commons license.

n-type-doped polysilicon layer is formed on top of the SiO_x layer to further enhance the passivation at the rear surface by field-effect passivation. This cell structure is an example of a so-called passivated contact cell structure. The charge carriers can move through the thin interfacial SiO_x by either pure tunneling or pinhole-assisted tunneling [10]. Moreover, due to band bending and high doping of the poly layer, the structure provides carrier selectivity. Advantages of TOPCon technology over PERC technology are among others a higher energy conversion efficiency potential (at the moment of writing, the highest reported efficiency for a TOPCon solar cell is 26.7% [12]) and the absence of the need to make point-contact holes at the rear surface. As a result, it is expected that TOPCon devices will soon replace PERC as the dominant technology in industrial silicon PV production (see Fig. 3).

SHJ. The SHJ solar cell is another example of a so-called passivated contact cell structure that is finding its way into mass production. The schematic structure of a two-sided contacted SHJ solar cell is shown in Fig. 5(c). The main feature of SHJ cells is the use of thin intrinsic and doped a-Si:H layers of a few nanometers on both sides of the crystalline silicon absorber to passivate the silicon and to create emitter and back surface field (BSF) (or front surface field) layers. This symmetric cell structure allows to extract electrons and holes selectively and can be created via low temperature processing, which makes SHJ cells compatible with the use of thin crystalline-silicon wafers. The highest energy conversion efficiency obtained at the moment of writing this article with the two-sided contacted SHJ cell architecture is 26.8% [8].

Backcontact solar cells. Finally, silicon backcontact solar cell architectures aim at achieving even higher energy conversion efficiencies by placing both n-type and p-type

contacts at the rear of the cells, thereby reducing the shadowing losses at the front of the cell [4]. There are different types of silicon backcontact solar cells that can be divided into three classes [13], namely back-junction cells [e.g., interdigitated backcontact cells (IBCs); see Fig. 5(d)], emitter wrap-through (EWT) cells, and metallization wrap-through (MWT) cells. In this section, we focus on IBCs since these cells are currently the closest to mass-scale industrialization and have the highest efficiency potential. To reach the highest energy conversion efficiencies, the IBC architecture can be combined with the use of carrier-selective contacts (TOPCon or SHJ). In May 2024, the company Longi broke the world record energy conversion efficiency for a single-junction crystalline silicon solar cell with an SHJ–IBC solar cell showing an efficiency of 27.3% [14].

2.2b. Thin-Film PV Technologies

Thin-film PV refers to PV devices that are based on the use of a thin film of material as sunlight absorber. Since crystalline silicon has an indirect bandgap, crystalline silicon wafers used in PV are typically around 150–200 μm thick to enable sufficient absorption of the incoming light without the need of very advanced light trapping schemes. However, when a material with a direct bandgap is used as sunlight-absorbing layer, much thinner absorbers can be used and these absorbers can then be deposited as thin films on top of a substrate (e.g., glass or metal foil).

The basic architecture of a thin-film solar cell consists of a sunlight-absorbing layer sandwiched between two contact layers [10]. One or more layers may be further required to passivate the interfaces between the layers. Thin film solar cells can be grown in two different configurations, namely substrate or superstrate configuration [10]. In substrate configuration, the sunlight enters the device from the opposite side of the substrate onto which the device has been grown. In superstrate configuration, the sunlight enters the device through the substrate onto which the device has been grown and, hence, that substrate needs to be transparent in this case. In this section, we briefly describe the main thin-film PV technologies.

Cadmium telluride. In 2023, CdTe PV had the second biggest market share worldwide after crystalline silicon PV. One of the reasons for the success of CdTe PV lies in its combination of a high energy conversion efficiency potential with low processing costs. CdTe is a polycrystalline p-type semiconductor material belonging to the II–IV group with a direct bandgap of 1.45 eV [10]. Whereas the theoretical maximum energy conversion efficiency is above 30%, the highest efficiency demonstrated for a small area CdTe cell is currently 23.1% [15]. Because of its direct bandgap, a CdTe layer thickness of around 1 μm is sufficient for sunlight absorption purposes, which also relaxes the minority carrier lifetime requirements of the material. Typically, a CdTe solar device consists of a heterojunction between p-type CdTe and n-type CdS [10]. Some of the main challenges of CdTe PV are directly related to the absorber material used, namely toxicity issues related to cadmium and the scarcity of tellurium. Both issues limit the mass production and widely spreading of the technology.

CIGS. $Cu(In,Ga)(S,Se)_2$ is another thin-film solar cell technology that is being produced industrially, although it is still in relatively small quantities compared with crystalline silicon PV and even CdTe PV. The CIGS semiconductor material has a chalcopyrite crystal structure with a tunable bandgap in the range of 1.0–1.6 eV [10]. CIGS is a direct bandgap material with p-type conductivity that arises due to Cu vacancies [10]. The conductivity of the material can therefore be tuned by changing the In-to-Cu ratio during deposition. Similar to CdTe, a CIGS solar device also makes use of a heterojunction with an n-type material such as CdS or Zn(O,S) [10]. At the end of 2023, the highest independently confirmed energy conversion efficiency

demonstrated for a small-area CIGS cell was 23.6% [15]. Some of the main challenges of CIGS PV are the use of the scarce element In, and homogeneity problems of the compound material when grown on large areas which typically leads to much lower energy conversion efficiencies for large devices compared with small lab-scale devices.

III–V semiconductors. Materials such as InP and GaAs are direct bandgap semiconductors with significantly higher sunlight absorption compared with silicon [16], and have been used for PV devices for many decades. Their high sunlight absorption allows for the fabrication of ultrathin, reliable, and highly efficient solar cells. III–V solar cells can be single junction devices (such as a GaAs cell), or they can be multijunction devices in which multiple III–V semiconductor materials with different bandgaps are grown or stacked on top of each other [17]. The cost of III–V solar devices is significantly higher (up to two orders of magnitude) than that of silicon solar cells, making them mostly used in niche applications such as space solar cells and CPV [16]. The highest energy conversion efficiency ever reached with a solar cell to date is 47.6% which was achieved in 2022 with a four-junction wafer-bonded III–V solar cell (GaInP/GaInAs; GaInAsP/GaInAs) under an irradiance of 665 Suns [15,18].

Amorphous silicon. Hydrogenated amorphous silicon (a-Si:H) has been used since the 1970s for PV applications. It has a direct bandgap of around 1.6–1.8 eV (tunable by changing the hydrogen content) and can be deposited at low temperatures on a variety of substrates [10]. Due to its direct bandgap and comparatively high sunlight absorption coefficient, a-Si:H layer thicknesses of just a few 100 nm are sufficient for solar cell purposes. The main drawbacks of a-Si:H solar cells are their low energy conversion efficiencies and their instability under light illumination called the Staebler–Wronski effect [10]. Since the highest stabilized energy conversion efficiency reached with an amorphous silicon solar cell is only 10.2% [15], multijunction devices have been investigated in which the a-Si:H material is combined with so-called nanocrystalline silicon (nc-Si) or amorphous SiGe alloys to boost the efficiency. This had led to tandem devices with a best efficiency of 12.7% and triple junctions with a best efficiency of 14.0% [15].

Organic PV. These cells make use of thin films of organic semiconductors to convert sunlight into electricity, and offer the potential of low-cost, flexible devices and semitransparency [19]. The organic semiconductors used are π-bonded small molecules or polymers that are made up of carbon, hydrogen, and other atoms such as nitrogen, sulfur, and oxygen [19]. Light absorption in these organic materials generates tightly bonded Frenkel excitons instead of free charges in inorganic semiconductors [19]. Organic solar cells typically consist of a bulk heterojunction formed by a donor material and an acceptor material to enhance exciton dissociation and charge collection. Over the last two decades, many different photo-active organic materials have been synthesized and tested for organic PV. The resulting energy conversion efficiency of organic solar cells is highly dependent on the materials used. Moreover, morphological control of donor and acceptor domains on the nanoscale is needed to enhance efficient exciton diffusion and dissociation, carrier transport, and suppression of recombination losses [20]. The highest certified energy conversion efficiency reported for organic PV to date is 19.2% [15,20].

Perovskites. The term perovskite refers to a class of materials with the general chemical formula ABX_3 that typically have a cubic or octahedral crystal structure [21]. Perovskite materials with PV properties are typically hybrid organic–inorganic perovskites containing both organic (e.g., methylammonium CH_3NH_3) and inorganic components (e.g., inorganic cations such as Pb and Sn, as well as halides based on

I, Cl, and Br). One of the most widely used perovskite materials for PV are methylammonium lead iodides ($CH_3NH_3PbI_3$) with an energy bandgap of 1.55 eV [21], but by tuning the material composition (e.g., mixing various halides) different material properties such as different bandgaps or different electrical transport characteristics can be achieved. The most successful perovskite-based solar cells have the planar heterojunction device structure in which the perovskite light-absorbing layer is sandwiched between an electron transport layer (ETL) and a hole transport layer (HTL). Electron-hole pairs are generated in the perovskite layer by sunlight absorption and charge carrier separation and collection is facilitated by the band alignment between the HTL, perovskite, and ETL. Depending on whether the sunlight first enters through the ETL or the HTL, the solar cell is called a n–i–p or a p–i–n device, respectively. The highest certified energy conversion efficiency reported for single-junction perovskite solar cells to date is 26.7% [15].

2.2c. Multijunction PV Technologies

In the previous two sections, we briefly described the main single-junction PV technologies based on crystalline-silicon wafers or thin-film absorber materials. In this section, we discuss so-called multijunction solar cells in which two or more sunlight absorbers with different bandgaps are placed or grown on top of each other to increase the energy conversion efficiency of the solar device. The main energy losses in a single-junction solar device come from the nonabsorption of the photons with an energy below the bandgap of the absorber material and from thermalization losses of the excess energy of the absorbed photons. As a result, the upper theoretical energy conversion efficiency limit of the most common single-junction solar cells is in the range 29–33%, depending on the bandgap of the absorber material used [22]. By stacking multiple junctions made of materials with a different bandgap on top of each other, the upper theoretical energy conversion efficiency limit can be pushed upward (e.g., to a value well above 40% for devices with two junctions, so-called tandems) by a more efficient conversion and utilization of the incoming photon energy. In the last few years, tandem devices based on a crystalline-silicon bottom cell are heavily being investigated because single-junction crystalline-silicon solar devices, even those in industrial production, are rapidly nearing their practical energy conversion efficiencies, and tandems are seen as the way forward to crystalline-silicon-based device efficiencies beyond the single-junction limit [3]. In particular, perovskite materials are attracting a lot of attention as potential high-bandgap top cell for silicon-based tandem devices. Currently, the highest independently confirmed energy conversion efficiency for a perovskite/silicon tandem device is 34.6% [15], which is indeed well above the record efficiencies for single-junction crystalline-silicon and perovskite solar cells.

2.3. Challenges Related to the Further Deployment of PV

To keep the Earth's average temperature rise to less than 1.5°C, as set by the Paris Agreement in 2015, requires rapid decarbonization coupled with a transition of the energy system to 100% renewable energy, using solar PV energy along with wind, hydro, geothermal, and biomass energy, to power directly or indirectly all sectors of the economy and society [23]. A massive electrification of the world's energy system is therefore needed, with an estimated required global PV generating capacity of about 50–70 TW_p by 2050 [23,24], whereas at the end of 2023 only 1.5 TW_p was installed (see Section 2.1). The PV industry therefore needs to rapidly grow its production capacity to about 3 TW_p per year to reach this objective [23], which is roughly a tenfold increase from the current yearly production rate. This required massive deployment of PV modules in the coming three decades with production and installation rates of several TW_p per year, will lead to important socioeconomical

challenges as well as to new challenges in the field of material and system technology besides the traditional R&D subjects such as performance increase and cost reduction.

In the following subsections, we describe the main technological challenges and how optics can help resolve those challenges. For the socioeconomic challenges we refer to Ref. [25].

2.3a. Sustainable Production of PV Systems

Although solar radiation is an inexhaustible renewable energy source, the future required large-scale production and deployment of PV technology demands a sustainability analysis in terms of raw materials demand, energy required to manufacture the PV systems, and environmental impacts of production and operation of the PV systems [26]. In particular, sustainable PV production should ensure the proper usage of materials (e.g., minimizing the use of rare materials and avoiding toxic materials), the minimization of energy usage and greenhouse gas emission during the production process, and the proper way of dealing with the end of life of PV modules and systems. Ensuring a true long-term sustainable production of PV systems in the future will require new materials, adapted device concepts, and improved production technologies.

Advanced and novel optics can be of help here in many different ways, as we illustrate in Section 4 of this article. That section shows that by a smarter ecodesign of the PV devices, we can make fewer critical rare materials such as indium and silver while maintaining high device performance. Section 3, on the other hand, illustrates the general optical concepts in PV that can help to reduce the thickness of the silicon solar cell wafers which will reduce the CO_2 footprint of the technology.

2.3b. PV Modules with Higher Energy Conversion Efficiencies

In 2023, the cost of a large-scale PV system (>10 kW_p) was determined for 70% by the cost of the BOS and only for roughly 30% by the cost of the modules [4]. It is expected that the relative cost of the PV modules in the total PV system cost will lower even further in the coming years to roughly 20% [4]. Since the BOS cost typically scales with the area needed for the system, this increases the need for producing PV modules with very high energy conversion efficiencies. As a result, the industry is currently switching from the production of PERC-like devices toward the production of devices with passivated contacts (such as TOPCon and SHJ; see Section 2.2a) [3], since the latter lead to PV modules with higher conversion efficiencies. On the medium to long term, multijunction solar devices will be needed to reach energy conversion efficiencies at module level beyond 30%.

2.3c. PV Systems with Higher Energy Output

With the rapidly increasing number of PV systems installed worldwide, it has becomes increasingly important for these systems to operate at maximum performance and for the energy system operators to be able to accurately predict the energy output of the PV systems connected to the electrical grid. The higher the energy output of a given PV system or PV power plant over its period of operation, the lower the resulting levelized cost of electricity (LCOE). The maintenance and analysis of failures of PV systems and PV power plants are therefore becoming increasingly important [27]. To further lower the LCOE of PV systems, one possible way is the enhancement of the operational lifetime well beyond 30 years. In the past, PV modules were made in mass production without discrimination to the climate in which the modules would be used. This has sometimes led to systems that showed an actual operational lifetime of only 10–12 years instead of the typical 20–25 years warranty lifetime [27]. To avoid early failure of

PV modules and systems, especially for integrated applications where the operational conditions might be completely different from those in standard PV powerplants, the PV module design, and the materials used need to be tuned to the specific operation conditions (e.g., climatic conditions) that the system will likely undergo during its lifetime. Currently, a lot of research is ongoing into advanced energy yield (EY) and lifetime prediction models that will help to increase the operational lifetime and EY of various standard and integrated PV applications.

Again, optics can contribute a lot to increase the energy output of PV systems, hence decreasing their LCOE. Section 10 deals with state-of-the-art illumination models that can accurately predict the (spectral) irradiance of PV modules, which is crucial to obtain reliable EY modeling tools for both standard as well as integrated PV applications. Moreover, thermal management, as described in Section 9, also helps to extend the operational lifetime of PV modules and systems, while also increasing the EY of the system.

2.3d. Integration of PV Systems in Their Environment

The massive deployment of PV systems also raises the question of where all these systems should be installed, especially in densely populated areas such as Western Europe. The ability to use a certain space or land for multiple uses including energy generation is therefore very important. So-called integrated PV, in which the PV system is integrated seamlessly into its environment, provides this possibility. Examples are among others building-integrated PV, vehicle-integrated PV, infrastructure-integrated PV, and agrivoltaics (the combination of agriculture with PV). Integrated PV have an enormous potential and typically have better aesthetics and therefore can also lead to easier social acceptance. For these applications, the PV technology needs to be adapted to the specific operating conditions in which it will be used and a customized fabrication technology is needed to meet customer requirements for aesthetics (color, layout, and shape), flexibility in shape and size, and integration (facades, canopies).

2.4. Summary

In this section, we described the various device architectures in production for crystalline-silicon PV as well as the various absorber materials being used and developed for thin-film PV. We also explained why multijunction PV technology is considered the future of PV technology. We identified four major technological challenges (Fig. 1) for future mass production and deployment of PV technology in order to achieve the goal of climate neutrality and indicated how optics could help resolve these challenges. The four main challenges (Fig. 1) are:

- Sustainable production of PV systems;
- Higher energy conversion efficiencies;
- Higher energy output and operational lifetime;
- Integration of PV systems in their environment.

In the following sections we delve deeper into the details of how optics will further improve PV solar energy technology in the future.

3. OPTICAL CONCEPTS IN PV

K. Jäger, B. Bläsi, H. Helmers, R. Saive, and M. Schmid

For a highly efficient PV module the absorption of light in the absorber layer of the solar cells must be maximized. To maximize the absorption, first, reflective losses should be minimized or, *vice versa*, coupling of the incident light into the solar cell should be maximized. Second, for weakly absorbing semiconductors, such as silicon, the absorption should be maximized, which is known as *light trapping*. Third, parasitic absorption in the supporting layers must be minimized. These three strategies are often summarized under the term "light management." For multijunction solar cells optical concepts are used to redistribute the light between the junctions. Further, optics also can be used to improve the aesthetics of solar cells, for example by making them appear in a certain color.

In this section, we explain the different optical concepts, mention historical milestones and we discuss the relevance of these concepts for photovoltaics (PV) on terawatt scale. The section starts with the very basic concept of antireflective coatings (ARCs) in Section 3.1, we discuss the probably most relevant concept of *textured interfaces and structured materials* in Section 3.2 and also emphasize the importance of *parasitic absorption* in Section 3.3. After that we elaborate on *spectrally selective concepts* in Section 3.4, look at optimizing the energy yield (EY) in Section 3.5 and concepts using *concentrated light* in Section 3.6.

3.1. Antireflective Coatings

ARCs, as illustrated in Fig. 6(a), are applied to the surface of solar cells and cover glass for PV modules to increase light absorption and conversion into electricity. They reduce the reflectance of the solar cell, allowing more light to enter the cell. The coatings are designed to have a refractive index between that of air and the front material of the solar cell or PV module. Reflection is minimized, when the thickness of the coating is one quarter of the wavelength. Then the phase shift between the beams reflected from the front and rear is $\Delta\phi = \pi$. In the early years after the first "modern" crystalline silicon (c-Si) solar cell was produced in 1954 [30], ARCs from SiO_2 and TiO_2 were used. In 1972, an optimized ARC made from tantalum oxide (Ta_2O_5) was used to build a "violet" solar cell with a significantly boosted optical performance [31]. Other materials used for ARCs are silicon nitride (Si_3N_4), lithium fluoride (LiF), and magnesium fluoride (MgF_2). SiO_2, TiO_2, and Si_3N_4 also are used as passivating layers in silicon solar cells [32].

3.2. Textured Interfaces and Structured Materials

Texturing the front of a solar cell has a antireflective effect for a large angular and spectral range. In particular, for large incident angles textures can outperform ARCs. For wavelengths much shorter than the typical dimensions of the texture, the antireflective effect can be explained with the effective medium approach. For textures much larger than the wavelength, the antireflective effect can be explained with geometrical optics [33]. Further, texturing increases the absorption in the low-absorbing region because of path length enhancement, as illustrated in Fig. 6(b). In the very low absorbing region of the wavelength spectrum close to the bandgap, texturing can increase the absorption by up to a factor of $4n^2$, where n is the refractive index of the absorber [34].

Random textures are created by etching or crystal growth processes. However, depending on the thickness of the solar cell layers, the typical dimensions of these textures differ largely and therefore cover different optical regimes: while the interaction of light with the large pyramids used in c-Si solar cells, illustrated in

Figure 6

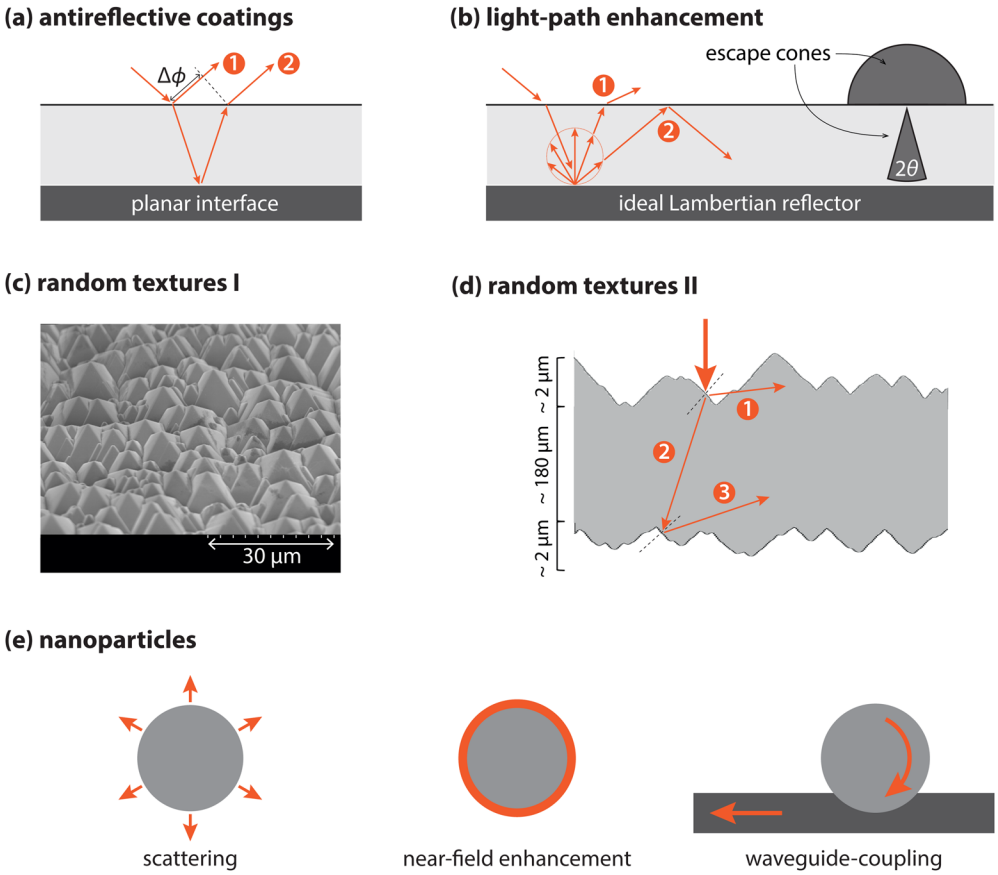

Optical concepts used in PV. (a) In ARCs the strongest antireflective effect is achieved, when the phase shift $\Delta\phi$ between the beams reflected from the front (1) and rear (2) is π, 3π, 5π, ... (b) Schematic of light with energy close to the bandgap passing through a thin silicon slab with an ideal Lambertian reflector on the rear side. The escape cone with opening angle $\theta = 16.3°$ within the silicon and the air escape/acceptance cone that corresponds to the full hemisphere are shown. Depending on its angle, scattered light reaching the front surface will either (1) escape or (2) encounter total internal reflection. (c), (d) Random textures. (c) Scanning electron microscopy (SEM) image of a textured silicon solar cell. (d) Schematic showing three ways in which pyramids randomize light: (1) reflecting on textured front, (2) transmission through textured front, and (3) reflection on textured rear. (a)–(d) Adapted from [28] under a Creative Commons license. (e) Effects of nanoparticle–light interaction: scattering, near-field enhancement, and coupling into waveguide modes. Schmid, Review on light management by nanostructures in chalcopyrite solar cells, Semicond. Sci. Technol. **32**, 043003 (2017) DOI: 10.1088/1361-6641/aa59ee [29], © IOP Publishing. Reproduced with permission. All rights reserved.

Figs. 6(c) and 6(d), can be described with *geometrical (ray) optics*, the interaction of the small textures used for thin-film silicon solar cells is in the wave-optical regime.

In 1974, Haynos and co-workers presented a c-Si solar cell with square-shaped pyramids on top, which were created by etching [35]. As of 2024, anisotropically wet-etched pyramids are still a benchmark for light trapping in c-Si technology [8], because they

reduce reflective losses across the whole wavelength range and are almost-perfect Lambertian scatterers, enlarging the light path in the absorber. Therefore, they enhance the absorption in the long wavelength range, where silicon is weakly absorbing.

For c-Si solar cells, **inverted pyramids** were also investigated [36]. Combining pyramids with small **nanocones** leads to almost perfect light trapping. Here, special attention must be put on passivating the textured surface to preserve the electronic quality of the solar cell [37].

Since the 2000s, **advanced photonic concepts** have been studied. Numerical studies suggest that nanophotonic textures can enhance absorption even much stronger than $4n^2$ within narrow spectral and angular boundaries [38–40].

Despite extensive efforts to develop various photonic textures for improved light trapping, they have typically exhibited limitations, offering enhanced light trapping only within specific wavelength ranges or narrow incident angle tolerances [28]. For thin-film silicon solar cells, **periodic structures** yielded comparable optical performance as standard random nanotextures under broadband solar irradiation [41]. In some applications light trapping is only relevant within a limited spectral range, such that the restricted wavelength range is no considerable limitation. In fact, rear side gratings have contributed to record efficiencies [42,43].

Quasiperiodic structures enable broadband and wide-angle light-trapping capabilities. In contrast to random pyramid textures, quasiperiodic photonic structures with feature sizes on the order of 100 nm present a viable approach also for thin-film solar cell designs [44–49].

Another concept to realize strong absorption enhancement was the introduction of ***plasmonic*** **metal nanoparticles** (NPs) that support surface plasmons, which are excitations of electrons at the interface between a metal and a dielectric [50–53]. Despite the positive effects of large-angle scattering, coupling into waveguide modes, and field enhancement, illustrated in Fig. 6(e), plasmonic NPs have only found restricted applications in solar cells [54–56]. For thin-film silicon solar cells, they could not outperform standard random nanotextures for thin films [57,58].

As an alternative approach, **dielectric NPs** may be inherently stable and absorption-free while equally offering antireflection behavior, resonance effects, field localization, and light redirection [59]. They have found successful integration into different types of solar cells including, e.g., thin-film Si, GaAs, and CIGSe solar cells [60–63].

The tunable wavelength-selective response of photonic structures makes them attractive for tailoring the reflected, absorbed, and transmitted spectrum. However, so far only very few concepts have been able to demonstrate their potential to improve solar cell performance beyond the state of the art. Furthermore, the cost-efficient production of photonic structures on the large scale necessary for terawatt PV remains an open challenge.

3.3. Reducing Parasitic Absorption

To maximize the optical performance of solar cells, it is essential that light is predominantly absorbed within the active absorber layer. Hence, unintended absorption must be minimized in supporting structures such as ARCs, textured interfaces, photonic structures, NPs, reflectors, and electric contacts. For instance, parasitic absorption can be significantly reduced utilizing lowly absorbing transparent conductive oxides (TCOs) [64] such as zirconium-doped or hydrogen-doped indium oxide (In_2O_3) [65,66], and low-doped zinc oxide (ZnO) [67,68]. Parasitic absorption in the back metal is caused

by the excitation of surface plasmons and can be strongly reduced by interlayers consisting of TCOs [69,70] and dielectrics [70].

3.4. Spectrally Selective Concepts

3.4a. Semitransparency

Although, in most cases, reflection and transmission are to be minimized, for some applications absorption is desired only in a very specific spectral range. Partial transmission or semitransparency find a variety of applications such as solar windows, agrivoltaics, or multijunction solar cells. Deliberately, not all of the incident light is absorbed by the solar cell: instead, the spectrum required for, e.g., indoor lighting, crop cultivation, or bottom solar cell operation is transmitted. For semitransparent solar cells, wavelength-selective optical concepts such as thin-film coatings or nanophotonic concepts, as outlined previously, can be used. Finally, semitransparency may also be exploited for bifacial operation [71,72].

3.4b. Multijunction Solar Cells

In multijunction solar cells, solar cells with different bandgaps are stacked onto each other. In addition to light incoupling and light trapping, here light management has to account for a third task: optical structures that redistribute the light between the subcells, and increase the transmission of light into the bottom cell. The role of optics for multijunction solar cells is discussed in detail in Section 7.

3.4c. Spectral Shaping

An effective strategy to counteract the challenges posed by the broadband nature of sunlight involves altering the incident spectrum impinging onto the solar cell, achievable through downshifting, downconversion, or upconversion processes. Downshifting involves the absorption of a high-energy photon followed by the emission of a low-energy photon. In downconversion, one high-energy photon can result in the emission of two lower-energy photons. Conversely, upconversion entails the absorption of two or more photons that excite a state within a material, leading to the emission of a single photon of higher energy upon radiative recombination. These techniques can be integrated into layers in front or behind of the active solar cell layer, respectively, or employed within uminescent solar concentrators to which solar cells are attached or optically coupled through free space, as outlined in Ref. [73]. This approach not only mitigates losses due to sunlight's broad spectrum but also enhances the efficiency of solar cells by more effectively harnessing the available light. Spectral shaping is discussed in detail in Section 8.

3.4d. Color Appearance

With the further integration of solar modules in buildings, *aesthetics* become more relevant. Different optical concepts have been used to make solar modules with attractive color appearances. Section 11 is devoted to the role of aesthetics and color for PV.

3.5. Optics for Optimized Energy Yield

To be relevant for terawatt scale, optical concepts not only must perform well in laboratory settings under standard testing conditions, but also demonstrate enhanced performance under real-world outdoor conditions. Outdoors, light not only reaches a solar module directly from the Sun but is also scattered by clouds and surroundings, resulting in what is known as scattered light, incident from various angles and with spectral distributions deviating from the standard solar spectrum.

To assess the performance of PV modules in the outdoors, the concept of EY is used, which is the total amount of energy harvested from a PV system installation, taking into consideration seasonal and daily variations in irradiation conditions, spectrum, temperature, as well as other relevant details of the PV system.

An elegant solution to capture light from diverse angles is the utilization of *bifacial* solar panels, which accept light not only from the front but also from the rear. It is noteworthy that around 85% of currently produced solar cells are bifacial, and it is projected that the majority of modules will follow suit within a few years [3]. The EY also can be increased by texturing the module cover for improved in-coupling of radiation incident under large angles. Light-redirecting films can increase the performance from guiding light away from solar-cell edges [74]. For multijunction solar cells, fine-tuning of bandgaps and absorber thicknesses can increase the yield under different illumination conditions.

The increased acceptance of light from different angles underscores the importance of considering ground-reflected light, known as *albedo light*. Moreover, there is potential to strategically design albedo to achieve enhanced EYs under realistic conditions. Understanding, bench-marking, and designing the effects of albedo remain active areas of research, demanding robust optics knowledge and modeling capabilities. More details on these topics can be found in Section 10.

3.6. Concentrated Photovoltaics

In concentrated photovoltaics (CPV) systems [75] direct sunlight is concentrated by factors in the range of several hundreds to a thousand, so that the amount of required energy-intensive and costly semiconductor material for solar energy conversion is reduced greatly. As a consequence, CPV has shown the lowest embodied energies and fastest energy payback times of all PV technologies [76]. Moreover, the solar cell efficiency increases under concentration due to higher carrier concentrations and resulting gain in output voltage. Record efficiencies have been demonstrated with III–V-based multijunction concentrator solar cells (see Section 7).

In **micro-concentrated** PV [77–80] the solar-cell size is reduced to the submillimeter range, as illustrated in Fig. 7. This reduction in size reduces the heat load per cell, eliminating the need for specific heat sinks and enabling the use of simple and low-cost circuit board substrates. In addition, reduced current lowers series resistance losses and very high-voltage modules become feasible, while series/parallel interconnection schemes offer flexibility in adjusting for cell-to-cell tolerances [81].

However, miniaturization also leads to an increasing influence of perimeter recombination, which is counterbalanced by high enough concentration: for a 500-μm cell and a concentration ratio of 1000, the related voltage loss is below $1\%_{rel}$ [78]. In terms of manufacturing, miniaturization requires accurate assembly and interconnection of thousands of microconcentrator solar cells per square meter. In this regard, parallelized and/or high-throughput processes from other industries, such as panel level packaging in micro- and optoelectronics, micro-/mini-light-emitting diode (LED) display technology, and advanced circuit board technologies can be applied and promise low cost. For example, surface-tension-driven self-alignment [82–85] enables micrometer-precision without the need for accurate chip placement. In fact, the forced motion of the chip during solder melting caused by an initial displacement has been shown to even increase the self-alignment accuracy [84,85]. For $Cu(In,Ga)Se_2$ microabsorbers both top-down [86,87] and bottom-up [88,89] fabrication processes were explored.

Another concept are luminescent solar concentrators (LSCs), which consist of large sheets of transparent materials embedded with pigments known as dyes or

Figure 7

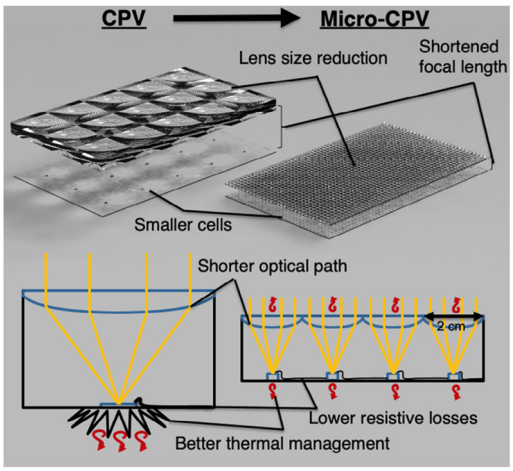

Illustration of the main functional benefits of micro-CPV modules compared with conventional CPV. The reduction of the solar cell size and the optical aperture result in shorter optical paths, lower resistive losses, and better thermal management. An additional benefit is more flexibility for different interconnection schemes and for tracking, which can avoid power losses generated by misalignments between solar cells and optics. Reprinted from [77] under a Creative Commons license.

luminophores. Luminophores absorb sunlight and subsequently re-emit fluorescent light, which is then guided and concentrated toward small solar cells positioned either at the back or at the edges of the sheet. This dramatically reduces the area of solar cells needed, as in traditional concentrators. Unlike conventional light concentrating methods (i.e., with lenses), LSCs can effectively concentrate diffuse irradiance, a significant component of solar radiation scattered by the atmosphere and terrestrial surfaces, and, thus, it eliminates the need for tracking. More details on LSCs are given in Section 8.3.

3.7. Summary

In this section, we have briefly discussed essential optical concepts for PV. After introducing *ARCs* in Section 3.1, we discussed *textured interfaces and structured materials* in Section 3.2 and *parasitic absorption* in Section 3.3. Then, we elaborated on *spectrally selective concepts* in Section 3.4, looked at optimizing the EY in Section 3.5 and concluded the section with optics for *CPV* in Section 3.6. The concepts presented in this section establish a foundational understanding that will support the advanced topics explored in the subsequent sections.

Table 1. Supply Risk and Economic Importance for Different CRMs used in PV Technology[a]

Material		Supply Risk	Economic Importance	Composite Index
Indium	(In)	0.6	2.6	0.68
Copper	(Cu)	0.1	4.0	0.52
Silver	(Ag)	0.8	4.6	0.49
Silicon metal	(Si)	1.3	4.9	0.40
Cadmium	(Cd)	0.2	4.1	0.38

[a]As assessed by the European Commission in 2023 [93]. Also includes a composite index for a global ranking of critical materials, as defined by the International Renewable Energy Agency (IRENA) in 2024 [94]. A larger number means a larger supply risk, economic importance, or criticality, respectively.

4. ECODESIGN FOR SOLAR CELLS BY USING EARTH-ABUNDANT OPTICAL MATERIALS

D. Munoz, H Sai, T. Gageot, and W. Favre

4.1. Introduction to Ecodesign

Ecodesign is defined by the International Organisation for Standardisation (ISO 14006, 2011) [90] as "the integration of environmental aspects into the design and development of products, with the aim of reducing negative environmental impacts throughout the life cycle of a product." Therefore, ecodesign is an approach that reduces the negative impacts of a product throughout its life cycle while maintaining its quality of use (cost, technical performance, etc.). Adopting an ecodesign approach consists in three steps [91]. First, an environmental assessment is necessary to provide a good initial understanding of the environmental problems caused by the reference product. Second, ecodesign strategies are suggested to reduce the environmental impacts in the development of the new solution. Finally, these strategies need to be validated from social, technical, and economic points of view. It is important to highlight that the ecodesign is not limited to environmental evaluation but must also include strategies to improve the product before production.

The life cycle assessment (LCA) approach allows for the assessment of environmental impacts by using relevant and appropriate information about the product for each phase of its life cycle: raw material extraction, manufacturing, distribution, use, and end of life. The carbon footprint is one of the many output parameters [92].

4.2. Ecodesign Definition in PV

Regarding PV technology development, carbon footprint reduction is key but depends mostly on the energy mix in the production country [92], which has little effect on technology design. In contrast, raw material use is extremely relevant in the design phase. The ecodesign criteria defined by the French government consider the reduction of critical raw material (CRM) as a mandatory step for the ecodesign approach (among others). Several CRMs as assessed by the European Commission [93] are used commonly in photovoltaics (PV). Their criticality is defined according to supply risk and economic importance, some examples are presented in Table 1, which also includes a composite index for a global ranking of critical materials as defined by the International Renewable Energy Agency (IRENA) [94].

As indicated by Table 1, indium, which is commonly used in silicon heterojunction (SHJ), thin-film, and perovskite solar cells, is the most critical material today, followed by copper and silver. Metal silicon is a CRM because of its economic importance, supply risks, and significant environmental impact during production, even though silicon is among the most abundant elements. The challenges of PV community today are to reduce or even replace these materials with more abundant ones and to ensure their 100% recyclability in the context of an rapidly growing demand for the upcoming years.

4.3. High-Efficiency Solar Cells and Raw Materials Limitations

Crystalline silicon (c-Si) solar cells dominate the current PV market, and this trend is expected to continue in the coming decades, whether in single-junction or tandem configuration. To date, the highest efficiency among various types of c-Si solar cells has been achieved with SHJ architecture [8].

One of the optical functional materials used in SHJ cells is transparent conductive oxides (TCOs), which provide both high light transmittance and high electrical conductivity simultaneously. TCOs are also important building blocks for thin-film solar cells including metal-halide perovskite and perovskite/c-Si tandem cells. The most-common TCO material is indium oxide. In_2O_3-based TCO offers the best optoelectronic performance among various TCOs, but as a CRM, it significantly limits the production capacity of SHJ, perovskite, and perovskite/c-Si tandem cells [95]. In response to this issue, R&D toward In-lean or In-free SHJ cells is currently under way to pave the way for the massive industrialization of the technology, as discussed in Section 4.3a. The concern about silver (Ag) usage pertains to the metallization of all silicon-based solar cell technologies, as the demand for this element in PV manufacturing has already reached 13% of the global demand [96]. The PV community is following a similar strategy for reducing In usage: both Ag usage reduction or complete replacement are being explored through different technological approaches, as discussed in Section 4.3b. Regarding silicon, many improvements are ongoing to reduce and optimize material use (thickness, kerf loses, recycling, etc.), and proposals for the next technology of direct wafer manufacturing are being explored. However, this is beyond the scope of this work. The usage of poly-Si for a Si PV cells has decreased from 6.8 g/W in 2010 to 2.3 g/W in 2022 [97].

4.3a. Indium Concerns and Optical Improvements

Figure 8 summarizes the state of the art of the conversion efficiencies of SHJ solar cells as a function of In reduction in TCO layers. The highest efficiency of front/back contact SHJ cells is 26.8%, achieved by Lin *et al.* with In-rich TCOs on both sides [8], as plotted in the top left corner of this figure. Other reference cells with In-rich TCOs are also aligned at an In fraction of 100%, with a wide range of efficiencies [98–100].

There are several approaches for reducing In consumption in SHJ cells. The simplest approach is to replace In-rich TCOs with In-free TCOs, such as ZnO-based [103,109,110,114–119] or SnO_2-based [108,120] TCOs (In-free approaches). Another approach is to reduce the thickness of In-rich TCOs (In-lean approach) [70,101–113]. In this approach, thin In-rich TCOs are combined with dielectric layers or other TCOs to meet optical requirements, such as antireflection effect on the front. The advantage of this approach is the possibility to leverage the extensive knowledge about standard In-rich TCO-based SHJ cells, though it still requires a certain amount of In. Another interesting approach to eliminate In consumption is TCO-free solar cells, which do not incorporate any TCO layers, whether In-based or not [121–123]. All approaches can be applied either one side or both sides of the cells. Hereafter, we discuss these approaches. It should be noted that hetero back-contact (HBC) approach [14,124,125] is also regarded as an In-lean SHJ cell since it does not use any TCOs on the front side. However, it is out of the scope of this section due to the additional technological difficulties of rear-side fine patterning.

(a) In-free TCOs. Here, we discuss the study of replacing the TCO on one or both sides of the SHJ cell with an In-free TCO, as schematically shown in Fig. 9. This family of In-free materials mainly concerns ZnO-based and SnO_2-based materials [64]. Zn has a much larger resource availability than In, and therefore ZnO-based TCOs have been expected and developed as an In substitute material for many years

Figure 8

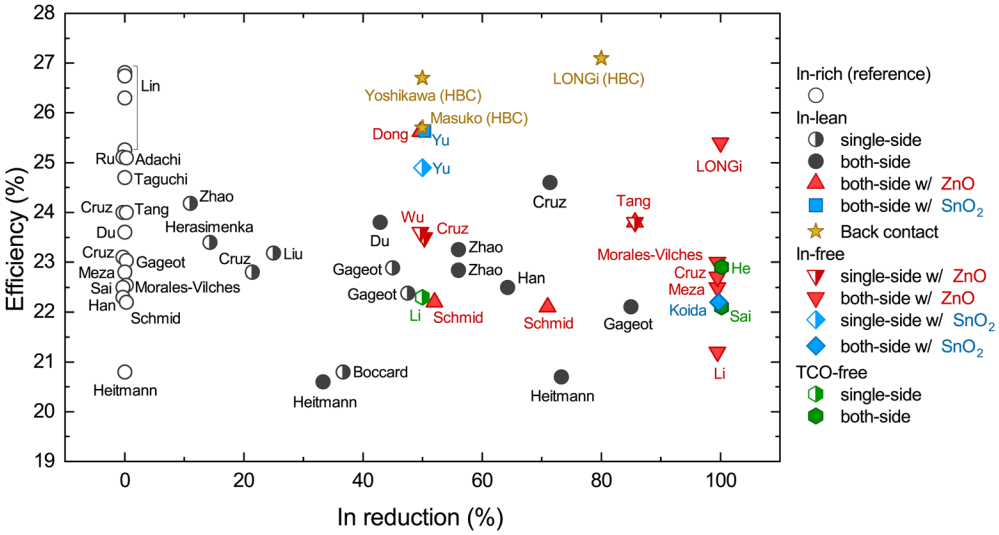

State of the art of the conversion efficiencies of SHJ solar cells as a function of In reduction in TCO layers. Symbols at In reduction = 0% indicate benchmark SHJ cells with In-rich TCOs [8,98–100]. The different symbols indicate different approaches to reduce In consumption in SHJ cells: thin In-rich TCOs with dielectric layers or other TCOs [70,101–113], In-free TCOs (ZnO or SnO_2) [103,108–110,114–120], and TCO-free SHJ cells [121–123]. All the approaches can be applied either one side or both sides of the cells. 100% In-reduction means completely In-free SHJ cells. A hetero back-contact (HBC) approach [14,124,125] is also regarded as an In-lean SHJ cell as it does not use any TCOs on the front side. The name next to each symbol indicates the first author of the corresponding publication.

[126]. An important advantage of ZnO-based TCO materials is that high conductivity TCOs can be obtained by low-temperature processes such as sputtering, similar to In_2O_3-based materials, though they are slightly inferior to In_2O_3-based materials in terms of optoelectronic properties. This is crucial to apply TCOs to solar cell devices with low heat resistance, such as SHJ cells and perovskite cells. In SHJ cells, many groups have reported studies on the use of Al-doped ZnO as a TCO. In fact, high initial efficiencies comparable to those of In_2O_3-based TCO have been reported, as shown in Fig. 8 as the downward triangle symbols [103,109,110,114–119]. In-free AZO-based SHJ cells with efficiencies of 21.2–23% were reported in 2019 [103,115–117]. Recently, an excellent example of In-free ZnO-based SHJ cell with an efficiency of 25.4% was reported by LONGi [119].

However, a problem inherent to ZnO-based materials is their weakness to moisture and poor long-term stability. Therefore, ZnO-based SHJ cells have not yet been commercialized. As described later, the chemical stability of ZnO-based TCOs can be improved by capping with In_2O_3-based ones, compared with ZnO-based alone. Alternatively, there is an approach to compensate for this lack of chemical stability in the module sealing technology. In fact, a double glass structure is used to achieve robust sealing in thin-film Si solar cells [127] and CuInGaSe solar cells [128] that were commercialized using ZnO-based TCO. For full-scale commercialization, further research is expected to improve the optoelectronic properties and chemical stability.

SnO_2-based TCOs can also be interesting to replace In_2O_3-based ones. Indeed, SnO_2-based TCOs (SnO_2:F, SnO_2:Sb, and SnO_2:Ta) are excellent TCO materials and widely used in various applications, including thin-film Si and CdTe solar cells [129,130].

Figure 9

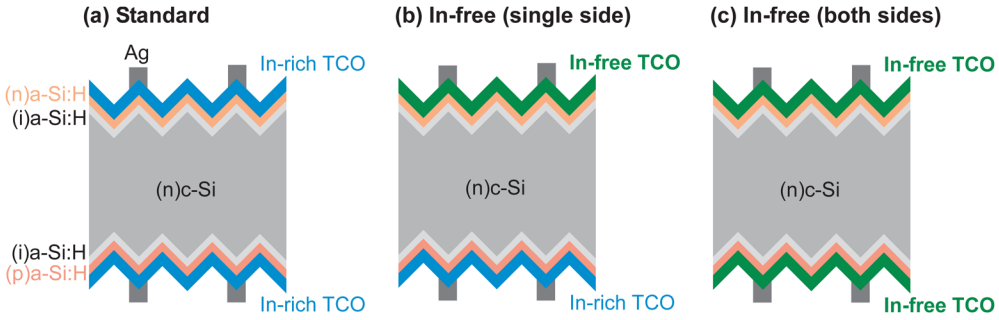

Schematic illustrations of SHJ cells with (a) In-rich TCOs on both sides, (b) In-free TCO on a single side, and (c) In-free TCO both sides.

Such SnO_2-based TCO films are typically deposited by chemical vapor deposition (CVD) or sputtering at high temperatures of 400–600°C. The resulting film is polycrystalline with excellent chemical stability. However, the electrical properties of the SnO_2-based film decrease significantly when the deposition temperature is lowered [131]. Therefore, SnO_2-based TCOs have not yet been applied to temperature-sensitive devices such as SHJ and perovskite/Si tandem cells. Recently, it has been reported that amorphous SnO_2 (a-SnO_2) can achieve high transparency and reasonable electrical properties even by low-temperature deposition. a-SnO_2 films deposited by reactive plasma deposition (RPD) method have shown resistivity of the order of 10^{-4} Ωcm [120]. The potential of In-free a-SnO_2-based SHJ cells has demonstrated by a lab-scale SHJ cell with a-SnO_2 films on both of front and rear sides by Koida *et al.* [120] as plotted as the blue diamond symbol in Fig. 8. Moreover, the development of a-SnO_2 films by sputtering method is also progressing. Although the resistivity is still higher than that of RPD method, a RJ SHJ cell with sputtered a-SnO_2 on the front side with an excellent efficiency of 24.9% was reported by Yu *et al.* [108] as plotted as the half-filled blue square (In reduction = 50%) in Fig. 8. One advantage of SnO_2 over ZnO is its high tolerance to humidity, which leads to long-term stability for solar cell applications [120].

In summary, the research and development of TCO materials without In, such as ZnO-based and SnO_2-based materials, is steadily progressing. For the relaxation of resource constraints, early commercialization of c-Si solar cells and perovskite/c-Si tandem solar cells with these materials are expected. Today, those TCOs raise issues with poor contact with Ag or a-Si:H [109,117,118,132], FF losses [109,110,112,117,118,132], higher sputtering damage leading to lower V_{oc} [109,110,112,132,133], lower J_{sc} [109,110,112,118,132], and poor reliability against humidity [109,117] compared with In-rich TCOs. Potentially, SnO_2-based TCOs are supposed to be more reliable than ZnO-based ones from the material point of view, but this must be confirmed by extensive reliability tests.

(b) In-lean approach. To overcome issues with In-free TCOs, other approaches have been studied in recent years, such as multilayer antireflective coatings (ARCs). Indeed, it is also possible to reduce the indium content by reducing the In-rich TCO layer thickness. On the rear side, the thickness can be lowered by 60% without efficiency losses [134]. However, on the front side, since the TCO acts as an ARC, the thickness reduction needs to be compensated by adding another layer. In this case, two different approaches exist as follows:

Figure 10

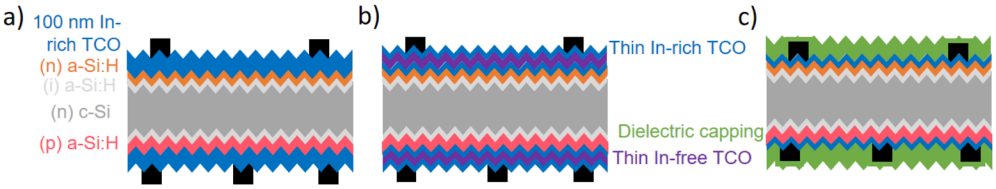

(a) Classical SHJ cell, (b) In-free + In-rich TCO multilayer cells, and (c) thin In-rich + dielectric layer or multiple ARCs. Note that the TCO changes are represented on both side of the cells, which is not the case in all the cited studies.

In-free + In-rich TCO multilayer To circumvent the poor contact of AZO with a-Si:H layers, some studies added a thin In-rich layer between the two layers, as shown in Fig. 10(b) [109,110,112,132,135,136]. When the In-rich contact layer is used below the AZO layer, it also protects the a-Si:H layer from the higher sputtering damage of AZO. On another hand, to cope with the poor damp heat reliability of pure AZO and allow a better contact with the Ag grid, a thin In-rich TCO layer can be used as a capping layer, thus providing a barrier against humidity [109]. By using two contact layers, Tang *et al.* reached efficiencies as high as 23.6% (compared with 23.7% for the ITO references) with an 85% In reduction [110]. Dong *et al.* achieved an impressive certified cell efficiency of 25.62% with a 50% In reduction on the front side (only an In-rich contact layer between the selective layer and the AZO layer) [112].

Thin In-rich TCO + dielectric layer or multiple antireflective layers Another solution is to use a completely transparent but nonconductive layer as a dielectric layer (SiN_x, $SiON_x$, SiO_x, MgF_2, or AlO_x) [70,101,102,105–107,113] to compensate for the thickness reduction of the TCO layer as shown in Fig. 10(c). Using this solution, the lateral transport is carried out only in the thinner TCO layer (and in the substrate), so optimization of the thinner TCO toward high conductivity is necessary to avoid fill-factor losses. Indeed, since the sheet resistance is inversely proportional to the thickness, a thinner TCO leads to higher sheet resistance. It must be noted that the deposition of a hydrogen-rich dielectric can improve the underlying TCO electrical properties by hydrogen doping: the resistivity of the TCO layer can be reduced by up to a factor of three [101,113]. On the other hand, since dielectric layers are more transparent than TCOs, current gains can compensate for small FF losses: the thinner the TCO layer, the lower the parasitic light absorption. Thus, a compromise between FF losses and current gains will dictate the thickness reduction potential. It was also shown that a dielectric capping can improve the damp heat reliability of the cells [104,113,137] and that, in some case, the thinner ITO layers can show an enhanced ultraviolet (UV) reliability [113]. Using this type of architecture, Cruz *et al.* [70] reached a remarkable cell efficiency of 23.9% (while the 100% In rich TCO reference is 0.2% lower) using a 20-nm-thick In-rich layer on both sides and a SiO_2 capping layer. Another recent study showed that lowering the TCO thickness on the rear side below 20 nm affects dramatically the efficiency, but that it is possible to use ITO layers as thin as 10 nm on the front side without efficiency losses (90% In reduction) [113].

(c) TCO-free approach. The last approach we discuss here is TCO-free solar cells, in which no TCO layers are used, regardless of whether they are In-based or not. This might be a promising approach in SHJ solar cells because the photogenerated carrier density in c-Si cells under illumination becomes rather high by applying state-of-the-art passivating contact technologies such as SHJ. Therefore, the sheet resistance of the base c-Si wafer can be low and comparable to that of TCO layers [138]. In such

Table 2. Aluminum and Silver Usage for the Different Silicon-based Solar Cell Mainstream Technologies[a]

	Efficiency (%)	Power (W)	m_{Al} (mg)	c_{Al} (mg/W)	m_{Ag} (mg)	c_{Ag} (mg/W)
m-PERC	23.2	7.7	900	117	84	11
b-PERC	23.2	7.7	300	39	84	11
TOPCon	23.9	7.9	0	0	160	20
SHJ	24.2	8.0	0	0	200	25

[a]As taken from Ref. [4] for year 2022 as reference. The area is 330.69 cm^2 (M10 wafer size) for all; m and c in the table stand for "mass" and "content per watt," respectively.

a situation, the lateral carrier transport could be supported by the c-Si wafer itself without the help of TCO layers. In addition, a TCO-free approach is attractive for cost reduction since the TCO deposition process occupies a nonnegligible portion of the production cost of SHJ cells.

TCO-free approach was first demonstrated by Li *et al.*, showing an efficient rear-junction SHJ cell with a TCO-free front contact structure [121]. In addition, He *et al.* took one step further and realized TCO-free SHJ cells using dopant-free contacts on both sides [122]. Sai and Matsui also developed both-side TCO-free SHJ cell with an initial efficiency of >22% [123]. In that work, it was found that low contact resistivity at carrier selective contacts is more crucial in TCO-free SHJ cells than in normal SHJ cells. It was also pointed out that TCO-free cells suffer from metal diffusion into Si layers, which deteriorates the long-term PV performance of SHJ cells. These results suggest that TCO-free SHJ cells with a high initial efficiency are achievable, and many examples for TCO-free devices are given, but the issue of stability was not discussed. New metallization process/architecture are required to solve this reliability problem in the future.

4.3b. Silver Concerns

Metallization of c-Si-based solar cells must allow charge carriers collection and transport up to the interconnection ribbons or wires while ensuring low recombination, resistive, and optical losses, and be reliable under thermal and mechanical stresses. The mainstream process for metallization is screen-printing using conductive pastes, which are a mix of metallic particles, solvents, and other components depending on the cell technology. For high-temperature Si devices such as passivated emitter and rear cell (PERC), with dielectric passivating layers (SiO_x, SiN_x:H, AlO_x), etching agents are needed to ensure a connection to the silicon through these insulating layers (activated during the firing step). Al–Ag-based pastes enable contact on p-type silicon, whereas Ag-based pastes are used for contact on n-type Si [139]. For high-efficiency cells, technologies such as TOPCon and SHJ, there is a limited (TOPCon) or no (SHJ) direct contact with silicon, which allows for drastically reducing recombination losses and achieving higher open-circuit voltages (V_{oc}) [140]. In the currently developed TOPCon technologies, both front and rear sides of the device are contacted with pastes involving a high-temperature firing step. For SHJ, the deposition of both sides' metallization is on top of TCO layers, followed by drying and low-temperature sintering steps (<200°C). A major drawback of this technology is the higher silver content compared with higher curing temperature pastes. The schematic illustrations of PERC, TOPCon, and SHJ cells are shown in Fig. 11.

PERC devices use Al on the rear side and Ag on the front side [3]. TOPCon and SHJ require different metallization-paste properties, leading to increased Ag usage, with typical laydown of 160 and 200 mg, respectively. Table 2 summarizes the metal content in these mainstream devices considered as M10 size in 2022.

Figure 11

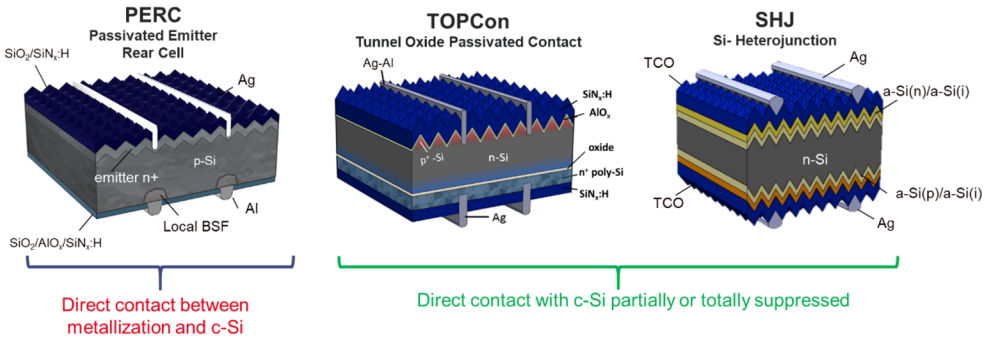

Representation of bifacial PERC, TOPCon, and SHJ devices and corresponding layers, including metallization approaches with direct, partial, or no contact with the silicon absorber.

Projections on silver demand for the PV sector to meet the net-zero emission by 2050 underline the need to drastically limit the silver content per cell, with an upper limit proposed at 5 mg/W and corresponding Ag demand upper limit at 5 kt/a [96].

Metal laydown using a screen-printing technique has seen significant reduction in use in recent years, mainly due to an increase in the number of busbars (BBs). This strategy allows for the deposition of narrow fingers (improving shadowing) with higher line resistance, as the charge carriers will be transported over shorter distances. The transfer of metal particles through narrow screen openings could lead to nonconform or cut lines, but the development of knotless screens with new emulsions enables the processing of lines less than 20 μm in width. Current technologies generally use 9 to 12 BBs for M10 devices, and some suppliers are expected to release products up to 24 BBs for G12 wafer size soon. Reducing the silver content at the finger level implies a greater metal usage for the BBs, increasing the complexity and costs for interconnection and metal consumption at the module level (more ribbons or wires). At some point, this becomes detrimental to photon collection by the PV module, as more ribbons or wires generate more shadowing, even with specific nonflat structures (see Section 3). Furthermore, the module reliability can be affected by the most-aggressive metal laydown.

Alternatively, interesting results have been found for TOPCon with direct contact of new Al-based pastes compatible with n+ poly-Si or lines deposited in two steps: (i) Ag paste dots in contact with the poly-Si layer; (ii) a copper full line on top [141]. For SHJ, metal pastes loaded with Ag-coated Cu particles have recently attracted much attention, as they are compatible with screen-printing and can reduce Ag laydown by more than 40%. Integration of such pastes at the rear side or on both sides in 6-BB SHJ devices shows that it is possible to reduce the Ag content by 30% with only a slight effect on efficiency. Thus, 11 mg_{Ag}/W is reached with less than 0.3% absolute efficiency loss, as presented in Fig. 12. These results are very promising, and efficiency loss related to higher line resistances (compared with the pure Ag ones) can be reduced using higher quantity of BBs or BB-less designs.

Alternative techniques for metallization of Ag pastes, allowing narrow fingers with high aspect ratio, such as pattern transfer printing (PTP) also referred as laser transfer printing (LPT), dispensing, rotary printing, and inkjet printing have been proposed [139,142]. Although LTP has been used to allow front-side shadowing lower than 2% and reached record efficiency for SHJ devices, its compatibility with high-throughput and reduced silver usage still needs to be demonstrated [143].

Figure 12

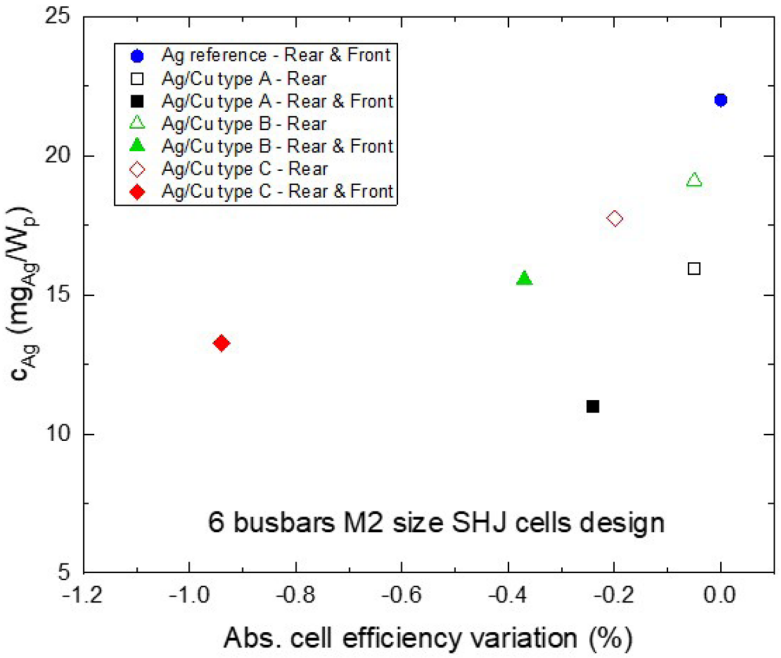

Influence of Ag content reduction in Ag-coated Cu low-curing-temperature pastes on relative efficiency for 6-BB SHJ devices prepared on CEA SHJ pilot line. The reference (blue circle) is a standard Ag paste and the Cu/Ag pastes have been applied only at the rear side (open symbols) or on both sides (solid symbols).

Copper plating processes for Si-based solar cells allow for reducing or removing Ag usage. Several works show possible process flows compatible with the different existing Si cells technologies and record efficiencies. The higher cost of this metallization technique compared with screen-printing, together with possible process issues such as parasitic plating and reliability losses, are some of the points preventing its entrance into mass production [144–146]. It is worth noting that in the approaches involving the usage of Cu, its diffusion into silicon must be avoided as it could cause strong reliability issues (local shunts, bulk lifetime degradation). Laser contact opening (LCO) process optimization or the presence of a barrier such as TCO for SHJ are possible strategies for this purpose. There may also be a need to have the Cu metal layer covered by another metal, as its oxidation could strongly affect its conductivity and color, and also lead to reduced module reliability. Finally, moving to interdigitated back solar cell (IBC) technologies enable to suppress entirely front side reflections due to metallization and some have already demonstrated their compliance with strong Ag reduction [9,147].

4.4. Summary and Advances Required

In conclusion, considering the impressive trend of solar PV installations reaching ≈ 1.5 TW worldwide in 2023 [97], the PV community needs to rethink PV solar systems based on an ecodesigned approach where efficiency, reliability, and environmental constraints are mandatory. This means that strategies for CRM reduction (or removal) should be at the core of research and innovation activities in the lab to make these processes and technologies possible. Moreover, designing for 100% recyclability is also necessary to maximize material recovery in a circular ecosystem for PV. In the future, the optical challenges in this context can be summarized as follows:

CRM reduction or removal: Reduction or alternative technologies for CRMs used in mainstream crystalline silicon solar cells and modules. Typically, the development of device and module technologies that reduce Ag, In, Bi, etc., are required. As for optoelectronic materials, urgent tasks include the development of low-temperature-formed TCO materials with reduced or no In, applicable to heterojunction solar cells and perovskite/Si tandem solar cells, control of interface properties, and verification of long-term stability.

Recycling technologies: Recycling technologies for PV modules, or the development and dissemination of PV modules that are easy to recycle. In relation to optics, laser processes are widely used in the manufacturing process of solar cells, and efficient module disassembly technologies utilizing lasers are also an interesting research subject.

5. LUMINESCENCE I

P. Manley, U. Aeberhard, M. Ledinsky, and S. Burger

5.1. Introduction

This section covers luminescence, the light leaving the cell or subcell of a multijunction device. We show that the luminescence of a solar cell gives us insight into both the electrical and optical properties. Furthermore, internal luminescence can be exploited to increase the voltage in single-junction solar cells and the current in multijunction solar cells via the luminescent coupling effect.

5.2. Luminescence

In the detailed balance analysis of Shockley and Queisser, many loss channels are assumed to be negligible in order to obtain upper limits of solar cell performance [22]. One loss channel that cannot be set to zero is the emission of photons from the solar cell, called luminescence. This is due to the fundamental reciprocity between absorption and emission [148]. For light to enter the solar cell, we must allow for the fact that it will also be able to leave the solar cell. An interface that is perfectly transmissive for light from one direction and perfectly reflective from the other direction requires rather exotic physics and is not applicable to a solar cell [149,150]. Second, if we allow that light can be absorbed in the solar cell, thereby producing an electron-hole pair, it must be possible for electrons and holes to radiatively recombine and emit light [22].

When an ideal solar cell is illuminated under open circuit conditions, all of the generated electron-hole pairs recombine radiatively and produce luminescence. In reality, both Auger and Shockley–Read–Hall (SRH) recombination will lower the amount of luminescence by nonradiative recombination [151,152]. The luminescence is a measure for how close our real system is to an ideal one. By increasing the measured luminescence of a solar cell operating at open circuit, we imply that the nonradiative recombination rates have been reduced in comparison to the radiative recombination rates [148].

The real-time monitoring of luminescence may serve as a direct indicator of the evolution of defect states contributing to nonradiative recombination during the growth or crystallization of semiconductor thin films. A notable example involves the utilization of combined *in situ* photoluminescence and grazing-incidence wide-angle x ray scattering (GIWAXS) measurements for investigating the deposition of halide perovskite films through the solution process [153]. The findings allowed for the delineation of two distinct stages in halide perovskite growth. The initial stage is characterized by the rapid growth of individual perovskite grains, as revealed by GIWAXS, accompanied by a linear increase in the luminescence signal. In contrast, the second stage exhibits a significant decrease in growth speed detected by GIWAXS, coupled with a pronounced quenching of the luminescence signal. This phenomenon arises from the formation of grain boundaries when the individual grains begin to interconnect. Grain boundaries, being regions of high defect density, result in a substantial quenching of luminescence by two orders of magnitude due to nonradiative recombination. Interestingly, similar observations have been made through *in situ* measurements of evaporated halide perovskite [154] and films prepared using so-called pizza oven deposition [155].

Due to the wealth of information that is gained from the spectrum, overall intensity, and lifetimes of the photoluminescence from a solar cell, this will become a key characterization technique, especially for high-efficiency devices.

5.3. Radiative Efficiency

The external radiative external efficiency η_{ext} of a solar cell is the ratio of the external emission rate R_{ext} to the combined total of the external emission rate and nonradiative recombination rate R_{nonrad},

$$\eta_{\text{ext}} = \frac{R_{\text{ext}}}{R_{\text{ext}} + R_{\text{nonrad}}}. \tag{1}$$

Increasing the external radiative efficiency, which is primarily achieved by reducing the nonradiative recombination rates, will reduce the voltage loss of the solar cell at open circuit, V_{oc}, compared with the ideal radiative open circuit voltage $V_{\text{oc,rad}}$,

$$V_{\text{oc}} = V_{\text{oc,rad}} + \frac{kT}{q} \ln \eta_{\text{ext}}, \tag{2}$$

where kT/q is the thermal voltage. The open circuit voltage is determined by the quasi-Fermi-level splitting in the absorbing material upon illumination, which, in turn, depends on the density of generated charge carriers and recombination mechanisms [152,156]. When charge carriers recombine radiatively, their emission with respect to the angle inside the absorber may be isotropic, in-plane, or out-of-plane polarized, depending on the material system and photonic environment. Due to the higher refractive index of the absorbing layer compared with the exterior, some of the internal emission is trapped within the device due to total internal reflection. This is reabsorbed to create an electron-hole pair, which restarts the cycle that is also termed *photon recycling*. A schematic overview of this process is given in Fig. 13(a), which does not show nonradiative recombination effects present in realistic devices. Note that Fig. 13(a) represents operation at a voltage below V_{oc} as some carriers are collected at the contacts. For planar layers, most of the internal emission is trapped due to the very small escape cone [148]. This leads to a higher photon density inside the absorbing layer, resulting in a higher charge carrier density. As previously established, this will directly increase the V_{oc} [157,158]. This effect has been studied in GaAs, Si, and perovskite devices [159–162]. Due to weak absorption at the band edge, Auger recombination in crystalline silicon is dominant, and thus the radiative efficiency remains far from the ideal limit [151].

The V_{oc} of a solar cell can be brought closer to the ideal value by an optical design that more readily traps light inside the absorbing layer. This requires large η_{ext}, since otherwise the photon and charge carrier densities do not significantly build up with repeated emission and reabsorption events. For low η_{ext}, the energy is instead lost as heat. The optical design must also not trap light for those angles corresponding to the external solar illumination, otherwise light would not be able to enter the solar cell. In order to reach the efficiency limit for single-junction devices, the optical design must also take into account the photonic environment for light emission inside the absorbing layer. This involves including a high reflectivity rear side with low parasitic absorption (favoring dielectric mirrors over metallic reflectors), suitable modification of the front side to provide antireflection in the narrow band of angles that receives solar radiation and high reflection of all higher angles [148,158,163]. Such a system would be suitable for very low levels of diffuse light and would require a two-axis tracking system. Section 10 contains a discussion on modeling the diffusivity of sunlight based on average local weather conditions and including aspects such as tracking into cost calculations.

5.4. Luminescent Coupling

Multijunction solar cells have two or more layers absorbing sunlight. Typically, they are arranged from front to back in descending bandgap energies. This allows all of the light with energies below the bandgap to be naturally transmitted to the underlying cells. In

Figure 13

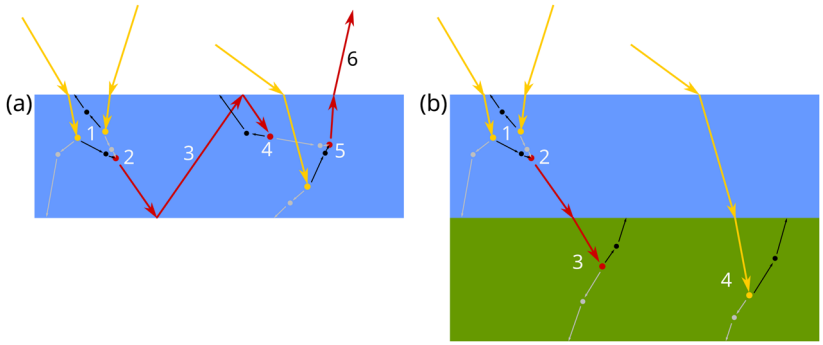

Schematic description of (a) photon recycling and (b) luminescent coupling in solar cells at the operating voltage. (a) (1) Solar radiation (yellow arrows) incident to the solar cell (blue) is absorbed, generating electron-hole pairs. Some charge carriers are collected at the contacts. (2) Some charge carriers recombine to emit luminescence (red arrows). (3) Depending on the emission angle, the luminescence can be trapped via total internal reflection. (4) The corresponding internal photon may be reabsorbed creating a new electron-hole pair. (5) Another recombination event leading to (6) a photon that is extracted via luminescence. (b) Steps (1) and (2) are the same as in (a). (3) Due to low reflection between the upper (blue) and lower (green) absorber, the internally emitted photon is able to enter the lower absorber and to generate an electron-hole pair. (4) Some fraction of the incident solar radiation will also reach the lower absorber.

such a configuration, the luminescence produced by each subcell will also be absorbed by the underlying cells but not by those that are closer to the front. If the luminescence from a subcell is absorbed by a lower lying subcell, it will contribute as an extra illumination source, thereby increasing the current in the lower lying subcell. This process is called luminescent coupling and is shown schematically in Fig. 13(b). Note that the extra current in the underlying subcell comes from the incomplete conversion of absorbed light to current in the upper subcell. The luminescence absorbed in the lower lying subcell will undergo thermalization of the charge carriers that reduces the energy yield (EY). Despite this, it is still preferable for the luminescence of subcells to be absorbed by lower lying subcells rather than to be emitted to the environment. This effect has been experimentally verified in high-quality multijunction systems, typically involving III–V materials [164,165], but also in perovskite tandems [166].

Section 7.1 describes the challenge of current matching in series connected multijunction devices. This requirement is easily met for a given illumination spectrum, incidence angle distribution and temperature. Under real-world conditions, the solar irradiance will change its angular spectrum throughout the day and year. Cloud cover may dramatically reduce the intensity, spectral weighting, and angular distribution of the solar irradiance. Furthermore, the temperature dependence of the current and fill factor will generally not be equal for the two subcells. Due to overall current being limited to the lowest current of all subcells in a multijunction device, such fluctuations in the illumination or temperature can reduce the overall efficiency much more than for a single junction.

The voltage increase due to the external radiative efficiency has also been studied for multijunction solar cells [167]. The key challenge here is to include wavelength selective reflectors to confine the luminescence for each subcell while allowing the transmission over photons with lower energies.

Luminescent coupling may act as a stabilizing effect to counteract fluctuations in the illumination [168,169]. Often, these fluctuations cause an absorption that is too high in the higher lying subcells and a too low absorption in the underlying subcells. If the conversion of absorption into current in the upper subcell is incomplete, it may luminesce and emit light to lower lying subcells. Thereby directly increasing the absorption there, as shown in Fig. 13(b). Note that this also requires a high radiative efficiency in the upper subcell. In addition, the photonic environment should be constructed to allow light to be preferentially emitted to lower lying subcells. For a two junction solar cell this is usually the case as the refractive index of the lower lying cell is much higher than that of air outside the device. This means the escape cone for light is much larger for emission to lower subcells. For devices with more than two junctions, the situation is significantly more complicated, and requires a careful design to ensure the luminescence is primarily directed downward to increase the luminescent coupling.

By tailoring the amount of luminescent coupling, the current in a multijunction device can be more easily balanced. This can directly raise the efficiency under ideal conditions, i.e., a clear day with the Sun at the optimal azimuth and altitude, in the case of a bottom-limited device, for instance a perovskite–silicon tandem with insufficient primary photogeneration in the low-absorbing silicon subcell. Luminescent coupling can also reduce the efficiency drop seen for nonideal conditions, i.e., cloudy day or Sun at a nonoptimal azimuth and altitude. To quantify the effect of luminescent coupling under ideal and nonideal conditions, it should be included in EY models discussed in Section 10. This includes modeling of both the electrical and optical properties [170,171].

5.5. Modeling Internal Emission

We have seen that modeling the luminescence of solar cells is crucial for reaching the highest efficiency devices. There is a lot to gain by an optical design that preferentially manipulates the luminescence. To achieve such an optimal design, modeling tools are required. Approaches present in the literature have handled the light emission via ray optics with either planar interfaces or approximations to structured interfaces using the idealized Lambertian scattering law [172]. For structures much larger than the wavelength of light, a ray optical picture is appropriate. An approach based on first determining the scattering matrix of such an interface and using this to determine the self-consistent internal field of the absorbing layer can model the radiative efficiency. With knowledge of the SRH recombination rate, the Auger coefficient for the material and the angular-dependent rear reflectivity, the luminescence at open circuit can be determined. This directly relates how close the device V_{oc} is to the ideal limit. If the absorbing layer is thick compared with the internal wavelength, interference effects may be neglected. For thin films, the escape probability will be dependent on the position of the photon emission within the absorber due to phase effects.

If the device structuring is on the same order or below the size of the internal wavelength, rigorous simulations are needed to realistically model the wave optical nature of light. Due to the stochastic nature of the internal light emission, we may treat individual emission events as independent from and incoherent with one another. A widespread model to describe the characteristics of light emission in thin-film optical cavities is dipole radiation theory [173,174], heavily used in the fields of organic light-emitting diodes (OLEDs) [175,176] and of the emerging perovskite LEDs [177,178]. Assessment of PV performance at the radiative limit, which includes consideration of photon recycling, requires quantification of both internal emission and external light-outcoupling [179]. Conventionally, internal emission and reabsorption is evaluated by measuring the power dissipated by a radiating dipole in the active medium, whereas the

Figure 14

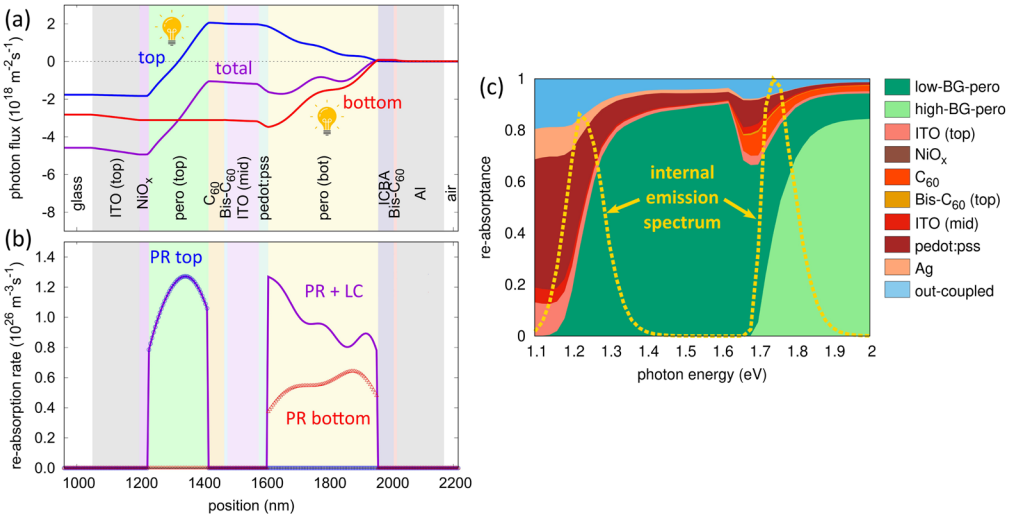

Optical modeling of internal emission and reabsorption in an all-perovskite tandem solar cell based on the Green tensor formalism. (a) Subcell contributions to the total photon flux due to internal emission (blue, top; red, bottom; magenta, sum/total). (b) Spatial profiles of secondary photogeneration rates due to PR and LC. (c) Spectrum (dashed), layer-resolved reabsorptance (green, PR and LC; red, parasitic) and outcoupling (blue) of internally emitted light. Aeberhard *et al.*, Sol. RRL **8**, 2400264 (2024) [184]. Copyright Wiley-VCH Verlag GmbH & Co. KGaA. Reproduced with permission.

outcoupled flux is measured via the Poynting vector of the electromagnetic fields generated by the radiating dipoles [180]. In contrast to the situation in optically bulk-like media, where the Van Roosbroeck–Shockley relation linking absorption coefficient and local emission rate can be used [172,181], the internal emission in thin films depends on the local density of photon states in the cavity. A consistent description regarding dependence on the cavity modes of both internal emission rate and external flux is found on the basis of the electromagnetic Green's tensor of the dipole fields [180]. An important challenge remains in the propagation of the optical rates of emission, reabsorption, and outcoupling to the electrical performance of the solar cell. To this end, the expressions for the local rates and the Poynting vector in terms of the Green dyads need to be connected to the local value of the quasi-Fermi-level splitting [182,183]. This consistent formulation of light emission, propagation, and reabsorption can also be used to assess, on equal footing, the contributions of photon-recycling and luminescent coupling in multijunction solar cells based on thin films, such as all-perovskite tandems [184] (Fig. 14). For tandems including subcells with incoherent optics, such as perovskite–silicon tandems, the Green dyad formalism can be coupled to net radiation or even ray-tracing models (in the presence of scattering at large-scale textures) for this purpose [185].

At the same time, device structuring on the nano-scale often results in periodic structures. Models of periodic structures are typically restricted to a single unit cell of the repeating structure. Such a model is valid for a periodically repeating coherent ensemble of sources that differ only by a phase factor. Since we instead wish to model a single incoherent source, we need either to simulate a large supercell of the repeating periodic structure [186,187] or integrate over values of the phase in reciprocal space [188]. Although large supercells are conceptually more straightforward, the reciprocal space integration may offer more room for an efficient approach. The integrand involved

is typically highly singular which requires special mathematical treatment, but opens the door to adaptive schemes and rational function interpolation schemes, which may vastly reduce the computational effort required. It should be noted that such issues also appear in integrals of the angular spectrum of simpler structures such as planar interfaces due to the bound waveguide modes. There, reciprocal space integration techniques could also be applied to reduce the computational effort. Indeed, divergences in dissipated power at large values of in-plane photon wave vector in absorbing media are a common issue in dipole radiation theory, and are usually mitigated by a rather arbitrary wave vector cutoff [177] or the introduction of nonabsorbing domains around the dipole position [180,189]. Since these divergences originate in the presence of near-field energy transfer by longitudinal components of the Green tensor related to the use of a continuum model of the dielectric medium response at microscopic distances, they are removed by transition to a purely transverse Green tensor [182].

Simulation of the entire optoelectronic response of solar cells is crucial to achieving the highest efficiencies. The challenges highlighted in this section require the continued development of multiphysics approaches in order to accurately and efficiently evaluate device performance.

5.6. Advances Required

Luminescence will play a key role both as an analytical tool and as a design parameter for high-efficiency solar cells. The following aspects will be crucial for improving devices efficiencies:

***In situ* measurements:** Luminescence will be used as an analytical tool both for fully completed devices and for manufacturing processes through real-time monitoring of *in situ* device deposition. This allows for fast and low-cost measurements that provide direct information on how well the device is functioning, allowing for challenges that develop during the deposition process to be investigated and overcome.

Radiative efficiency: Future designs of high-performance solar cells will need to incorporate strategies to increase the radiative efficiency. This will primarily bring the open circuit voltages and, hence, the efficiency closer to the theoretical limit.

Luminescent coupling: For multijunction devices, luminescent coupling will be included in the design process, thereby allowing multijunction devices with monolithic connections to obtain higher efficiencies and to operate over a wider range of illumination conditions.

Modeling internal emission: For luminescence to be included in the design process, improved optical and electronic models are required. These models need to include a range of factors including the statistically incoherent light sources, full wave propagation, nanostructuring, and multiphysics. The Green dyad presented in this section provides an approach combining many of these components, with the development of further models needed to incorporate other specific factors, e.g., nanostructuring.

Figure 15

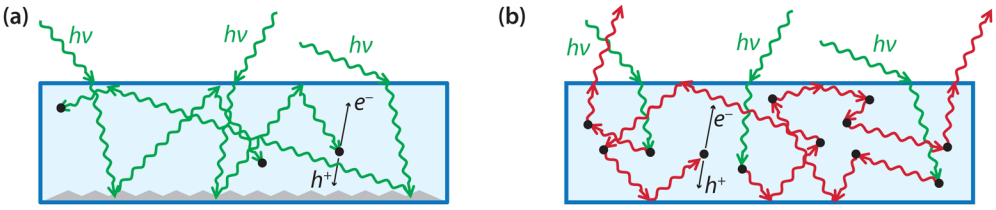

(a) Photon gas formed by weakly absorbed solar photons (in green), reflected from the random scattering rear surface. The internal brightness is $4n^2$ larger than the incoming sunlight. (b) Other internal photon gas (in red) formed by luminescent IR photons. © 2012 IEEE. Adapted, with permission, from Miller *et al.*, IEEE J. Photovoltaics **2**, 303–311 (2012) [158].

6. LUMINESCENCE II: THERE ARE TWO DISTINCT PHOTON GASES PRESENT INSIDE EVERY SOLAR CELL

E. Yablonovitch and Z. Omair

6.1. Introduction

It has gradually been recognized that incoming sunlight can be trapped within a high-refractive-index semiconductor, $n \approx 3.5$, owing to the narrow 16° escape cone. The solar light inside a semiconductor is $4n^2$ times brighter than incident sunlight [34]. This is called light trapping and has increased the theoretical and practical efficiency of solar panels. However, there is a second photon gas of equal importance that has been overlooked. Inside every forward-biased solar cell, there is a gas of infrared (IR) luminescence photons, also trapped by total internal reflection. We introduce the idea of *super-equilibrium*, when the luminescence photon gas freely exchanges energy with the two quasi-Fermi levels.

Nonetheless, the loss of a single photon from either gas is equivalent to the loss of a precious minority carrier. Therefore, optical modeling and design become equally important as electron–hole modeling in high-efficiency solar cells. It becomes possible to approach the idealistic Shockley–Queisser limit [22], by proper material selection and design of the solar cell optics.

Inside a solar cell, the incoming solar photons tend to be trapped by total internal reflection. As illustrated in Fig. 15(a), weakly absorbed rays of sunlight experience multiple internal reflections, forming a photon gas with $4n^2$ absorption enhancement [34], increasing both current and voltage. At the same time, there is second photon gas, illustrated in Fig. 15(b), inside every solar cell. The presence of a nonzero voltage is accompanied by an IR luminescence photon gas, significantly brighter than Planck' blackbody radiation.

These two photon gases are very important for solar cell operation. If a single photon is lost from either photon gas, it is equivalent to the loss of a precious minority carrier. Thus, the photon gases need to be included in solar cell modeling, and must be treated on an equal footing with the electron gas, and with the hole gas, that are also present in every solar cell.

6.2. Generalized Planck Theorem

In thermodynamic equilibrium, there is only one Fermi level (or chemical potential μ) for electrons in a system. Semiconductors are unusual in that they separately sustain both an electron gas and a hole gas. In the best materials, the electrons and holes recombine rarely compared with their individual momentum relaxation rates, and

they barely interact. The electrons and holes fail to mutually equilibrate, and they have separate Fermi levels. Since they are out of global equilibrium, the separate Fermi Levels are called quasi-Fermi levels, E_{Fn} and E_{Fp} respectively, where $E_{Fn} - E_{Fp} = \mu = qV$ with the elementary charge q and the voltage V. The quasi-Fermi-level separation $\mu = qV$ represents the internal free energy buildup by sunlight.

In a solar cell there is a further type of equilibrium: the internal luminescent photon gas exchanges energy with the electrons and holes, and can establish a form of equilibrium that includes photons, electrons, and holes. We suggest the name *super-equilibrium* when the IR photon gas exchanges energy between the two quasi-Fermi levels. The photon gas brightness, $\mathcal{B}$, then deviates from the Planck blackbody formula,

$$\mathcal{B}(\nu, \mu, T) = \frac{8\pi n^2 \nu^2}{c^2} \frac{1}{\exp\left(\frac{h\nu - \mu}{kT}\right) - 1}, \tag{3}$$

where the brightness $\mathcal{B}$ is the photon number per area, per unit bandwidth, per unit time, and per 4π steradians; n is the refractive index, ν is the photon frequency, T is the temperature, and kT is the ambient thermal energy. This is sometimes called the "generalized Planck formula." It was first derived by Ross [157], and further elaborated on by Henry [190], and in Ref. [191]. If there is no excess carrier concentration, and only a single quasi-Fermi level, there is global equilibrium, $\mu = qV = 0$, and the ordinary Planck formula would apply. However, if $\mu \neq 0$, then the "super-equilibrium" would apply, as represented by the "generalized Planck formula," Eq. (3).

It is odd that a photon spectral distribution, Eq. (3), would contain a chemical potential, μ. Since the photon number is not conserved (photons can be freely created and destroyed), it is usually understood that the creation of photons costs zero free energy, $\mu = 0$. However, that only applies to perfect thermal equilibrium. In our case, the photons are closely coupled with, and exchange energy with, the carriers of an excited semiconductor. The photon distribution, Eq. (3), then contains the chemical potential of the semiconductor carriers, the quasi-Fermi-level separation.

The quasi-Fermi-level separation can be regarded as causing the luminescent IR photon gas. In "super-equilibrium," this IR gas brightness $\mathcal{B}$, can be reinterpreted as measuring the voltage V in the photovoltaics (PV) cell,

$$qV = \mu = E_g - kT \ln\left(\frac{8\pi n^2 \nu^2}{\mathcal{B}(\nu, \mu, T)c^2} + 1\right). \tag{4}$$

In human experience, we rarely confront light at or near thermal equilibrium. In virtually all human experience, light is much brighter than the thermal equilibrium intensity, except perhaps on a very dark starless night. To the extent that there is sufficient ambient light, Eq. (4) can assign a chemical potential $\mu>0$ to the light brightness we deal with in our daily lives. It is perfectly reasonable to ask on a sunny day: "What is today's chemical potential as given by Eq. (4)?" It would be like a weather report, and combined with ambient temperature, would provide an upper physical limit for that day's PV cell voltage.

Luminescent IR photons are not lost to PV. Owing to light trapping, only the small fraction $1/4n^2 \approx 2\%$ of the internal IR luminescence escapes. A total of 98% of the IR luminescence is trapped upon each front surface reflection and is subject to reabsorption. Therefore, modeling of solar cell performance must include a full optical analysis, on an equal footing with the analysis of minority carrier transport. Indeed, in a good solar cell, the minority carrier properties are usually close to ideal, and the performance is completely determined by the PV optics [158]. This is certainly true

for the current flat-plate record solar cell [15], which surpassed the previous record by further improving rear-surface reflectivity.

The remaining 2% of internal IR luminescence photons, lost to escape from the front surface, are not really lost. The front surface of a solar cell must be open to allow the entry of sunlight. At open-circuit conditions no current is drawn. According to the detailed balance limit [22], those incoming solar photons are replaced by outgoing luminescent photons, from the internal photon gas that is $4n^2$ times brighter than the incident sunlight. Thus, the 2% photon escape is a necessity, not a loss mechanism. This also led to the slogan: "A great solar cell also needs to be a great light emitting diode" [158].

In some forms of PV cell modeling, it is necessary to know the B-coefficient, where Bnp is the rate of spontaneous emission from electron-hole recombination. However, the spontaneous emission coefficient can be bypassed by using detailed balance [181] to compute the spontaneous emission; where luminescent emission $L(\nu,\mu,T)=\alpha(\nu,\mu,T)\times\mathcal{B}(\nu,\mu,T)$ is exactly balanced by optical absorption of the internal luminescence photons. Then spontaneous luminescence is

$$L(\nu,\mu,T)=\frac{8\pi n^2\nu^2}{c^2}\frac{\alpha(\nu,\mu,T)}{\exp\left(\frac{h\nu-\mu}{kT}\right)-1}. \tag{5}$$

When the material is only moderately excited, $\mu \ll \nu h$, the absorption spectrum is unchanged from that of unexcited material, replacing $\alpha(\nu,\mu,T)$ with $\alpha(\nu,0,T)$. Thus, the spontaneous emission can be known without a knowledge of either the B-coefficient, nor the intrinsic carrier density, n_i, in the semiconductor. Indeed only the conventional absorption coefficient $\alpha(\nu,0,T)$ is needed, and Eqs. (3)–(5) in this section apply equally well to dye molecules as to semiconductors. A dye molecule can have an internal chemical potential determined by the excess probability p_{ex} of being in the excited state, relative to p_0 the usual Boltzmann probability, $\mu = kT\ln(p_{\text{ex}}/p_0)$.

6.3. Ergodic Light Trapping

Light trapping inside the solar cell improves the voltage, current, and fill factor. However, it was not exploited in the first 40 years of the PV industry. One reason is that the first generations of PV cells consisted of a plane-parallel slab. In semiconductors, the refractive index is high, $n \approx 3.5$ in silicon. By Snell's law, the refraction inside the slab would always be within an angle $\arcsin(1/3.5) \approx 16°$, a cone adjacent to normal. As shown in Fig. 16(a), the simple geometry of a plane-parallel slab fails to scatter light rays in directions outside this narrow cone which only accounts for $(1/4n^2) \approx 2\%$ of 4π steradians. The other 98% of angles remain inaccessible. This problem is solved by simply leaving the rear surface of silicon rough, as saw-cut, to break the plane-parallel slab symmetry. The light propagation becomes ergodic as discussed in Fig. 16(b), and shown in Fig. 15(a). Scattering the internal light by >16°, which would require an 8° rear facet, is usually sufficient. Although Lambertian rear light scattering is sufficient for $4n^2$ ergodic light trapping, it is not necessary. Any deviation from perfect symmetry by more than 8°generally converts a nonergodic geometric shape into an ergodic light trapping shape, providing a voltage and current boost.

Light trapping was not generally adopted by the PV industry until the late 1990s, but it was already thoroughly exploited in Martin Green's passivated emitter and rear cell (PERC) [6] a decade earlier. The benefit is to increase the internal optical brightness by $4n^2$, and the optical free energy by $kT\ln(4n^2)$, and the PV output voltage by $(kT/q)\ln(4n^2)$.

Figure 16

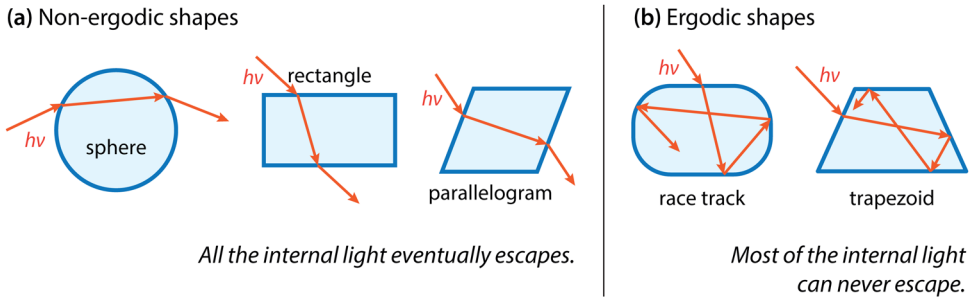

(a) Nonergodic: the term ergodic refers to the time-averaged trajectory of a light ray being the same as the phase-space average. The simple geometric shapes, sphere, rectangle, and parallelogram fail this test. A light ray that enters such a shape but rapidly escapes, and fails to fill all possible internal angles. (b) Ergodic: in the case of odd shapes, the trapezoid or the race track, light rays scatter at unusual angles, filling the full internal angle space. The light intensity builds up increasing brightness by $4n^2$, and free energy by $kT\ln(4n^2)$, and the PV output voltage by $(kT/q)\ln(4n^2)$. Almost all but the simplest geometric shapes are ergodic.

In their analysis of fundamental solar cell efficiency, Shockley and Queisser idealized the optical situation [22]. Optical absorption jumped from zero to infinity at the band edge. The material itself had 100% luminescence efficiency, and the luminescence was immediately reabsorbed with no losses. There was no need for a distinction between internally trapped light and external luminescence. All of the solar cell optical physics were effectively idealized away, and there was no need to talk about the two internal photon gases.

Shockley and Queisser achieved their goal of placing an upper limit on solar efficiency. The purpose of this section is to consider the parasitic optical effects, and to show that these deleterious effects can be largely overcome by proper optical management and design. By maximizing the optical reflectivity in the context of ergodic optics, and selecting materials with very high internal luminescence yield, we can approach the idealized Shockley and Queisser performance.

6.4. Nonideal Solar Cells

We now consider a series of nonideal solar cells, shown in Figs. 17(b)–17(d). However, Fig. 17(a) is an exception: there, we have done the best possible job with the optics. There is a high reflectivity mirror, so that none of the photons are lost. Ergodicity is provided in two ways: by the textured rear reflector and by the reabsorption and random angle reemission of the IR luminescence. The spectral shape of optical absorption and reemission can be taken into account using the Shockley–Van Roosbroeck [181] principle. The result for GaAs is 33.5% efficiency [158] for standard air mass 1.5 illumination [192], similar to the Shockley and Queisser result, but without the idealistic assumptions. In GaAs, a direct bandgap semiconductor, we benefit from the very low Auger recombination relative to internal luminescence.

The nonidealities in GaAs solar cells prior to 2011 are represented by several cases in Fig. 17. In Fig. 17(b), the material is of top epitaxial quality, but the film rests on the original growth substrates. The substrate is thick, relatively impure, and has no proper rear mirror. The optical quality is assumed poor. The substrate is essentially a sink for band edge luminescence. This immediately wastes 98% of the luminescent photons, like losing 98% of the minority carriers at open circuit. The main effect is to lose $\approx (kT/q)\ln(4n^2)$ in open-circuit voltage, V_{oc}. Eliminating this problem by

Figure 17

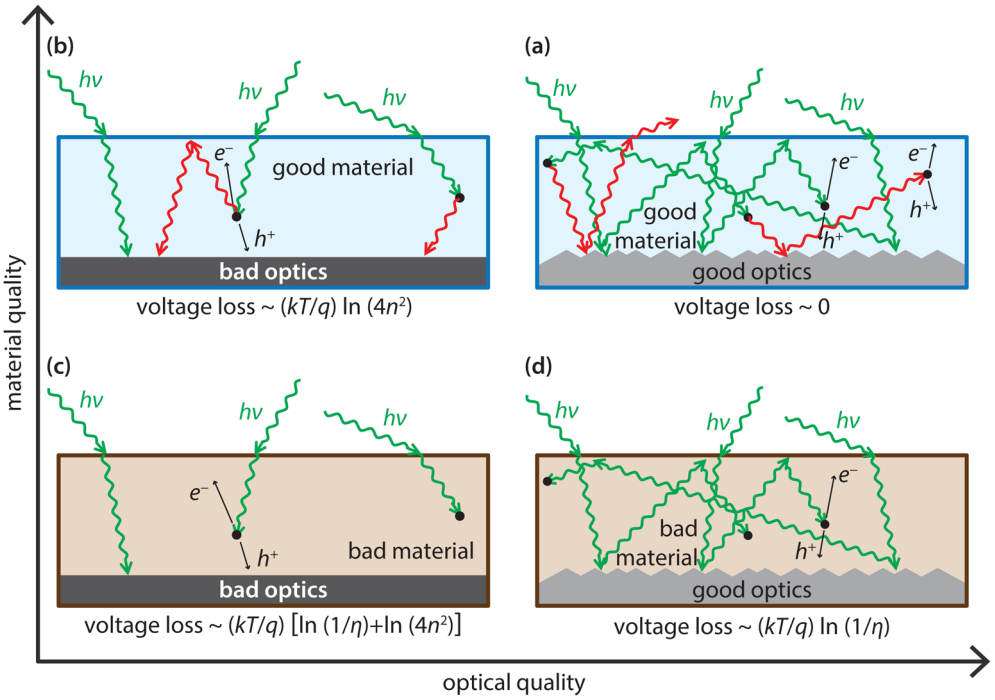

Comparison of the effect of light-trapping optics on the operating point voltage penalty ΔV_{op} from poor internal luminescence efficiency, η, and/or poor optical design. Case (a) is the ideal case of a perfect scattering rear mirror for ergodicity, combined with the record-breaking internal luminescence efficiency of epitaxial thin GaAs film separated from their growth substrates by epitaxial liftoff. Case (b) represents epitaxial GaAs solar cells before 2011, which were still attached to the original GaAs growth substrates that were so thick as to effectively absorb band edge luminescence. Case (c) is a modern Si solar with good light management, but the material is labeled bad since the indirect gap prevents high (>90%) internal luminescence efficiency. Case (d) represents the older generation of silicon solar cells, (pre-1990), still indirect, but also with no implementation of light trapping.

epitaxial liftoff was the reason for all the new solar cell efficiency records in the 2010s.

Consider the opposite nonideality in Fig. 17(c). The optics are good as in modern c-Si solar cells, but the material is handicapped by being indirect. Although Si is indirect, it still luminesces, and can be an light-emitting diode (LED) [193]. Nonetheless, Si is not efficient enough to build up a high brightness of luminescent photons, which requires an internal luminescence efficiency >90% owing to the multiple absorption/reemission events. The loss of luminescent photons reduces luminescent brightness and by Eq. (3.4) leads to a corresponding drop in open-circuit voltage V_{oc} by $\approx (kT/q)\ln(1/\eta)$, where η is the internal luminescence yield in the material.

However, there is ample motivation for good optical design, in Fig. 17(c), despite Si being an indirect semiconductor. Good optical design increases the effective optical absorption coefficient by about $4n^2 \approx 50$, and allows the silicon to be thinner by the same factor. The photocarriers from the Sun are effectively compressed into a thinner layer, and reside at a higher density by $\approx 4n^2$ times. The higher density corresponds to less entropy and more voltage. The designer who uses good optics to make their

Si solar cell thinner would then gain $\approx (kT/q)\ln(4n^2)$ in V_{oc}. However, good optical design is already assumed in both Figs. 17(a) and 17(c).

Such good optical design is one of the reasons that Si solar cells are far exceeding the theoretical limits that were projected in the 1970s [194,195]. The other reason is that higher-performing cells require good material quality. But good material quality also includes low recombination on the surfaces and interfaces. If the surfaces and interfaces dominated the electron–hole recombination, there would be no benefit in making the solar cell thinner. This was first achieved by Swanson [196,197] using point contact openings on oxidized Si, effectively creating the first double heterostructure [198,199] on silicon. The oxide coating was particularly compatible with good optical mirror reflectivity.

The remaining case is shown in Fig. 17(d), corresponding to the old-fashioned silicon solar cells before light trapping and Si heterojunctions became standard. In those days, the rear reflectivity was rather poor, i.e., bad optics, and the material being indirect was yet a second penalty. The material had to be thick enough to absorb the solar photons, with no help from light trapping.

A thicker solar cell means a lower minority carrier concentration, since the same injected carriers occupy a larger volume. Thus, the open-circuit voltage is penalized by $\approx (kT/q)\left[\ln(1/\eta) + \ln(4n^2)\right]$, once for the poor luminescence efficiency, and again for poor optical absorption, necessitating greater thickness.

6.5. Conclusions and Advances Required

For the reasons given in this section, the PV industry employs solar light-trapping in almost all cases. However, there is now a second mechanism with the recognition of the internal IR luminescent photon gas that can build up to a high brightness, many Suns, inside direct bandgap materials. If this IR luminescent photon gas is properly conserved, absorbed, reemitted, and reflected, then the Shockley–Queisser limit can be approached even under a realistic practical optical design.

In lower-performing solar cells, the luminescent photon gas is very weak, hardly drawing any current away. Nonetheless this second photon gas is present, inextricably linked to voltage by Eq. (4), and that voltage is boosted by $\approx (kT/q)\ln(4n^2)$ using sound optical management.

We now know how to approach the Shockley–Queisser limit, but it does require material with a high internal luminescence yield, such as GaAs or perovskites. As we have argued in this section, these solar cells need good light management to utilize the full luminescent potential.

7. LIGHT MANAGEMENT FOR MULTIJUNCTION SOLAR CELLS

C. Becker, B. Ehrler, H. Helmers, O. Höhn, K. Jäger, and M. Schmid

The photovoltaics (PV) module right now accounts for only one third of the total costs of a PV system, as the fixed cost essentially scales with the installed module area (see Ref. [4] and Section 2). Therefore, the increase in solar cell efficiency is the most-effective parameter for the further reduction of the levelized cost of electricicty (LCOE) (see Section 2). Silicon PV technology is already so far developed that it reaches efficiencies close to its physical limit. Multijunction solar cells are regarded as the most promising concept to surpass this limit.

In this section, we briefly introduce the general multijunction solar cell concept (Section 7.1) and provide a brief overview of recent multijunction solar cell technologies based on III–V semiconductors, silicon, CIGS, and perovskites, identifying the specific scientific and technological questions (Section 7.2). In the end, we discuss the specific optical challenges occurring in such devices (Section 7.3).

7.1. Multijunction Solar Cell Concept

Figure 18(a) illustrates the spectral irradiance of the Sun under standard testing conditions (AM1.5G, gray area) and an upper limit estimation of the usable energy by a solar cell based on a semiconductor with electronic bandgap $E_g = hc/\lambda_g$ considering the detailed balance limit [22]. Here h, c, and λ denote Planck's constant, vacuum speed, and wavelength of light, respectively. The sketch next to Fig. 18(a) visualizes that photons with energies below the bandgap cannot be absorbed at all, whereas higher-energy photons lose a part of their energy due to thermalization to the band edges. As an example, the red area marks the exploited irradiance of a solar cell with $E_g = 1.1$ eV. In addition to the aforementioned nonabsorption and thermalization losses also extraction losses according to the detailed balance limit are considered. When a second solar cell, here with $E_g = 1.7$ eV, is added on top of this bottom cell, thermalization losses are reduced and higher-energy photons are converted more efficiently (blue area).

The electrical connection of the subcells in a multijunction device is an essential point to consider. Figures 18(b) and 18(c) represent example configurations of four- and two-terminal (4T and 2T) tandem devices. In the simplest approach, the top and bottom cells are electrically independent [i.e., four connections in total: 4T; Fig. 18(b)], and are only optically, possibly mechanically, stacked. The main benefits are the opportunity to manufacture top and bottom cell separately, which is particularly interesting when high-temperature processes in combination with temperature-sensitive layers are involved, as well as the independent operation of the two cells in their respective maximum power points. Neither concerns about junction directions are needed, nor is the effect of changing performance with varying irradiation conditions relevant. Yet, parasitic losses will be high since the full number and thicknesses of contacts are required for lateral charge carrier extraction in the top cell, whereas the lower current in the bottom cells relaxes slightly the conductivity requirements to the contacts.

In 2T tandems, the top and bottom cell are, mostly monolithically, connected in series [Fig. 18(c)]. The orientation of the two cells' junctions has to be aligned. The current will directly pass from one to the other cell, e.g., via a recombination junction. Thus, the intermediate layers and with them parasitic optical absorption are minimized, allowing for maximum light exploitation. In return, the current between top and bottom cell needs to be matched because the lower current of the two will dictate the device performance. The current matching in 2T configuration is a key aspect of the optical design of multijunction solar cells next to minimizing parasitic absorption.

Figure 18

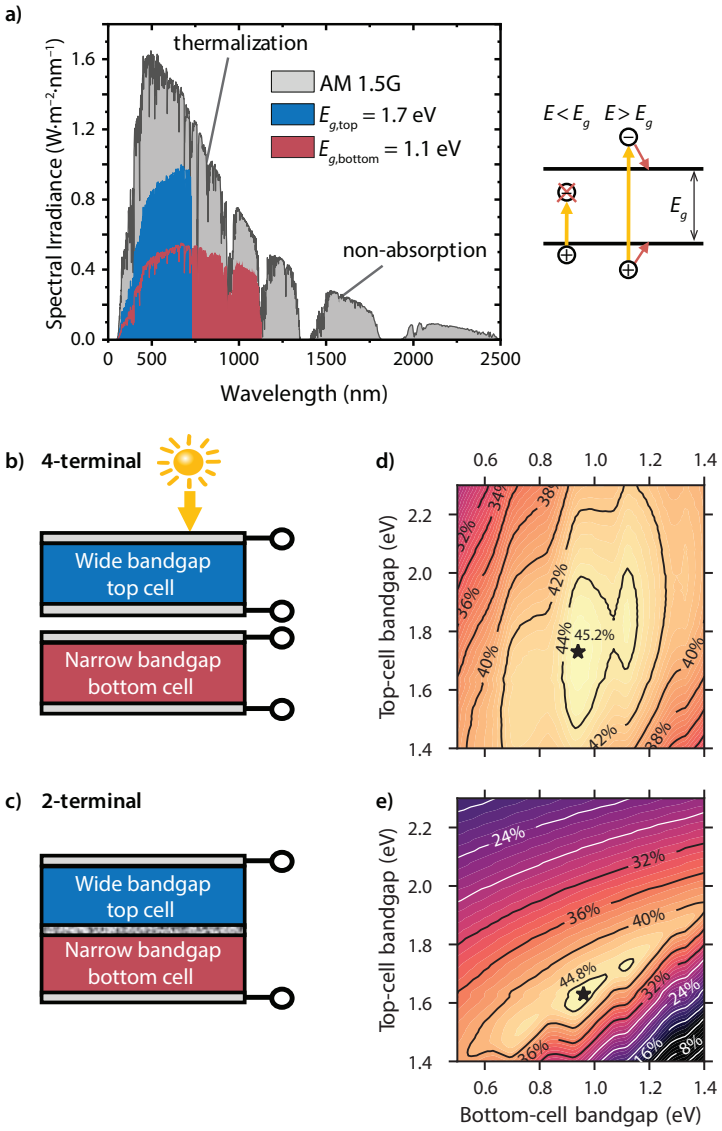

Multijunction solar cell concept. (a) Exploitation of the solar irradiation (AM1.5G spectrum in gray) by a multijunction solar cell composed of two subcells with bandgaps E_g = 1.1 eV (red) and E_g = 1.7 eV (blue) considering extraction losses according to the detailed balance limit. Sketch on the right: unabsorbed photons with energy lower than the bandgap and thermalization losses of higher energetic photons. (b) and (c) Tandem configurations with four terminals (4T) and two terminals (2T), respectively. (d) and (e) Theoretical efficiency limits for tandem solar cells as functions of the top and bottom cell bandgap energies in 4T and 2T configuration, respectively. (d) and (e) Jäger and Albrecht, *Hybrid Perovskite Solar Cells*, Chapter 17, 463–508 (2021) [200]. Copyright Wiley-VCH Verlag GmbH & Co. KGaA. Reproduced with permission.

Figures 18(d) and 18(e) show the theoretical efficiency limits for tandem solar cells as functions of the top and bottom cell bandgap energies for 4T cells and for 2T cells, respectively. In this theoretical efficiency limit calculation, we consider the detailed balance approach for single-junction solar cells [22]. For 4T cells the efficiencies of the two subcells can be treated nearly independently. That means only the bandgap of the top cell affects the short-circuit current density of the bottom cell. In contrast, for 2T cells the two subcells are electrically connected and the same current density flows

through both subcells. Due to this current-matching constraint for the 2T configuration, the power conversion efficiency (PCE) depends much more on the subcell bandgaps than for the 4T configuration. Details on the calculation can be found in Refs. [200,201]. 2T tandem solar cells can act as a direct replacement for single-junction solar cells, however, the implementation of 4T devices is more challenging, requiring, e.g., more cabling and more complex module design.

7.2. State-of-the-Art Multijunction Solar Cell Technologies

Here we give a brief overview of the four classes of semiconductor materials, which are currently leading to the highest power conversion efficiencies in multijunction solar cells. We describe selected state-of-the-art multijunction devices, which are currently discussed in the PV community. Figure 19 summarizes the highest power conversion efficiencies as of October 2024 of (a) single-junction and (b) 2T multijunction solar cells as a function of bandgap (a) and bottom cell bandgap (b), respectively.

7.2a. Absorber Materials for Multijunction Solar Cells

Crystalline silicon is the most widely used material in PV for good reason. It is nontoxic, earth-abundant, and stable. Further, silicon is well-known due to its long history in research and development in semiconductor chip industry and PV. In comparison with the other solar cell materials described previously, it has one special feature: it is an *indirect*-bandgap semiconductor, that means to excite charge carriers from valence to conduction band (E_g = 1.12 eV) they must not only change energy but also momentum. For the optical properties of silicon, this has far-reaching consequences. The absorption coefficient is comparatively low with around 10^3 cm^{-1} for a wavelength of 800 nm. Even if considering perfect Lambertian light trapping (see Section 3), absorbers with several tens of micrometer thickness are required to ensure >95% absorption of sunlight with $E>E_g$. Further, radiative recombination and all effects associated with it, such as luminescent coupling and photon recycling, can be neglected. Auger recombination and Shockley-Read-Hall (SRH) recombination will dictate the achievable open-circuit voltage. The detailed balance efficiency limit of silicon single-junction solar cells considering Auger recombination has been calculated to 29.43% [203] and 29.56% [204] without and with exact calculation of an ideal Lambertian light trapping scheme, respectively.

Most **III–V compound semiconductor materials**, such as gallium arsenide (GaAs) and indium phosphide (InP), are direct semiconductors. With an efficiency of 29.1% for a single-junction GaAs solar cell [15], III–V semiconductors have demonstrated the overall highest efficiency among single-junction solar cells [Fig. 19(a)]. Due to their direct bandgap nature, they have much stronger absorption than silicon. Typically, only a few micrometers are sufficient to absorb the targeted sunlight.

Due to their high radiative efficiency, photon recycling [158,205–207] and in multijunction solar cells also luminescent coupling [207] are relevant (see Section 7.3). This high radiative efficiency in combination with excellent rear side reflectors enabled efficiencies close to the thermodynamic detailed balance limit. It should be noted that luminescent coupling is also of particular relevance for multijunction solar cell measurements, especially of external quantum efficiencies (EQEs). If the devices are highly radiative even at low irradiances, the determination of absolute EQEs becomes challenging [43]. Measured EQE can have an artifact caused by luminescence coupling that is similar to an artifact caused by low parallel resistance [208]. A key advantage of III–V semiconductors extends beyond the highest radiative efficiency and is the tunability of the bandgap. Adjusting the composition of ternary, e.g., AlGaAs and InGaP, and quaternary compounds, such as GaInAsP, allows for tuning the bandgap of III–V semiconductor from 0.7 to 2 eV by changing the composition. To decrease

Figure 19

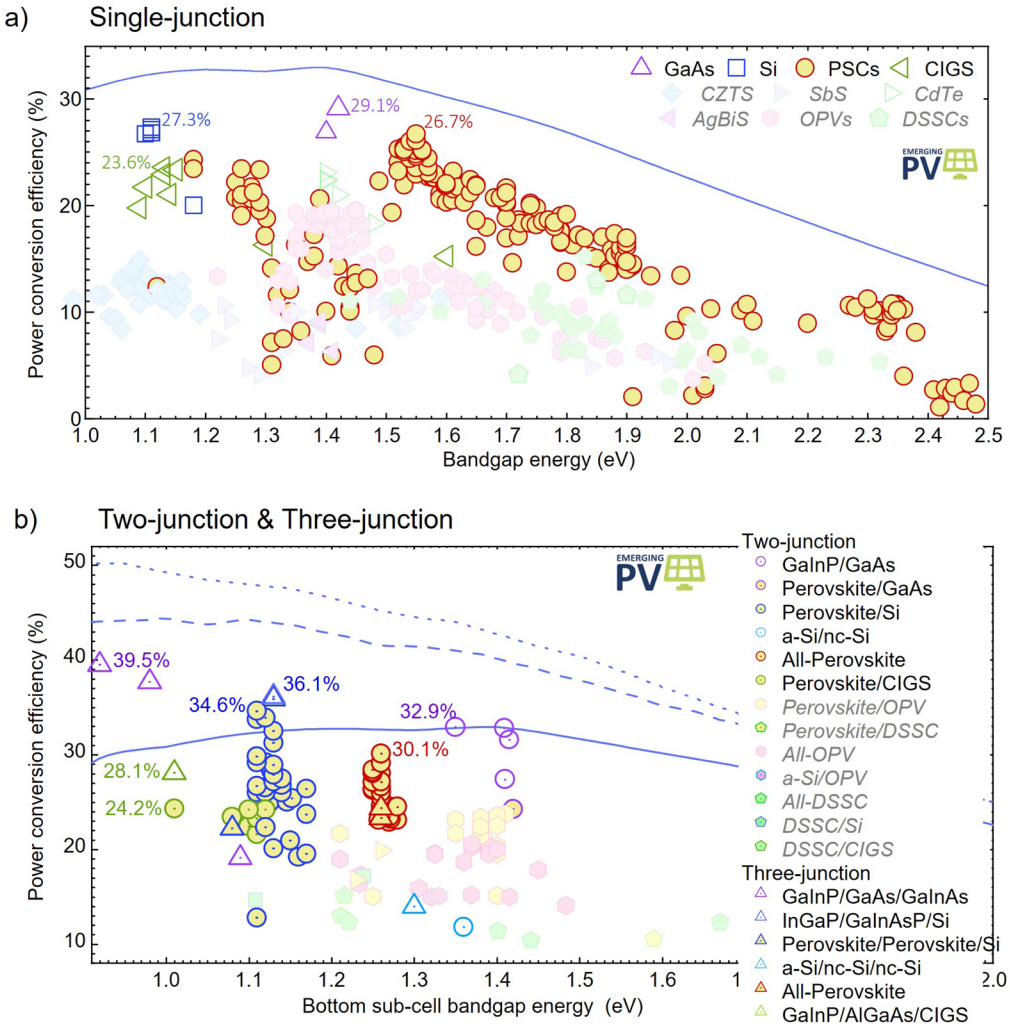

Power conversion efficiencies for (a) single-junction and (b) 2T multijunction PV research cells, including up to three junctions as a function of the absorber bandgap energy of the single-junction cell (a) or the bottom subcell of the multijunction device (b), respectively, for various PV materials as of October 2024. Materials that are not explicitly considered in this section are shaded. The solid, dashed, and dotted lines in the efficiency graph indicate the single-junction, the top-subcell-optimized and top- and middle-subcell-optimized detailed balance efficiency limits for single-junction, double-junction, and triple-junction PV cells, respectively. Adapted from [202] under a Creative Commons license. Data courtesy of the emerging-pv.org database.

material consumption and cost, ultrathin solar cells utilizing multiresonant photonic structures have receive considerable attention [209–211]. Remarkable efficiencies of 19.9% have been achieved using only 205 nm of active III–V absorber material [212].

Chalcopyrite materials Cu(In,Ga)(S,Se)$_2$ (CIGSSe) are characterized by a direct bandgap and a related absorption coefficient around 10^5 cm^{-1}. Compared with crystalline silicon, they can hence be fabricated as thinner films of approximately 2 μm thickness while maintaining complete absorption of photons above the bandgap and simultaneously enabling flexible, lightweight, and semitransparent applications with tunable thickness. The challenge of containing rare indium and gallium may be tackled

by ultrathin absorbers joint with light management strategies that are indispensable for efficient multijunction devices [213]. One major benefit of the CIGSSe material system is the tunability of the bandgap, ranging from 1.04 eV for pure CISe over 1.45 eV for CIS and 1.68 eV for CGSe up to 2.38 eV for CGS [214]. CIGSSe may hence be used for any absorber of the multijunction device and all-chalcopyrite devices appear feasible. It has to be noted that for CIGS materials, the increase in bandgap above 1.4 eV is a remaining challenge as the V_{oc} deficit significantly increases when the gallium to gallium plus indium ratio surpasses 0.3 [215]. The reasons are amongst others deep defects, grain boundaries, interfacial recombination, and microdomains [216]. In addition, CIGSSe stands out due to its high radiative recombination and high stability making it suitable even for space applications [217].

Metal halide perovskites, characterized by the ABX_3 structure, are particularly suited for multijunction solar cells because of their wide-bandgap tunability and excellent optoelectronic properties for many of these bandgaps. The A-site cation can be a small organic molecule or Cs, the B-site metal is typically lead or tin, and the X-site anion is typically a halide, often a mixture of bromide and iodide. Much of the research has been focused on bandgaps that are suitable for tandem combination with crystalline silicon (1.5–1.6 eV), and those solar cells perform close to the detailed balance limit (see Fig. 19) [202]. These perovskites typically contain a large fraction of iodide, and their remarkable performance is a result of the so-called defect tolerance, originating in the fortunate incidence that the valence band contains a large fraction of antibonding orbitals [218]. As a result, materials made with simple procedures show remarkably high photoluminescence quantum yield (PLQY) [219]. The high PLQY and small Stokes shift has led to interesting light-management questions, for example the luminescent coupling between various subcells [169], the effect of photon recycling [161], and self-absorption [220]. The research field is increasingly focusing on improving the efficiency of the narrow- and wide-bandgap compositions. These are necessary for all-perovskite multijunction solar cells, but there is a gap between the performance of perovskite solar cells with these bandgaps and the detailed balance limit (see Fig. 19). For the narrow-bandgap solar cells, the tin-based compositions show a reduced photocurrent, related to the deficiency in charge transport. Conversely, the wide-bandgap compositions suffer from a voltage loss that is partially related to the tendency for the (bromide-rich) compositions to phase segregate [221] and partially to the lack of suitable transport layers [222]. While the performance of perovskite semiconductors remains remarkable, the long-term stability does not match other solar-cell materials. Extrinsic factors such as sensitivity against water and oxygen can be managed by proper encapsulation [223], intrinsic factors such as ion migration [224] and the phase segregation [221] might pose a more fundamental challenge, whereas issues with reverse bias instability pertain to tandem applications [225].

7.2b. Selected Multijunction Solar Cell Technologies

Here we give a brief overview about selected multijunction solar cell technologies that are currently widely discussed in the PV community [see Fig. 7.2(b)] and where we believe that they shall play an important role in future PV energy conversion.

III–V/Silicon multijunction solar cells are suited for both 2T and 4T operation. Champion efficiencies of 2T III–V-on-silicon devices (record 36.1% [43]) are currently higher than their 4T counterparts [226]. While the optical interface between the two stacked cells of 4T tandems requires careful investigation, 4T tandems promise to be less sensitive for spectral variation outdoors and, thus, show an increased energy yield (EY) in the field. However, it has been shown that this difference can be small

if the 2T devices are well designed [227,228]. In the last years, the focus was on GaInP/GaAs/Si triple-junction solar cells as they show the highest efficiency potential, but two-junction devices with an AlGaAs-based top solar cell [229] are of interest because of their potential for lower epitaxy cost. The currently best 2T GaInP/GaAs/Si are realized utilizing a direct wafer bond. To this end the top solar cell is usually grown inverted on a growth substrate, i.e., GaAs or Ge wafers, and then wafer-bonded to a polished silicon bottom solar cell [42]. Afterwards, the growth substrate can be lifted and potentially be reused, and the cell structure can be processed into a solar cell. Whether this approach can lead to an economically attractive solution remains to be shown, but the method clearly proves the efficiency potential of the concept. Another option is to use the silicon bottom cell itself as the growth substrate [230].

One option is to use transparent conductive adhesives [231,232] to bond a III–V cell onto the silicon bottom cell. In this case, a challenge lies in the optics at the interface. The adhesive usually has a low refractive index leading to two counterbalancing effects: reflection losses of the incident light, but also strong internal reflection of radiatively emitted light supporting photon recycling and thus increasing device voltage.

Last, effective light trapping is especially important for the silicon bottom cell. Several different structures have been tried here. The mature random pyramids at the front side cannot easily be used, as for all three sketched routes flat surfaces are required. Thus, light trapping needs to be implemented at the rear side. Here wet chemically etched structures such as random pyramids or the acidic texture as used formerly for multicrystalline silicon are one candidate. Another option is a metallic photonic grating that scatters light into defined modes [233]. This approach is especially interesting if a planar rear side of the silicon bottom cell is desired, e.g., when using the TOPCon silicon technology.

All-III–V multijunction solar cells are a very mature technology delivering highest efficiencies so far. Due to the relatively high costs they are used mainly in space applications, but are also being considered for vehicle-integrated PV applications, drones, and high-altitude pseudo-satellites (HAPS) [234]. It can be beneficial to grow III–V subcells on a Ge substrate, which then also yields an active Ge bottom subcell by using a diffused emitter. One standard product has been a triple-junction GaInP/Ga(In)As/Ge solar cell on Ge substrate, however, also approaches with more stacked junctions are available for space.

A distributed Bragg reflector below the Ga(In)As helps to reduce the subcell thickness, mitigating degradation in space and enhancing end-of-life performance, crucial for space solar cell efficiency [235]. Alternatively, inverted grown metamorphic cells on metal foil allow direct rear-side processing and mirror implementation, improving performance [236] but adding fabrication complexity and cost [237].

III–V multijunctions also have terrestrial applications, where high efficiencies or superior power-to-mass ratios are required. Here, a GaInP/GaAs tandem cell, also often grown inverted, with rear side mirror is an interesting option [238]. Also in these devices, the mirror enhances the absorption in the bottom cell, but even more importantly it severely improves photon recycling and, thus, increases the voltage of the device. The currently best device of this approach has an efficiency as high as 32.8% [15] under the AM1.5G spectrum. A triple-junction solar cell even allows for 37.9% efficiency [15,239], or even 39.5%, where the middle cell bandgap was modified using thick GaInAs/GaAsP strain-balanced quantum well (QW) solar cells [15,240]. This is the overall highest efficiency under one Sun.

Although those multijunction devices for one Sun on Earth are still a niche, four- to six-junction solar cells are state of the art in concentrated photovoltaics (CPV)

(see Section 3). The highest efficiency, 47.6%, was achieved with a wafer-bonded four-junction solar cell under 665-fold concentrated sunlight (AM1.5D spectrum) [18]. A six-junction solar cell reached 47.1% efficiency under 143-fold concentrated sunlight [241]. Although these cells are lab cells, industrial five-junction solar cells on germanium are available for CPV. Lab records are often optimized for 25°C, but CPV operating temperatures are around 60–90°C. Here, the bandgaps can be tailored in a way to ensure that the subcell absorptances do not shift into the absorption lines of the solar spectrum avoiding current mismatch [242].

Perovskite/silicon tandem solar cells are currently attracting a great deal of attention worldwide. They present an excellent extension to the well-established silicon technology for large-scale applications, meanwhile demonstrating power conversion efficiencies of more than 34% [243,244], clearly exceeding the efficiencies, which are demonstrated, and theoretically possible, in silicon-only devices. Regarding optical optimization, many research and development efforts concentrate on the compatibility of perovskite top cell growth on silicon bottom cells with industrial standard micrometer-sized pyramidal surface textures (see Section 3). Such textures are necessary for optimum light in-coupling and light absorption. A combination of perovskite solution processing, so far leading to the highest perovskite single-junction efficiencies, with these large pyramidal silicon textures is not easily possible. Here, the silicon front surface textures have to be adapted by decreasing their size below the perovskite layer thickness, using nanopyramids [245–248], tailored nanophotonic structures [249], or adapted black silicon [250]. Alternatively, the perovskite deposition method is adapted, for example by using the so-called hybrid approach, where the perovskite top cell is conformally grown on the pyramidal textures by evaporation and subsequent infiltration with solution [251], or by evaporation only [252].

Multijunction-specific optical topics (see Fig. 20) discussed in the context of perovskite–silicon tandem solar cells are the consideration of realistic outdoor illumination conditions (see Section 10) including spectral deviations from the AM1.5G solar spectrum and bifacial illumination [253–257]. Accurate knowledge of the spectral illumination is crucial in order to ensure current-matching in monolithic 2T devices. Further, the above-mentioned high PLQY of perovskites leads to interesting effects via luminescent coupling in 2T [166,200,258,259] and 4T [260] tandem solar cells, which can relax current-matching constraints. Further, effective spectral splitters have been discussed conceptually [261].

Perovskite/CIGS tandem solar cells are currently the most popular and highest efficient tandems with CIGSSe bottom cells, even though the material system would also be suitable for various other combinations as outlined above. We focus here on the recent development of perovskite/CIGSSe tandems from 2022 onward as earlier literature is summarized in Ref. [200]. In 2022 a 2T tandem made of a $Cs(MA,FA)Pb(I,Br)_3$ top cell (E_g = 1.68 eV) and a CIGSe bottom cell (E_g = 1.1 eV) with 24.2% certified efficiency was reported [262]. The remaining current mismatch was assessed numerically and an efficiency of 30% was predicted. A slight variation in material compositions and, hence, bandgaps led to 23.5% certified efficiency [263]. The triple-cation perovskite had a bandgap of 1.59 eV and the bottom CIS had a bandgap of 1.03 eV, which together with perovskite layer thickness optimization and application of an antireflective coating (ARC) allowed an improved current match. Current matching as well as the remaining challenges of CIGSe surface roughness, and hence the risk of shunting due to a noncompact hole-selective layer of the perovskite top cell, can be circumvented in 4T configuration. An extensive optimization of a $CsFAPb(IBr)_3$/CIGSe tandem (bandgaps 1.64/1.04 eV) was conducted through significantly reducing parasitic absorption by replacement of the front and rear ITO by IO:H and IZO, respectively,

Figure 20

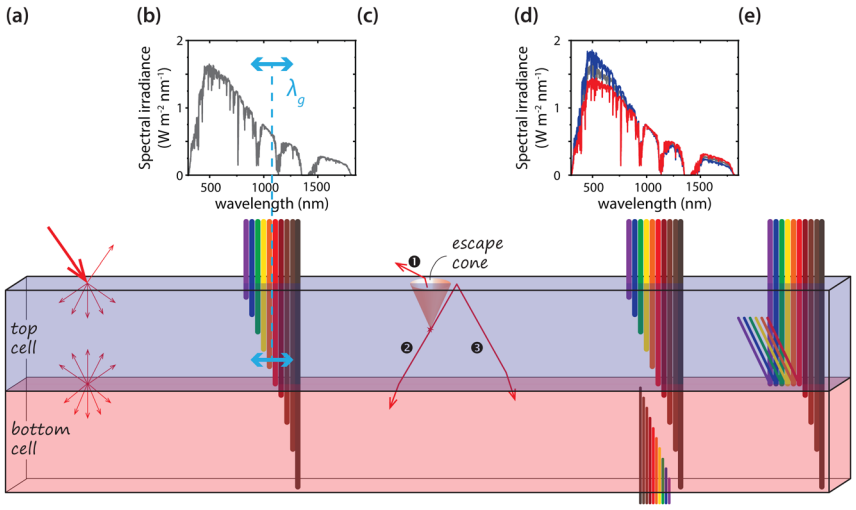

Optical design of multijunction solar cells requires the consideration of various aspects: (a) reduction of optical losses, (b) bandgap engineering, (c) luminescent coupling, (d) illumination different from standard testing conditions, and (e) effective spectrum splitting.

and through minimizing reflections by the application of MgF_2 ARCs, leading to 27.3% calculated (top plus shaded bottom cell) efficiency [264]. The latest record of (equally calculated) 28.4% 4T efficiency was achieved for a $CsFAPb(IBr)_3$/CIGSe tandem (bandgaps 1.67/1.04 eV) with improved perovskite material quality [265]. An efficiency maintained over 600 h underlines the persistent challenge of stability. A way out of stability issues may be all-chalcopyrite tandems if the challenge of low top-cell performance is overcome. Whilst the efficiency for the CGSe/CIGSe tandem remains below 10% (2T mechanical stack of 8.5% reported [266]), the integration of Ag enables (Ag,Cu)(In,Ga)Se_2/CIGSe tandems approaching higher efficiencies (13.9% in 2T beam-splitting configuration [267]). Further optimization appears feasible by improved material quality of wide-gap chalcopyrites, including alternative compositions.

All-perovskite multijunction solar cells offer cost-effective fabrication and lightweight, flexible solutions [268,269]. Their optical challenges fall into two categories: general light management tasks and multijunction-specific issues.

Losses by reflection and parasitic absorption losses must be reduced and, particularly in thin narrow bandgap perovskite layers, measures must be taken to increase the light path. Reflection reduction is mainly achieved by low-refractive-index antireflective layers or by using surface textures. In independently connected multijunction solar cells, such as 4T tandems, additional and thicker transparent electrodes cause parasitic absorption in the longer wavelength regime. This can be mitigated by the use of high mobility, low-free-carrier absorption transparent conductive oxides (TCOs) such as indium zinc oxide [270]. Narrow bandgap lead–tin (Pb–Sn) perovskites as used in all-perovskite multijunction solar cells exhibit a low near-infrared (NIR) absorptivity. A compensation by increasing the layer thickness is challenging because of low carrier diffusion lengths. Solutions for light path enhancement include light scattering resin particles in the narrow-bandgap Pb–Sn perovskite layer [271]. Yu *et al.* developed a SnOCl–basec hole transporting layer with a textured structure that reduces optical losses, simultaneously boosting the carrier diffusion length in the narrow bandgap

perovskite subcell [272]. The optical improvement potential of nanotextures has also been assessed numerically [273,274].

One major multijunction-specific challenge of all-perovskite solar cells is the bandgap engineering of different subcells. Perovskites of different bandgap cannot be fabricated with equally high quality and, hence, there are certain bandgap regimes where the single-junction efficiencies lag behind the others [Fig. 19(a)]. Narrow-bandgap perovskites are mainly limited by collection losses and low diffusion lengths, whereas wide-bandgap perovskites suffer from open-circuit voltage losses due to phase segregations and a lack of suitable transport layers. Luminescent coupling has been demonstrated experimentally in all-perovskite layer designs [166] and has shown to relax the current-matching constraint in 2T devices [166,275]. Studies have also investigated the influence of realistic illumination conditions, such as bifacial illumination [271,276,277] or deviations of the solar spectrum from AM1.5G [166,278] in all-perovskite tandem solar cells.

7.3. Advances Required

In conclusion, multijunction solar cells are currently developing at a rapid pace, which is reflected in rapidly increasing PCE records. In the future, the optical challenges in the field can be summarized as follows.

a) Reduction of optical losses. In every solar cell, regardless of the number of junctions, optical losses via reflection, transmission, and parasitic absorption in contact and recombination layers must be reduced to a minimum (see Section 3). The technological implementation of these measures varies greatly depending on which absorber materials are involved in the multijunction solar cell. For instance, random micropyramidal textures as used for the minimization of optical losses in silicon solar cells are not directly transferable to solution-processed perovskites or III–V semiconductors. Creative scientific and technological solutions are required enabling the implementation of optical loss reducing measures, which are compatible with the respective absorber material fabrication method.

As detailed in Section 7.1 the distribution of solar photons to the different subcells is crucial for obtaining the highest power conversion efficiencies in multijunction solar cells. For multijunction solar cells, which are connected in series (2T configuration), current-matching is even *the* central design aspect, as here the overall current of the device is limited by the subcell with smallest short circuit current density. From an optical point of view, several aspects must be therefore considered in multijunction solar cells as illustrated in Fig. 20.

b) Bandgap engineering. To tap the full efficiency potential of multijunction solar cells and to optimally harvest the solar spectrum, the bandgaps of the subcells must be matched to each other [Figs. 18(d) and 18(e)]. While deviations from the ideal bandgap combination have less influence on the maximum achievable PCE in the 4T configuration, there is a sharp maximum in the 2T configuration due to the current-matching constraint. The crystalline silicon bandgap can be regarded as fixed, whereas, in other solar cell material classes such as III–V semiconductors, perovskites, and CIGS, the bandgap can be more easily adapted by changing their compositions. It must be noted that bandgap engineering creates its own technological and material specific challenges such as a voltage deficit for wide-bandgap perovskite semiconductors and chalcopyrite materials (see Section 7.2).

c) Luminescent coupling is the sibling of the phenomenon photon recycling, which has already been described in Sections 5 and 6. It occurs in semiconductors close

to the radiative limit where excess carriers dominantly recombine by emission of radiation. The radiated photons from a subcell with a high bandgap can be coupled to an underlying subcell with a narrower bandgap and absorbed therein. Luminescent coupling can relax current-matching constraints if the multijunction device is limited by a lower bandgap subcell. In this case, excess generated carriers in the wide-bandgap subcell radiatively recombine and the radiated photons find their way to the narrow bandgap subcell where they can be absorbed.

d) Variable illumination conditions. Deviations from standard irradiance spectrum (AM1.5G) require solar cell design adjustments. In bifacial multijunction solar cells, the rear-sided narrow-bandgap subcell receives additional light, influenced by albedo, shadowing, and varying illumination conditions. Spectrum shifts (blue or red) affect photon distribution among subcells. Independently connected multijunction cells, such as 4T tandems, are less sensitive to spectral changes and do not need current matching. Detailed EY estimations (see Section 10), considering real solar spectra and annual yield, are necessary to determine the optimal configuration for bandgaps and layer thicknesses.

e) Effective spectrum splitting. Multijunction solar cells need tailored optical measures to ensure each subcell absorbs its designated part of the solar spectrum. In layer stack geometry, structures or films between subcells must transmit photons below the top cell's bandgap to the narrow bandgap subcells and reflect higher-energy photons back to the top cell to reduce thermalization losses. The spectrum can also be split using semitransparent mirrors guiding different parts of the solar spectrum to spatially separated solar cells. Such a spectral splitter could be accompanied by a photonic structure that guides the light into trapped modes to enhance absorption in the respective subcells.

Figure 21

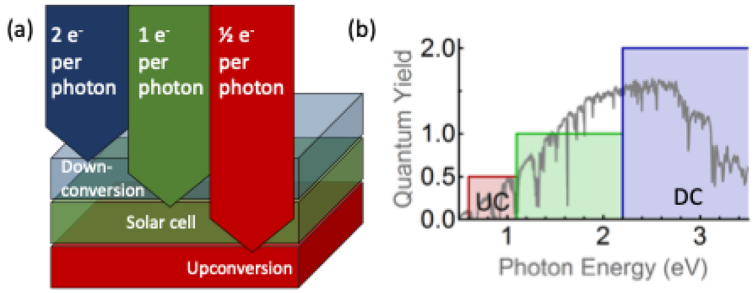

(a) Three-bandgap single-junction solar cell using a downconverter (blue, DC) to increase the energy converted from the high-energy part of the spectrum and an upconverter (red, UC) to convert previously unused below-bandgap photons, with (b) ideal quantum yield compared with the solar spectrum (gray).

8. SPECTRAL SHAPING/CONVERSION

E. Alarcón Lladó and B. Ehrler

Conventional single-junction solar cells are limited in efficiency because they absorb the broad solar spectrum by means of using a single, narrow bandgap. Any photon that is absorbed contributes the same energy for conversion, independent of the original photon energy. Tandem solar cells are the most prominent way to overcome this efficiency limitation, by dividing the spectrum into several parts, each absorbed by an individual subcell with better-matching bandgap (see Section 7). In this section we discuss optical ways to convert the solar spectrum into a spectrum that better matches to bandgap of the solar cell, which has a similar effect on the achievable efficiency [279,280].

Broadly speaking there are three ways to convert the solar spectrum for better energy conversion, all of which require advances in light management for increasing efficiency (Fig. 21). The first is downconversion, the conversion of high-energy photons into a larger number of lower-energy photoexcitations. The second is upconversion, where below-bandgap photons are converted into a (lower number) of above-bandgap photons. The third is to concentrate the sunlight at the expense of downconversion, often with luminescent solar concentrators (LSCs). All categories increase the excitation density of a solar cell and thereby its power conversion efficiency (PCE).

8.1. Downshifting and Downconversion

A downconversion layer would be placed in front of the solar cell because it converts the high-energy light into lower-energy particles, either photons or excitons. Downconversion to increase the solar cell efficiency can be achieved with a range of different mechanisms. The simplest one is the absorption of photons in an area of the solar spectrum where the solar cell performs poorly, usually the ultraviolet (UV) part, and emission in an area where it performs well, often called downshifting [281]. To increase the efficiency, however, the radiative efficiency of the downconversion layer needs to be close to 1, and the emission needs to be coupled into the underlying solar cell. Silicon solar cells have improved their performance in the UV part of the solar spectrum in recent years, so that need for such downshifting has shifted more toward a reduction of UV-induced degradation by absorbing the UV photons and downshifting them to a region where they can contribute to the photocurrent [282].

Downconversion by carrier multiplication, also called quantum cutting or photon multiplication, on the other hand, has potential for increasing the efficiency beyond

the detailed-balance limit for a single-junction solar cell. In fact, the thermodynamic efficiency limit is almost the same as with a 2T tandem cell [279]. In other words, a simple downconversion layer on a single-junction solar cell could be as efficient as a tandem solar cell.

The main material classes currently investigated for downconversion are organic materials that make use of singlet fission and rare-earth-doped materials, including rare-earth-doped high-bandgap perovskites. Singlet fission is a process in organic semiconductors by which a single photoexcited exciton is converted into a pair of excitons where each has roughly half the energy of the original excited state [283]. This conversion is possible because of the spin nature of the exciton state in organic semiconductors. The photoexcited exciton is in a singlet configuration, but in organic semiconductors with a large exchange energy, the triplet exciton has a much lower energy. The combination of two triplet excitons can be in a singlet configuration, so that the conversion of a single singlet exciton into two triplet excitons is energy and spin allowed. Efficiencies of this conversion of 200% have been observed for pentacene [284], tetracene [285], and other materials [286,287]. For the application in solar cells, these triplet excitons also need to have an energy larger than the bandgap of the solar cell, and the energy needs to be transferred to the solar cell. This transfer could be photonic by the transfer of the triplet exciton to a radiative emitter, but one could also imagine direct transfer of the charges or excitons. The direct transfer of energy has already been shown to contribute to the external quantum efficiency (EQE) of a silicon solar cell [288,289] and has even led to an improvement of the quantum efficiency recently [290]. However, each of these mechanisms has advantages and disadvantages, and it is not yet clear if any of these will be successful in increasing the overall solar cell PCE. To do so, very stringent requirements for each step in the process need to be fulfilled.

For exciton or charge transfer, the distance of the downconversion material to the solar cell active layer needs to be within the transfer distance (charge or Dexter energy transfer), which is only a few nanometers [291]. This poses a range of practical challenges, for example the surface passivation in case of silicon solar cells [292]. The challenges associated with photonic transfer are, perhaps expectedly, more photonic in nature [293]. The triplet exciton is in itself not emissive, but it can transfer its energy to an emitter, for example, a quantum dot (QD) [294,295]. Then the emission needs to be directed toward the silicon solar cell, which can, for example, be achieved by careful placement of the emitter on top of a dielectric structure [296]. In addition, the contrast in refractive index between the organic material and the underlying solar cells helps in this directionality of emission. The third challenge is to shape the emission spectrum such that it can be optimally absorbed by the underlying solar cell. In particular, in silicon solar cells, the absorption near the band edge is rather poor, so that the emission energy of the downconverter needs to be placed somewhat above the silicon bandgap. This poses a tradeoff, as the increase in emission energy also increases the energy from which it can absorb the photons it will downconvert (because of the thermodynamic requirement of energy conservation). Photonics can help in steering the light toward the underlying solar cell, and in increasing the absorption of the silicon solar cell in a narrow region around its bandgap [233]. Another, perhaps unexpected advantage of using an organic downconversion material is that it becomes transparent once it degrades. The downconversion foil then becomes a passive layer on top of the solar cell upon degradation, operating just like a normal single-junction solar cell [297]. This relaxes the requirement for the long lifetime of organic solar cells, which hampers many other applications of organic semiconductor in solar energy conversion.

Another way to efficiently downconvert high-energy photons is by the use of rare-earth-doped large-bandgap perovskites [298,299]. In these materials the term "quantum cutting" is commonly applied. Some rare-earth materials show emission close to the bandgap of silicon, and these materials are characterized by a very long emission time scale. To populate this emissive state, the strong absorption of the perovskite host is utilized. A large-bandgap perovskite, for example $CsPbCl_3$, absorbs at an energy above twice the silicon bandgap. Providentially, in this material some rare-earth ions such as Yb^{3+} assemble in a defect complex with a single metal vacancy and two Yb^{3+} ions. In this configuration, the excitation in the perovskite quickly splits into two excitations on the Yb^{3+} ions via a defect state [300]. Once the ions are excited, the state is very stable and emits on a long lifetime. If this emission can be directed toward a silicon solar cell, then the quantum efficiency for conversion of high-energy photons could be increased. In addition to the light-management challenges mentioned for the singlet fission downconversion systems, these quantum cutting systems experience power saturation, if the emissive states are populated faster than they emit light.

8.2. Upconversion

Upconversion for solar cells is an appealing prospect. All the photons below the bandgap energy in a solar cell are normally transmitted through the absorber layer and either emitted through the rear surface or, in case of a rear reflector, transmitted again though the absorber for emission through the front surface. On the way they have multiple occasions to be absorbed to generate parasitic heat. If these photons could be converted into electrical energy, the efficiency would be improved, and the cell temperature potentially reduced [301].

An upconversion layer would be placed behind the active layer of a solar cell to absorb only the photons transmitted by the cell. This requires both electrical contacts to be transparent, similar to a front cell in a 4T tandem solar cell, with all the light-management challenges associated with transparent contacts (see Section 4). Just like downconversion, upconversion can proceed via lanthanide ions or in organic semiconductor materials.

In organic semiconductors it proceeds via the annihilation of triplet excitons [triplet–triplet annihilation (TTA)], as the reverse process of the above-mentioned singlet fission. For a solar cell, the triplet excitons need to be photogenerated. Since the direct absorption of light to generate triplet excitons is spin-forbidden, it is extremely weak in materials with small spin–orbit coupling such as typical organic semiconductors. However, the triplet excitons can be generated by a sensitizer, such as an inorganic QD or metallated porphyrin molecules [301]. For solar cells, however, these donors would need to absorb below the bandgap of silicon. There are only few examples of semiconductors with triplet excitons that have an energy below the silicon bandgap and upconversion from that spectral region has only been demonstrated recently [302]. In lanthanide ions, the upconversion process combines the energy of two infrared (IR) photons to promote the upconversion material to a higher-energy excited state [303–305]. From this state, either a photon with an energy that is approximately doubled with respect to the initial IR photon is emitted to be absorbed by the silicon active layer, or the double-energy exciton is transferred to the silicon cell, and directly split into charges. Combinations of lanthanide ions with the proper energy level structure allows for the two consecutive energy transfer steps in which a neighboring lanthanide ion is raised from the ground state to an excited state. When the system is in the (long-lived) first excited state, a second transfer raises the ion to a higher excited state giving upconversion emission of photons of higher energy. Upconversion efficiencies of 12% have been realized for monochromatic excitation [306]. A known drawback of the lanthanide-based approach is that the IR absorption is weak and

Figure 22

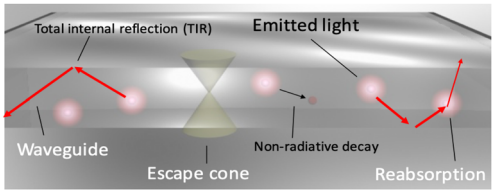

Schematic of the working principle of LSCs.

spectrally narrow. Similarly to the TTA upconversion, this can be overcome by functionalizing lanthanides nanoparticles (NPs) with antennas which transfer the absorbed energy to the NP core where the upconversion takes place. Broadband absorption in dye-sensitized upconversion has been reported for near infrared (NIR)-to-visible upconversion [307–309] but so far not for IR-to-NIR upconversion as required for c-Si solar cells.

8.3. Luminescent Solar Concentrators

LSCs consist of large sheets of transparent materials, such as polymers or glass, embedded with pigments known as dyes or luminophores. Luminophores absorb sunlight and subsequently reemit fluorescent light, which is then guided and concentrated toward small solar cells positioned either at the back or at the edges of the sheet (Fig. 22). This dramatically reduces the area of solar cells needed, as in traditional concentrators. Unlike conventional light concentrating methods (i.e., with lenses), LSCs exhibit the unique capability to effectively concentrate diffuse irradiance in addition to the direct irradiance, a significant component of solar radiation scattered by the atmosphere and terrestrial surfaces and, thus, it eliminates the need for tracking. Although the functional principle of LSCs was originally proposed in the late 1970s [310,311] reported concentration efficiencies are still far below the theoretical limit and scalability poses a challenge [312].

LSCs involve two key optical components: luminophores and the sheet waveguide. Luminophores are typically organic dyes or inorganic QDs that absorb well-defined spectral bands from the incident sunlight, which is then isotropically emitted with lower-energy photons due to the Stokes shift. Organic dyes, such as various types of chromophores, offer tunability in terms of absorption and emission wavelengths through chemical modification of their molecular structures. Inorganic QDs, on the other hand, exhibit size-dependent optical properties, allowing precise control over absorption and emission spectra by adjusting their NP dimensions [313]. Both organic dyes and inorganic QDs have been studied extensively and employed as luminophores in LSCs due to their high quantum efficiency, photostability, and compatibility with transparent substrates [314].

From the photonic perspective, LSCs are capable of concentrating light with a wide angular distribution into waveguided light with a narrow angular distribution, thereby reducing photon entropy. The second law of thermodynamics requires that this reduction in photon entropy is balanced by a reduction in photon energy, leading to a minimum required Stokes shift that increases logarithmically with concentration factor [315]. For instance, a concentration of 100 requires a minimum Stokes shift of $\approx$100 meV. While Stokes shifts as large as 200 meV have been reported, the practical concentration factor scales sublinearly with the sheet size or luminophore density [316].

Figure 23

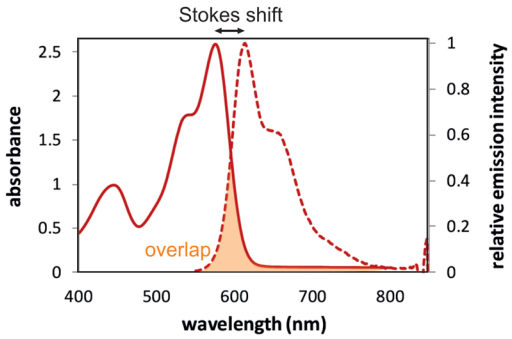

Representative absorption and emission spectra of a fluorescent dye [Lumogen F Red 305 (200 ppm) in PMMA], highlighting the spectral shift between the two processes (i.e., Stokes shift). The shaded area indicates the spectral overlap between absorption and emission. Adapted from Sol. Energy, **112**, Vishwanathan *et al.*, "A comparison of performance of flat and bent photovoltaic luminescent solar concentrators," 120–127 (2015) [317], with permission from Elsevier.

Just because a photon has been confined within the lightguide, it does not necessarily mean that it will actually make it to the PV element. Two main fundamental challenges hamper scalability of LSCs in terms of waveguide length. First, fluorescent light can be reabsorbed by other luminescent particles (or even the matrix material) intercepting the optical path of photons if the overlap between the emission and absorption spectra is large (shaded area in Fig. 23). Because fluorescent light is emitted in a random direction, light emitted within the escape cone of the glass–air interface will unfortunately outcouple from the waveguide. This results in the gradual reduction of light intensity with concentrator size [318].

Many efforts have been focused on the chemical manipulation of luminophores to minimize spectral overlap without excessive Stokes shift. Bronstein *et al.* [319] showed that LSCs doped with CdSe/CdS QDs can exhibit 30-fold concentration of irradiance. This is achieved by coupling of a wavelength-selective photonic mirror to an LSC to form an optical cavity where emitted luminescence is trapped. Li *et al.* [320] used colloidal core/shell QDs resulting in efficiencies of more than 10% for dimensions of tens of centimeters. For even larger LSCs one also needs to consider the matrix material, as even the weak absorption of vibrational modes can become significant [321].

8.4. Advances Required

In conclusion, spectral shaping and conversion could play a significant role in increasing the efficiency and applicability of solar energy. In the future, the optical challenges in the field can be summarized as follows:

Optical coupling. Increasing the PCE by upconversion and downconversion requires that the emission needs to be directed toward the solar cell, and the conversion efficiency of the underlying solar cell needs to be high enough in the spectral range where the photon multiplier emits. Therefore, directional emission of these photons, or scattering into the correct angular emission is required. The emission is typically very narrowband, which suggests that a suitable nanostructure could direct the light. Another aspect of optical coupling is to maximize the absorption strength of the solar cell in the spectral region where the upconverter or downconverter emits.

Power saturation. In addition to the optical coupling, the rare-earth photon multipliers pose an additional challenge. The slow emission efficiency of the rare-earth emitter yields power saturation once the incoming photon flux is too high [322]. The excitation rate cannot be higher than the emission rate, which means that the density of emitters needs to be maximized and at the same time the incoming power needs to be distributed in an optimal fashion throughout the downconverter. The power saturation only plays a role at high solar intensities, but can still limit the efficiency gain from the photon multiplier. Photonics could play a role by reducing the lifetime of the emitters by increasing the local density of states the material can emit into. Other optical ways to distribute the incoming solar intensity into different, spatially separated parts with its own emitters might further decrease the density of excitations that the rare-earth ions need to carry. Despite all these challenges, an increase in PCE has been demonstrated [323], which indicates the exciting opportunity these downconverters offer.

Transmission of upconverted light. The light management challenges for upconverters are subtly different from those for downconverters. While for upconverters the light needs to be steered toward the solar cell, this can be trivially achieved for upconverters with a simple mirror on the back of the solar cell stack. However, for solar cells the upconversion layer is ideally optically thick, which means that it absorbs all light below the silicon bandgap but above its own bandgap. However, this poses a challenge. The higher-energy emitted light is likely to be self-absorbed, reducing the number of upconverted photons hitting the solar cell. One way around this limitation would be to transmit the high-energy upconverted exciton into the solar cell by energy transfer or charge transfer, which has not been demonstrated to date. Alternatively, one needs to engineer a transmission window into the upconversion layer in the spectral range where the upconverter emits. This could be achieved by fabricating the upconverter from a dye that is optically thick in the IR, but has an transmission gap in the NIR. Alternatively, photonic strategies might be developed to generate the transmission gap.

Breaking reciprocity for efficient LSCs. Reciprocity requires that incoupling and absorption efficiency of sunlight must be the same as outcoupling and emission efficiency for the same photon energy and angle. This means that efficient incoupling of sunlight and waveguiding of emitted light can only occur simultaneously if there are large asymmetries in the angular and energy distribution of incoming and emitted light. Otherwise, any attempts to improve waveguiding will simply increase the reflection of sunlight from the LSC surface. New advanced photonic nanodesigns are needed to break the reciprocity, taking advantage of the fact that the wavelength of absorbed and waveguided light is fundamentally different. For instance, fine-tuning directional emission in the in-plane of the waveguide would minimize escape cone losses.

9. OPTICS FOR THERMAL MANAGEMENT OF PV MODULES

J. Mandal and A. P. Raman

A central challenge facing photovoltaics (PV) modules operating in the field is the elevated temperatures they typically encounter. Under hot ambient conditions and parasitic heating by sunlight, a typical solar module can easily reach 55–60°C in typical scenarios, and significantly higher temperatures in hot desert environments, where large PV systems are often deployed, or in concentrator architectures [324,325]. The source of this heating is both due to fundamental heat-generation mechanisms in the active PV material and also due to absorbed subbandgap light in other materials in the overall PV module architecture such as front and back sheets, metallic reflectors and cover glass. These elevated temperatures, distinct from the lab-scale conditions often used to report solar efficiencies, can greatly reduce both the practical operating efficiency and lifetime of the module [326]. Thus, in recent years, thermal management has emerged as an important research field to improve the real-world operating efficiency and lifetime of PV modules.

Optics and photonics hold the potential to play a unique, perhaps essential role in enhancing thermal management of PV panels through two separate but related mechanisms: (1) maximizing radiative cooling to the sky to enhance heat loss; (2) reflecting subbandgap photons that would otherwise parasitically heat the PV module and not be usable by the active layer. Here, we highlight past work on both these efforts and opportunities that lie ahead to enable effective scaling of these concepts to the terawatt scale.

9.1. Radiative Cooling of PV Modules

While the Sun represents the ultimate renewable heat source accessible to us here on Earth, our planet is also surrounded by the ultimate heat sink: outer space itself. Radiative cooling refers to the harnessing of this heat sink by radiative heat transfer of terrestrial objects that face the sky. As all terrestrial objects under the sky are heated by sunlight, so do they radiate some of their heat upward as longwave radiation. While the atmosphere does absorb and send back much of this thermal radiation, a significant fraction eventually escapes to space, thereby enabling a sky-facing surface to cool itself down passively below its surroundings [327,328]. Radiative cooling thus represents a complementary technology to solar-based technologies; where solar systems harness the heat of the Sun for either thermal or electrical ends, radiative cooling enables cooling that could also be leveraged for either thermal or electrical work.

Recent interest in radiative cooling has largely been motivated by subambient daytime radiative cooling, first demonstrated in 2014 [329]. The considerations for daytime radiative cooling are primarily around high solar reflectance and suitably high thermal emittance. Given the goal of daytime radiative cooling is to maintain subambient temperatures, it has also been noted that *selective* thermal emittance, preferential thermal emission within the primary atmospheric window between 8 and 13 μm, can allow objects to reach colder temperatures than with a blackbody, if the radiative cooling surface is sufficiently insulated. Such considerations however do not apply to radiative cooling of PV modules.

9.1a. Radiative Cooling Heat-Transfer Model

We briefly elucidate the radiative heat flows experienced by a PV module outdoors. Consider a PV module with spectral angular emissivity $\epsilon(\lambda, \Omega)$ at a temperature T. When the PV module is exposed outdoors it is subject to both solar irradiance, and thermal radiation from the atmosphere (corresponding to ambient air temperature T_{amb}). The PV module's steady-state temperature T is determined from the following

heat balance equation:

$$P_{\text{rad}}(T) - P_{\text{atm}}(T_{\text{amb}}) - P_{\text{Sun}} + P_{\text{cond+conv}} = 0. \tag{6}$$

In Eq. (6), the thermal emission power radiated out by the PV module as a whole is

$$P_{\text{rad}}(T) = \int \mathrm{d}\Omega \cos\theta \int_0^\infty \mathrm{d}\lambda\, I_{\text{BB}}(T,\lambda)\epsilon(\lambda,\Omega). \tag{7}$$

Here,

$$\int \mathrm{d}\Omega = \int_0^{\frac{\pi}{2}} \mathrm{d}\theta \sin\theta \int_0^{2\pi} \mathrm{d}\phi$$

is the hemispherical integral,

$$I_{\text{BB}}(T,\lambda) = \frac{2hc^2}{\lambda^5} \frac{1}{\exp\left(\frac{hc}{\lambda k_B T}\right) - 1}$$

is the spectral radiance of a blackbody at temperature T. Here h is Planck's constant, c is the velocity of light, k_B is the Boltzmann constant, and λ is the wavelength of emitted light. Furthermore,

$$P_{\text{atm}}(T_{\text{amb}}) = \int \mathrm{d}\Omega \cos\theta \int_0^\infty \mathrm{d}\lambda\, I_{\text{BB}}(T_{\text{amb}},\lambda)\epsilon(\lambda,\Omega)\epsilon_{\text{atm}}(\lambda,\Omega), \tag{8}$$

is the downwelling atmospheric irradiance absorbed the PV module.

$$P_{\text{Sun}} = \int_0^\infty \mathrm{d}\lambda\, \epsilon(\lambda,\theta_{\text{Sun}}) I_{\text{AM1.5}}(\lambda)\cos(\theta_{\text{Sun}}) \tag{9}$$

is the absorbed solar power (including, for example, subbandgap light) that collectively results in heating of the solar module. In Eqs. (8) and (9), we have used Kirchhoff's law to replace absorptivity with emissivity $\epsilon(\lambda,\Omega)$.

The angle-dependent emissivity of the atmosphere is given by

$$\epsilon_{\text{atm}}(\lambda,\Omega) = 1 - t(\lambda)^{1/\cos\theta}, \tag{10}$$

where $t(\lambda)$ is the atmospheric transmittance in the zenith direction. The solar irradiance is represented by the AM1.5 spectrum. The P_{Sun} is devoid of an angular integral, and the structure's emissivity is represented by its value at incidence angle θ_{Sun}. Finally,

$$P_{\text{cond+conv}} = h_c\,(T - T_{\text{amb}})\,, \tag{11}$$

is heat loss due to nonradiative heat exchange. Here h_c is a total nonradiative heat coefficient that accounts for conductive and convective processes due to the contact of the PV module with its immediate environment.

PV modules will necessarily operate at significantly above-ambient temperatures during the daytime under sunlight due to P_{Sun} being significantly larger than net cooling at T_{amb} at long-wave infrared (IR) wavelengths [i.e., $P_{\text{rad}}(T_{\text{amb}} - P_{\text{atm}}(T_{\text{amb}})$]. Thus, the primary goal of radiative cooling in the context of PV modules is to maximize their IR emissivity over all relevant thermal wavelengths, i.e., to ensure the module as a whole behaves as a blackbody [330,331]. This is distinct from goals of enable selective IR emissivity within the atmospheric window one typically encounters with daytime radiative cooling, where the goal is to reach subambient temperatures. Since we expect steady-state temperatures to be well above ambient, high broadband emissivity is the goal. While a nominally simple goal, this task has had a fundamental technical challenge associated with it: the glass panels that form the top layer of most PV modules have comparatively low emissivity (~0.84) due to the *Reststrahlen* band of SiO_2, the primary constituent material in typical solar glass.

9.1b. Photonic Strategies to Enhance Emissivity

Early work identified a remarkable opportunity if the emissivity of front-surface glass were enhanced to ≈ 1 while maintaining net transmittance into the underlying solar cell: in hot, desert conditions, where radiative cooling effects are particularly prominent, a temperature reduction of as much as 5°C might be accessible [330]. Later experimental work introduced a photonic crystal into the front surface of a silica wafer atop a silicon absorber, demonstrating a ∼1°C temperature reduction in more temperate weather conditions [332]. Crucially, this design demonstrated a slight light trapping effect as well, ensuring that the amount of sunlight reaching the underlying PV material actually exceeded that of the baseline glass scenario.

Motivated by these demonstrations, several strategies have been explored to enhance front-surface glass emissivity, from microspheres and voids, to multilayer thin films [333–338]. The latter strategy is the most easily scalable, but enhanced emissivity over long-wave IR wavelengths has resulted in quite thick designs, posing potential cost challenges. Such an approach may be particularly important for concentrated photovoltaics (CPV) [339], where strategies involving adjacent daytime radiative cooling surfaces for heat rejection have also been demonstrated [340].

9.2. Integrated Subbandgap Sunlight Reflection

A related thermal management strategy has also emerged in recent years: reflecting subbandgap sunlight, thereby minimizing parasitic heating from these otherwise useless photons in various constituent layers inside a PV module [335,337]. A key parameter explored has been placing such a selective reflector either on the front surface of the glass, or immediately beneath it [335,341–343]. An advantage of placing the spectrally selective reflector on the front surface is that one can, in principle, simultaneously optimize for three factors: (i) subbandgap reflection, (ii) IR emissivity, and (iii) antireflection over above-bandgap solar wavelengths.

This functionality, the ideal form of which is depicted in Fig. 24(a), could have a significant effect on overall operating temperature of a solar module, as illustrated in Fig. 24(b). In low-wind conditions, for instance, the net effect of this relative to a baseline glass-based solar module could be greater than 10°C temperature reductions.

9.3. Toward Cooler and More Climate-Friendly PV Panels

PV energy conversion, and the parasitic heating accompanying the process, mean that PV panels have two distinct effects on the climate. The conversion of solar energy to electricity is a zero carbon process and helps to reduce greenhouse gas emissions. This emissions reduction, in turn reduces greenhouse heat trapping in the atmosphere, making PV panels critical for climate change mitigation [344]. On the other hand, the dissipation of absorbed heat into the environment represents a weaker but significant antagonistic effect. The high operational temperatures of PV panels, arising from their parasitic solar heating and less than ideal thermal emittance, causes them to convectively and radiatively dissipate significant low-grade heat that is trapped in their environment. This warming effect on Earth, while significantly smaller than the cooling effect of CO_2 emissions reductions, does reduce the net environmental benefit. Second, heat from large-scale deployment of PV panels can lead to PV heat islands [345,346]. In built environments, this can raise cooling loads, causing part of the renewable energy generated by PV panels to effectively be used to mitigate their own heating effect. This reduces both the climate change reductions benefit and effective efficiency of PV panels.

By reflecting solar wavelengths that would be converted into parasitic heat, and increasing the emittance of PV panels in the long-wave atmospheric transmittance window,

Figure 24

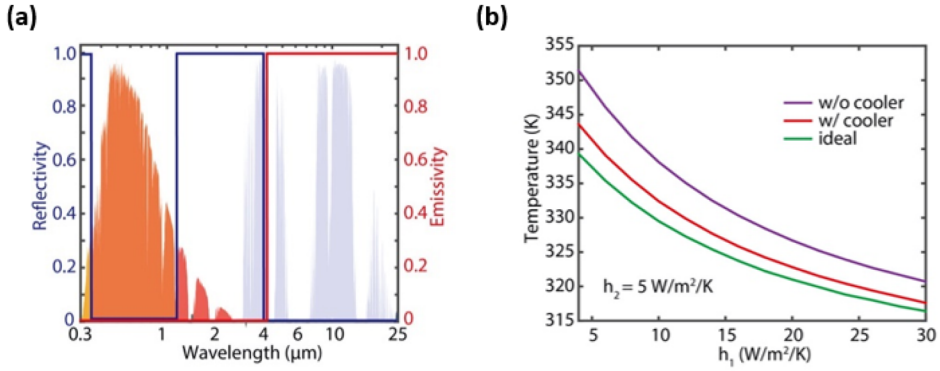

(a) Ideal spectral reflectivity and emissivity of a PV module. Subbandgap solar light is perfectly reflected (here assuming Si's bandgap), whereas over long-wave IR wavelengths > 1 μm the module exhibits unity emissivity. (b) Temperature effect of the ideal surface compared with a photonic design as well as baseline glass, for values of convective heat exchange on the front and back surface. In relatively modest wind conditions a temperature difference of >10 K is possible, yielding substantial gains in operating efficiency and improved module lifetime. Adapted with permission from Li *et al.*, ACS Photonics, **4**, 774–782 (2017) [335]. Copyright 2017 American Chemical Society, https://doi.org/10.1021/acsphotonics.7b00089.

radiative coolers cool PV panels by sending heat to space and reduce their heating effect on the environment. Relative to ordinary PV panels, this leads to a cooling impact, as well as better overall energy utilization by lowering self-generated cooling loads. While inferable from first principles, accurately quantifying these benefits of radiative coolers requires systematic studies that consider not only the energy-generation or optical and thermal aspects of PV panels, but also their intersections with the energy infrastructure, and built and broader environments.

9.4. Advances Required

While intriguing in its potential, the role of optics for PV thermal management faces numerous challenges. Optimal designs that can deliver functionality close to that of the ideal spectral response have entailed either very thick multilayer thin-film stacks, or complex patterning into the front surface of PV panels. Given the cost sensitivity of PV modules both these approaches face numerous practical challenges for wider adoption. An alternate approach has been to explore significantly simpler designs, often single or bilayer coatings made of low-cost materials. These designs can easily deliver small increases in subbandgap reflection (low tens of watts per meter squared reduction in heating), but ultimately may yield only ~1°C reductions in operating temperature.

Enhancing IR emissivity via a thin-film approach that preserves other optical requirements has typically entailed significantly thicker films. However, lower-cost materials, including a range of ultraviolet (UV)-stabilized polymer films with suitable emissivity may play a useful role here. Alternatively, low-cost chemical processing of the front surface of the glass to introduce tailored microstructures may yield desired optical functionalities. While a broad range of strategies have been explored in literature, a practical, scalable and low-cost approach that might yield multiple degrees Celsius of cooling remains lacking, and represents an exciting opportunity for terawatt-scale PV.

It is also important to note that the effect of radiatively cooling PV panels remain to be holistically calculated. Prior works in the literature have quantified the benefits for

individual PV panels [347]. However, such models assume major convective cooling into the environment: in reality, PV panels often exist as arrays, with convective heat dissipation affecting the performance of neighboring PV panels. In other words, convection may be less effective in such cases, and the impact of radiatively cooling PV panels on EYs may be considerably greater than what single-panel models indicate. Likewise, the potential urban climate impact of radiatively cooling widely deployed rooftop solar panels may also increase the effective efficiency of PV panels by reducing urban cooling loads. Further research on these topics can motivate material and optical design of thermal management strategies for PV panels.

10. BEYOND STANDARD TESTING CONDITIONS: ILLUMINATION MODELS FOR ACCURATE ENERGY YIELD PREDICTION

M. Jošt, U. Paetzold, and R. Saive

The performance of photovoltaics (PV) systems is assessed by a variety of key performance indicators such as levelized cost of electricity (LCOE), energy payback time (EPT), emissions per kilowatt-hour, or resource efficiency. All of these performance indicators assess the total amount of energy harvested from the PV installation, taking into consideration seasonal and daily variations in irradiation conditions, spectrum, temperature, as well as all the details of the installation (e.g., module orientation, type of tracking, shadows, and soiling). Therefore, predicting energy yield (EY) is pivotal for PV systems and device architecture design of solar modules. While reasonable extrapolations can be made from the power conversion efficiency (PCE) to the EY for many opaque single junction PV technologies installed in terrestrial locations, the PCE fails to provide accurate design rules for more complex device architecture or application scenarios. Prominent examples that require detailed EY modeling and discussed in the following are: (A) optimization of more complex multijunction PV technologies (e.g., perovskite–silicon tandem PV) and (B) bifacial PV. For example, it was shown that the PCE determined under standard test conditions is not suitable to determine the optimal bandgap combination of perovskite–silicon tandem solar cells nor the perovskite layer thickness in bifacial perovskite–silicon tandem solar cells [254,348,349].

10.1. Performing EY Calculations

In EY modeling, the energy produced over a whole year is calculated by integrating the generated energy of a solar module (or solar cell) produced for given time intervals, e.g., every hour over a year. The basic approach is illustrated in Fig. 25(a). It comprises, as depicted with green boxes, (1) determining the irradiation conditions and outdoor temperature, (2) determining the optics of the solar cell for a given angle of incidence, (3) the electrical characteristics of the solar cell for a given interconnection scheme and generation rate in each subcell, and (4) the EY calculation itself, which represents an integral over a representative time period, taking into consideration the installation aspects such as solar module, tracking systems or bifacial characteristics of the PV system. The EY modeling requires three key input parameters, depicted with blue boxes: (i) position of the Sun, spectral irradiance (diffuse and specular), and air (or module) temperature at a given time; (ii) optical response (external quantum efficiencies [EQE]) for a given angle of incidence and photon energy; and (iii) the electrical device performance for a given generation rate and temperature.

Obtaining the whole set of input parameters can be challenging. Part (i) depends on geographical parameters (position of the Sun on the horizon, surface) and weather conditions, namely direct and diffuse irradiance, air temperature and wind speed. The complete experimental datasets of spectrally and timely resolved irradiance that discriminates between specular and diffuse irradiance are extremely rare and, in most cases, only available for limited or incomplete periods (e.g., one or two years). Such short periods are not enough for general conclusions as the data could be from a hot and sunny, or cloudy and rainy year. For these reasons, most EY modeling studies are based on the typical meteorological year (TMY) dataset, which comprises the weather data of 12 years. The National Renewable Energy Laboratory (NREL) provides TMY dataset for the USA in their National Solar Radiation Database (NSRDB) database [352,353], and it has recently been upgraded to cover the whole world. Alternatively, Simple Model of the Atmospheric Radiative Transfer of Sunshine (SMARTS) model

Figure 25

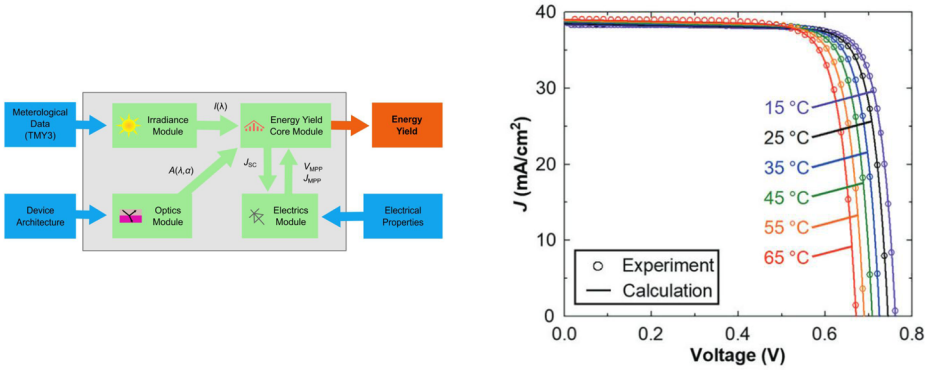

(a) (b)

Schematic flow of the modular EY modeling. The irradiance module computes the spectral irradiance I, the optics module the absorptance A, and the EY module calculates the short-circuit current density J_{SC} and EY with the help of the electric module. (b) Temperature variations of *J*–*V* characteristics of a Si heterojunction solar cell with a certified efficiency of 23.27%. The open circles show the experimentally derived data, whereas solid lines indicate the fitted results. (a) Reprinted with permission from Ref. [350] © Optical Society of America. (b) Kato *et al.*, Prog. Photovoltaics, **30**, 1198–1218 (2022) [351]. Copyright Wiley-VCH Verlag GmbH & Co. KGaA. Reprinted with permission.

can be used to generate, the so-called "clear sky" irradiance data [354,355]. In combination with a cloud model this data can provide an hourly and spectrally resolved dataset of specular and diffuse irradiance data for a wide range of locations covering most of the relevant climate zones. The module temperature is often calculated from ambient conditions through models such as the NOCT, Ross, or Duffie–Beckman model [356,357]. In particular, the NOCT model is often employed due to the absence of better models and/or a detailed knowledge of the temperature in the solar module. All in all, the inclusion of temperature into the EY model can induce a 5–10% penalty [262] (Fig. 26(b)), depending on the temperature coefficient of the studied structure. This makes an efficient thermal management key to obtaining high EY. For example, longwave heat flow, which is in details discussed in Section 9, can help reduce the operational temperature of the PV modules and increase the EY.

Part (ii) describes optical performance (EQE, and consequently J_{SC}) at different incident angles that occur during the Sun's path over the horizon. It is usually provided by performing optical simulations of the device stack using ray tracing and transfer matrix models, for which inputs are the thicknesses and refractive indices of the layers. These calculations can take some time, especially if the thicker, textured layers that require ray tracing are included, such as glass, encapsulant, and silicon. However, they can be prepared in advance for the selected device stack and integrated in the EY model [350].

Finally, for part (iii), the electrical performance at different temperatures and irradiances can be measured in laboratory by, e.g., changing temperature and irradiance of the Sun simulator in a wide range (25–85 °C and 100–1200 W/m^2) should cover most locations, Fig. 25(b), or by simulating *J*–*V* curves using one-diode parameters. For each interval in a year, a power at maximal power point from the *J*–*V* curve is selected based on outdoor conditions and optical response, and summed over a year.

The complete methodology of EY calculations has been thoroughly described in Refs. [349,350].

Further analysis of EY results can be used either in hourly intervals or integrated over a year. The latter is useful to compare locations, technologies and orientations and is analyzed in the following in more detail. The former, however, is especially handy when determining the short-term stability in outdoor testing of novel technologies, such as perovskite solar cells, where stability is measured in weeks or months rather than years as in the case of the established silicon modules. Thus, it is important to regularly and continuously track the degradation of devices. This is not trivial, since diurnal and weather changes make it hard to estimate devices performance [358] as the device output is determined by irradiance, angle of the Sun, and temperature, all important parameters of EY modeling. Therefore, by comparing the device output with the EY simulations [359] can serve as an efficient tool to estimate and monitor device performance in outdoor operation and, in turn, keep track of possible degradation or potential other effects, such as light soaking.

10.2. EY Modeling for Perovskite-based Tandem Solar Cells

A prominent example of the importance of EY modeling is the performance of multijunction solar cells in terrestrial applications. The multijunction concept and their main optic challenges are covered in Section 7, whereas here we focus on the perovskite-based tandem solar cells. To extract as much current out of the tandem device as possible, optimal balance between the two (or more) subcells has to be achieved, namely their current matching. This is typically done for AM1.5G irradiance as defined in standard test conditions (STC), optimizing the device layer stack in terms of perovskite bandgap and thicknesses of all the layers. Using simulations, one could easily compare the PCE potential of single-junction devices with tandem devices, either in monolithic 2T, 3T, or 4T configurations. Importantly, we could also optimize device fabrication toward record PCEs, measured at certification labs under STC.

While this is necessary to reach high certified PCEs, the outdoor conditions often significantly defer from STC, both in temperature, irradiance intensity, and its spectra. In particular, temperature and spectra influence the ratio between the currents produced in the subcells and their current matching [360,361]. For example, the irradiance spectra in several different Köppen-Geiger-Photovoltaic climate zones [362] in USA (National Renewable Energy Laboratory [NREL] database) is blue-rich, causing more current in the top cell compared with the AM1.5 condition and consequently not extracting all the potential from the tandem device. Thus, the AM1.5 optimization is often not the perfect case for best outdoor operation (Fig. 26(c)). Instead, a more thorough analysis involving EY calculations have soon appeared, providing fairer comparison through better and more complete results [349]. Optimizing tandem device architectures (in most cases this means perovskite bandgap and potentially also its thickness [363,364], Fig. 26(d) for maximal generated energy over the year has shown that wider perovskite bandgaps are required in case of blue-rich spectra. This result is not only important for tandem design to achieve the highest energy generation but also from stability perspective, since wider perovskite bandgap is obtained with higher bromide content and, thus, more prone to phase segregation [365].

Typical applications of EY in perovskite-based tandem research have been calculations of energy produced at different geographical locations. This allows comparison between sunnier and cloudier places as well as hotter, colder, and rainier. It can even indicate if the device stack has to be adapted for different locations or climate zones. Due to availability of the input weather dataset, such calculations have mostly been applied to locations within USA (Fig. 26). Similarly important are also comparisons

Figure 26

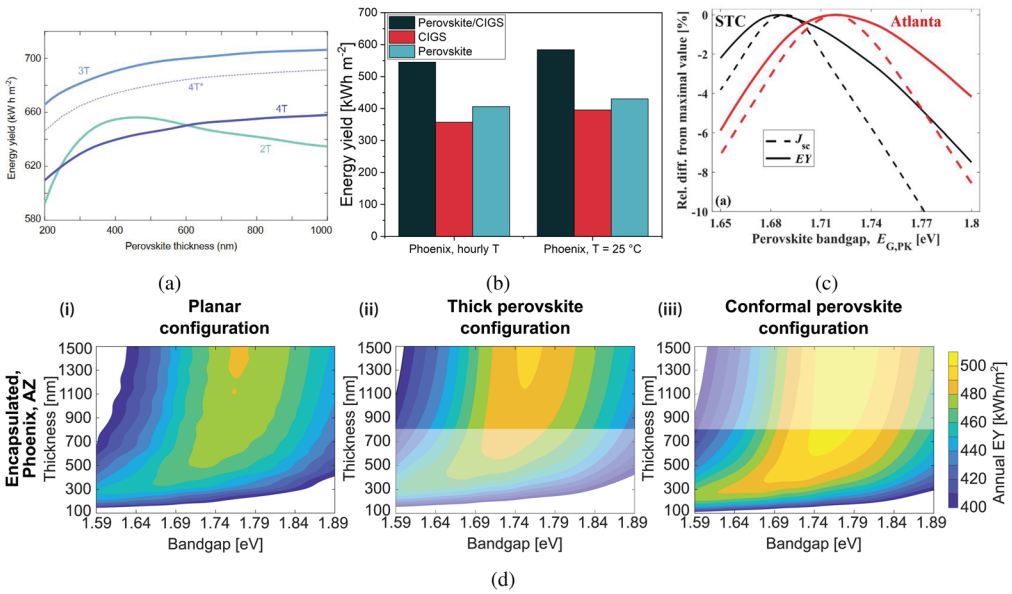

(a) Annual EY as a function of the perovskite thickness for 2T, 3T, and 4T architectures. Results for state-of-the-art morphologies: double-textured c-Si bottom cell, with conformal perovskite top cell in 2T and 3T architectures and planar top cell in 4T architecture are illustrated with solid lines. Results for a hypothetical 4T architecture with textured perovskite top cell, labeled as 4T*, are drawn with a dashed line. The bandgap of the perovskite layer is 1.72 eV. (b) EY of perovskite/CIGS, CIGS, and perovskite technologies. Encapsulated devices were considered. Bars on the left show the case where hourly temperatures (daily profiles) were considered, whereas the bars on the right show results where temperature was fixed at 25°C. (c) Relative losses of short-circuit current density and EY as a function of the perovskite bandgap for the cases of STC and Atlanta-specific realistic operating conditions. (d) Contour plots showing the PCE as a function of perovskite bandgap and thickness for encapsulated tandem solar cells with planar (i), thick perovskite (ii), and conformal perovskite (iii) morphologies. (a) Reprinted from Joule, **4**, Gota *et al.*, "Energy yield advantages of three-terminal perovskite-silicon tandem photovoltaics," 2387–2403, Copyright 2020 [348], with permission from Elsevier. (b) Reprinted from [262] under a Creative Commons license. (c) Reprinted from [349] under a Creative Commons license Creative Commons license. (d) Adapted from [364] under a Creative Commons license.

between single-junction and 2T or 4T devices (Fig. 26), as well as the analysis of bifacial modules that are entering the market as a single-junction technology but might become profitable also for the tandems [255,256]. Such calculations can present accurate benefits of tandem architecture and can also serve as guidelines for business models. For example, if the perovskite/silicon tandem produces 40% more energy than silicon single-junction device, then the additional costs of perovskite fabrication should not exceed 40%. Finally, static, one-axis or two-axis tracking operation can be efficiently estimated with EY [366]. The tracking can increase the generated energy by 30%, however, the amount of energy for tracking and cost of the tracking system often make such systems unprofitable.

10.3. EY in Bifacial PV: Challenges and Opportunities

In assessing realistic irradiance conditions, it becomes evident that the incident illumination in real-world applications of solar modules is not solely derived by direct

Figure 27

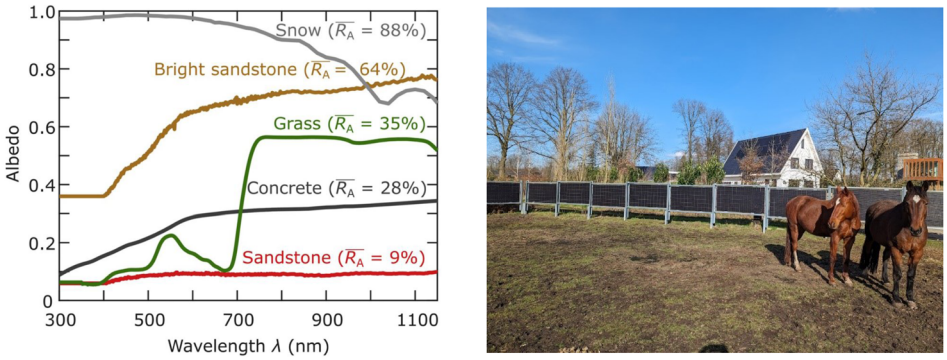

(a) (b)

(a) Reflection spectra of grounds used for the simulation of albedo irradiance. In addition, the mean albedo of each ground in the wavelength range of 300–1150 nm is specified in the legend. Reprinted from Sol. Energy Mater. Sol. Cells, **208**, Lehr *et al.*, "Energy yield of bifacial textured perovskite/silicon tandem photovoltaic modules," 110367, Copyright 2020 [254], with permission from Elsevier. (Original data taken from ecosystem spaceborne thermal radiometer experiment on space station (ECOSTRESS) spectral library.) (b) Bifacial solar fence used for a horse pasture.

sunlight and light diffused at the sky (i.e., clouds). Surrounding elements such as the ground and buildings also reflect light, contributing significantly to irradiance from below [367,368]. This phenomenon, typically measured as albedo or the reflectivity of a surface, plays a crucial role in determining the overall irradiance. For instance, water surfaces, with an albedo of less than 10%, absorb most sunlight, whereas snow, with an albedo of 90%, reflects nearly all incoming light. Given that the energy output of a solar power installation is highly sensitive to the incoming light spectrum, the spectral characteristics of albedo are vital for optimizing solar EY, as depicted in Fig. 27(a), which illustrates the spectral albedo of common surfaces.

Scattered light, emanating from both the sky and terrestrial surroundings, necessitates the design of solar modules capable of capturing light from multiple directions. Bifacial solar panels, which harness light from both their front and rear faces, have emerged as a solution, enhancing EY through novel configuration possibilities [369]. However, the integration of albedo light from various angles, combined with new application scenarios, significantly complicates accurate yield forecasting. To address this, recent efforts have focused on employing optics and optical simulation techniques [370–375] to refine EY predictions for bifacial installations under realistic conditions [367,368]. Such analyses must account for the spectral [376–380] and angular [367,368,381] distribution of incoming light, alongside realistic reflections on system losses and gains, necessitating advanced irradiance models or measurements and detailed optical simulations. This complexity underscores the need for efficient algorithms [382] capable of navigating vast datasets and multidimensional parameter spaces, presenting a ripe area for research and development within the optics community. The incorporation of machine learning and artificial intelligence stands to significantly expedite this process.

The International Technology Roadmap for Photovoltaics (ITRPV) 2024 [3] highlights the growing dominance of bifacial solar cells, which currently constitute 85% of the market, with projections suggesting an increase to 90% over the next decade. Although not all these cells are utilized in bifacial modules, the market share of such modules is

expected to rise from 50% to over 70% by 2034. This trend is buoyed by the enhanced performance and versatility afforded by bifacial technologies. Notably, applications such as bifacial solar fences (e.g., Fig. 27(b)) and sound barriers [383–385] are gaining traction. In addition, the burgeoning field of agriphotovoltaics (AgriPV), which synergizes PV systems with agriculture [386–391], stands to greatly benefit from bifacial technologies. Initial deployments integrating PV with crop cultivation and livestock rearing have yielded promising outcomes. In this context, optical modeling and optimization are paramount for enhancing yield predictions and achieving a balance between energy production, agricultural productivity, and aesthetic considerations. Vertical bifacial PV systems facing east and west also offer the potential for more evenly distributed energy generation throughout the day and across seasons, optimizing output in the morning and evening [369,390,392] and boosting the EY during winter [393,394].

10.4. Advances Required

In conclusion, EY modeling for PV is critical for accurately predicting the amount of electricity generated by solar panels over time. In the context of advancing optics for solar energy harvesting, EY modeling is of uttermost relevance for the following reasons:

Performance prediction: EY modeling allows scientists to accurately predict the performance of optics in solar cells/modules for a wide variety of application scenarios (e.g., different locations, orientations, tilt angles, and weather patterns). By simulating these scenarios, scientists can make informed decisions regarding the suitability of a novel optical component, coating or device architecture for the envisaged application scenario. For example, the optimal module orientation or color of a solar module can be determined even for nontrivial application scenarios, such as building integrated PV or bifacial PV.

Device optimization: EY modeling serves as a crucial tool for researchers and developers working on advancing PV technology. By simulating the performance of novel materials, new device architectures, and emerging PV technologies, scientists can identify promising avenues for research and development to enhance the efficiency, reliability, and affordability of PV systems. A prominent recent example in this regard are the multiple EY studies on perovskite/silicon tandem PV that are essential to guide the research on optimizing device architectures for this technology.

Assessment of imperfections and failures: EY modeling allows for the assessment of the actual performance of PV systems in real-world conditions. By considering factors such as device degradation, soiling, shading, unexpected weather conditions, and system losses, EY models provide insights into how much electricity a PV system will produce over its operational lifetime even in non-optimal installation conditions. In this regard, a very prominent research topic in the future will be in assessing the long-term performance of new PV technologies, such as perovskite-based tandem PV. However, for inclusion of long-term EY it is necessary to understand the optoelectronic performance of the studied devices. Thus, the theoretical application of EY modeling heavily depends on obtaining experimental data through thorough outdoor and lab testing. Several studies have already tried to connect indoor and outdoor testing results [359,395].

Cost–benefit analysis: The performance of PV systems is assessed by a variety of key performance indicators such as levelized cost of electricity, energy payback time emissions per kilowatt-hour, or resource efficiency. For all these performance

indicators, energy modeling is required to determine the lifetime energy production of a PV system under realistic conditions. In conclusion, EY modeling is essential for optimizing the performance, economic viability, and integration of PV systems into the energy landscape. By accurately predicting energy production and assessing the feasibility of solar projects, EY modeling plays a crucial role in advancing PV and, in particular, optics in PV.

11. COLOR AND AESTHETICS OF PV MODULES

J. C. Ortiz Lizcano, O. Isabella, B. Bläsi, and M. Schmid

The construction sector is one of the most significant contributors to greenhouse gas (GHG) emissions with an estimated global share of 35% [396]. The International Energy Agency (IEA) reports that by 2060, projected population growth will require an additional 240 million square meters of built area, representing the largest increase in human history [397]. The urban environment must transition from an energy consumer to an active producer. To achieve this goal, policies around the world aim to ensure that buildings meet near-zero energy standards in the near future. For example, Europe aims to mandate zero-energy housing by 2030, the United States is looking to retrofit half of its commercial building sector and transform them into net-zero projects, and similar efforts are beginning to occur in Australia, China, and Japan, to name a few [398]. Efforts toward a near-zero energy infrastructure include reducing the carbon footprint of materials used in the building sector, improving the energy performance of residences and office buildings, and the production of energy on site [399].

Installation of PV systems on site is becoming a common way to improve the energy performance of buildings. PV systems are versatile and straightforward, since their basic layout is consistent in small-, medium-, and large-scale topologies that require very moderate maintenance [400]. The implementation of PV systems in buildings is usually classified into two categories: building-added (or attached) photovoltaics (BAPV), where the modules are installed on existing building surfaces (such as roofs); and building-integrated photovoltaics (BIPV), where photovoltaics (PV) modules act as the building envelope, replacing conventional materials used for this purpose, such as facades and skylights [345].

BIPV systems are also an excellent alternative for renewable energy production in densely populated areas where land use is limited and needs to be reserved for other human activities, such as farming and preservation. By 2022, the BIPV market was valued at USD 19.82 billion with a projected compound annual growth rate (CAGR) of 21% until 2030, reaching USD 89.80 billion [401]. Experts have highlighted the importance of incorporating BIPV projects since the design stage of new building developments, particularly considering their aesthetic appeal [402]. Shape, texture, and color have been proven to be essential in accepting BIPV products, both for architects and homeowners [400,403]. Color, in particular, has been shown to be a critical factor in adoption, brand recognition, and purchasing decisions [404]. Studies indicate that potential customers are willing to pay premium prices for a colored BIPV system, and they are preferred over standard BAPV systems based on standard dark blue and black colors [405]. Discrete integration of PV energy is essential in heritage buildings [406,407], and stakeholders in rural and urban areas prefer to harmonize the color of PV modules with their surroundings [408]. This work summarizes the research and industrial efforts on the most commonly used coloring techniques in the production of BIPV modules. Note that these same approaches also apply to BAPV solutions.

11.1. Challenges for Colored BIPV Systems

The Photovoltaic Power Systems Division (PVPS Task 15) of the IEA categorizes the integration of PV modules into buildings by three main areas: roofs, facades, and external integrated devices [409]. Each of these functions can be divided into different categories of applications. For example, roofs can be divided into discontinuous, continuous, and atrium/skylights. Facade applications include rain screens, double skin, curtain walls, windows, and masonry walls. External devices can be parapets and balustrades or canopies and shading structures. One of the most challenging aspects

Figure 28

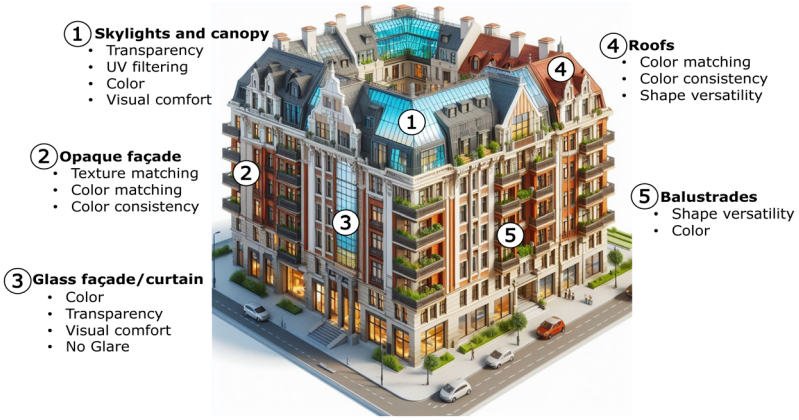

Different integration applications within the building environment. **1**, Skylight or canopy. **2**, Opaque facade. **3**, Glass facade/glass curtain. **4**, Roofs. **5**, Balustrades or external devices. Each application has its particular technical challenges. Image generated via Microsoft Designer – Dall·E3 image creator using the following query: *A colored 3D model of a European heritage apartment building with a portion of its roof as a glass ceiling.*

of BIPV products is that each application has specific technical requirements. These requirements range from fire safety certification, mechanical resistance, hygrothermal performance, and electrical insulation, among others [410]. Regarding the color appearance, Fig. 28 presents the main technical requirements for BIPV modules for every integration application. Depending on their applications, color PV modules can be required to be completely opaque, such as when replacing masonry facades, roofs, and specific external devices, or they can require certain levels of transparency.

For the case of opaque PV modules, one of the main requirements is to conceal its active area and mimic a wide variety of colors commonly used in the construction sector, such as those defined by the RAL system [411]. Color matching is essential for renovation projects that involve heritage buildings, where the aesthetic of the building must be maintained [412]. If PV modules replace masonry, architects are reluctant to implement them due to their glass-pane appearance and feel, so trying to match the texture of the material is important for this application [413]. The replacement of large facades and roofs can involve the use of a large number of PV modules, making color consistency essential. The coloring technique must ensure color stability at different observation angles and a reliable manufacturing process, ensuring minimal discrepancies between modules. The availability of bright colors is also preferred by architects and consumers, but glare should be avoided as it reduces visual comfort and can become a safety hazard [414].

Integrating PV into canopies, skylights, glass facades, and fenestration requires semi-transparency that ensures external and internal visual comfort. Internal visual comfort is estimated based on the color temperature and the color rendering index of the incoming ambient light [415]. This requirement represents an additional challenge for the PV module that replaces the glass structure and any color module whose reflectance can affect its surroundings.

The manufacturing techniques used to produce color PV must meet the above-mentioned requirements and be easily scalable and economically feasible for their market to reach terawatt scales of production. Moreover, the produced color must have a reliability equivalent to or superior to that of the PV module. BIPV products must

have lifetimes similar to the building materials they replace, so the coloring technique should not interfere with this objective by producing colors that change or fade after a few years.

The technological and economic evaluation of a BIPV system requires a complete understanding of the expected electrical performance, the available financial incentives, the social and environmental benefits, and other regulatory frameworks required for its installation. Gholami *et al*. [416] found that a life cycle analysis evaluation that considers this demonstrates that BIPV systems can become economically feasible. The authors expanded the methodology from the European scenario [417] to other places, such as Brazil, China, and Bahrain, obtaining similar conclusions. From a performance perspective, Zimmerman *et al*. [418] found that module efficiency and lifetime were critical parameters to verify whether a vertically mounted PV system could achieve levelized cost of electricity (LCOE) values similar to grid prices in the US.

Understanding the effect of coloring a PV device requires a combination of colorimetry, optical, and electrical models. Human color perception of a nonluminous object is modeled based on the CIE standard observer [419], which quantifies the chromatic response of human vision [420,421] to stimuli from a given light source and the observed object reflectance. The result of these calculations is the three-dimensional *XYZ* color space, which is the basis for deriving various alternatives using transformation matrices [422]. The most commonly used color spaces are sRGB, CIE La*b*, and hue, chroma, and luminosity (HCL). The last one is beneficial, as it is the basis of the formula for color difference [423]. This factor denoted ΔE_{00}, quantifies the difference between two colors and represents a valuable figure of merit for the validation of computational models and the analysis of color consistency. Theoretically, studies have estimated the maximum efficiency achievable in a colored PV device. Peharz and Ulm [411] and Halme and Mäkinen [424], for example, calculated that colors can induce relative power losses between 5% and 20% compared with a perfectly absorbing device. Both authors concluded that the most important colorimetry parameter is the luminosity (brightness) of the color, and the most affected performance parameter was the photogenerated current on the solar cells due to the reflectance loss needed to provide color.

The main challenge in modeling the electric yield of color BIPV systems is to accurately calculate the irradiance that effectively reaches the solar cells. Since the relationship between the output power of a PV module is nearly linear with the irradiance it receives, inaccuracies in estimating this parameter can lead to important errors in the obtained EY. Although several studies have focused on finding ways to reliably estimate this power output under the complex surrounding conditions of urban installations for standard modules [425–429], the same is not currently available for color modules. The additional reflectance loss and its spectral dependence on the coloring technique increases the complexity of accurately estimating the expected electrical efficiency. Furthermore, coloring a PV module has the potential to reduce its operating temperature [430], which can have a significant effect on its reliability [431]. A modeling tool that considers color perception, color stability, accurate EY, accurate operating temperature, and expected lifetime is instrumental to studying the feasibility of color BIPV products.

11.2. Approaches for Coloring BIPV products

Several techniques have been developed to provide color to PV modules. This section presents the techniques that have reached, or have the potential of reaching, large-scale production. Substantial information on all different coloring approaches can be found

Figure 29

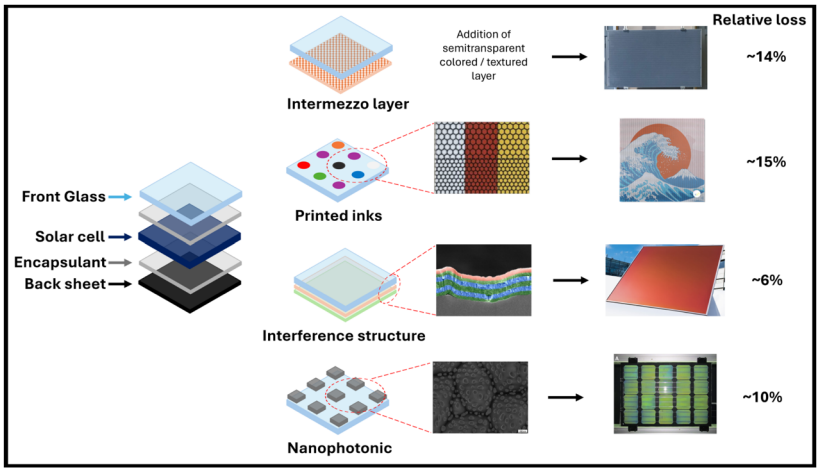

Coloring techniques for opaque PV modules. These techniques aim at concealing the active area (solar cells). From top to bottom: Color textiles or layers can be added to any of the front layers of the module to change its color appearance. © 2021 IEEE. Photograph used, with permission, from Gewohn *et al*., IEEE J. Photovoltaics, **11**, 138–143 (2021) [438] (permission conveyed through Copyright Clearance Center, Inc.). Digitally printed inks. Photographs reprinted with permission from Kameleon Solar [439]. Interference structures that selectively reflect light via interference effects. Image and photograph reprinted from [440] under a Creative Commons license Creative Commons license. Nanostructures that produce wavelength specific light scattering. Photographs reprinted from Renewable Energy, **109**, Peharz *et al.*, "Application of plasmonic coloring for making building integrated PV modules comprising of green solar cells," 542–550 [441], Copyright 2017, with permission from Elsevier. The last column indicates the reported average relative efficiency loss compared to a standard PV module.

in the review works by Meddeb *et al*. [432], Sehati *et al*. [433], Basher *et al*. [400], and Li *et al*. [434].

In practice, the coloration of PV modules is done using a wide variety of techniques. These techniques can be applied directly to the solar cells or at the module level by adding or coloring a layer of the PV module, such as the front glass, the encapsulant, or the back sheet. Examples of these different levels of application are found in the work of Pelle *et al*. [435], Kutter *et al*. [436], and Lisco *et al*. [437].

11.2a. Opaque PV Modules

For opaque PV modules, four techniques have industrial terawatt-scale potential given their large-area feasibility, high industrial throughput, and minimal effect on the standard manufacturing process of solar cells and PV modules. These techniques are summarized in Fig. 29 and are presented starting from those based on readily available industrial methods to those with potential for industrial production.

***Intermezzo* or added color layer**. This refers to retrofitting existing commercial PV modules to change their color. These approaches are based on techniques available in other industrial sectors, but are tailored to PV modules. An example is presented by Gewohn *et al*. [438], who developed imprinted textiles that can be laminated to existing PV modules via an inkjet hybrid printer using a halftone technique. The results show that the technique can effectively change the color of a standard PV module with current losses in the range of 15%.

Another example of intermezzo layering is the work of Morlier *et al.* [413] which proposes a way to provide standard PV modules with the look and feel of stone veneer sheets using different stone laminates. The main drawback of this method is its significant power loss. Relative losses for stone-shaped samples ranged from 47% to 76%. However, the successful integration of these aesthetic options is a promising starting point for future research.

Masuda *et al.* [442] carried out experiments to understand the feasibility of using automotive paints in PV modules. The aim was to investigate which of the best painting techniques commonly used in the automotive industry was suitable for manufacturing potential lightweight PV modules. The study concluded that mica pigments could confer a rich color to the module while maintaining a relatively high level of light transmittance, with relative efficiency losses around 20%.

Microscopic ink patterns on the front glass consists of creating patterns (such as dots or hexagons) separated in such a way that, at a distance, it is impossible to discern by the human eye. Basher *et al*. [443] present a concept that consists of creating a 50 μm separated dot pattern printed on glass using a ultraviolet (UV)-sensitive white ink (UV-curable technique). The area of glass covered by the ink transmits light within the UV and near-infrared (NIR) regions, while the gaps transmit the whole light spectrum. The result, from a distance, is a fully concealed PV module. Shin *et al*. [444] tested the screen printing method to create single-color PV modules. The technique prints the dotted pattern directly onto low iron glass and then fires it at high temperature to ensure adhesion. Riedel *et al*. [445] found that for ceramic inks applied via digital printing, the optical and electrical performance was almost independent of the geometry of the microscopic pattern. The aesthetic potential of this technique is essentially limitless, since any high-resolution image can be used to create any design of the PV module. The most commonly used techniques to apply color, silk screen printing, digital UV-printing and digital ceramic ink printing, all reach industrial scale status for large-scale production. In addition, digital ceramic ink printing has proven reliability. Kameleon Solar, for example, claims that this technique provides coloring with a useful life of close to fifty years [439].

Despite its aesthetic potential, the colors obtained through this technique have comparatively limited saturation values [436]. Furthermore, the absorptive nature of inks can produce significant relative losses, some colors almost halving the electrical output [445]. Modeling the effect of this technique is time-consuming and complex, and care must be taken in the design of the pattern as excessive irradiance inhomogeinity on the solar cells can lead to performance and reliability problems.

Interference structures are one of the most-studied techniques for coloring PV modules. These devices offer the advantage of producing color without absorbing dyes, thus reducing unnecessary optical losses. In addition, color saturation can be maximized by creating reflectance spectra that can be similar to those of a monochromatic source. They are manufactured by depositing thin dielectric layers in a given sequence (alternating high and low refractive indices). The width of reflectance around the created peak depends to some extent on the difference in the refractive index of the materials used [446]. Macleod [447] provides an in-depth mathematical approach to the engineering possibilities of these optical systems.

The materials most commonly used, given their suitable optical properties, are titanium dioxide TiO_2, silicon nitride SiN_x, silicon dioxide SiO_2, and magnesium flouride MgF_2. Soman and Antony [448], Røyset *et al*. [449], Wessels *et al*. [450], Ingenito *et al.* [451], Ortiz Lizcano *et al*. [430], and Bläsi *et al*. [440] present comprehensive examples of the aesthetic potential of this approach. Furthermore, this approach has

reached commercial status, due to manufacturing techniques readily available within the PV industry, such as sputtering and atomic layer deposition. Products such as those offered by LOF Solar [452], Soluxa [453], Kromatrix™ [454], and Megasol [455] are based on this technique. Similarly to the case of nanostructures, the relative losses reported using this technique are among the lowest. Bright colors can have relative losses as low as 5%.

One of the main drawbacks of interference structures is poor color stabilization and the potential to create significant glare. However, several studies have provided approaches to ameliorate these obstacles. Stabilizing color perception at different angles of observation represents an essential challenge for these devices. Bläsi *et al*. proposed the deposition of these optical systems on textured glass surfaces. This layout creates a three-dimensional interference structure named MorphoColor [440], which improves the stability of the color at different angles of observation. Furthermore, the use of second-harmonic designs made with materials with a high refractive index (such as TiO_2) can help create bright and stable colors. Similarly, a glass-based texturization layout with inverted pyramids on the front side and random texturing on the back, where the structure is deposited, provides excellent color stability for observation angles up to 80° [430]. Jolissaint *et al*. [456] also provide insight into how texturing the front glass helps reduce unwanted glare effects and helps conceal the solar cells. The above-mentioned works are only a few examples of approaches to coloring PV modules based on interference structures; other contributions using this approach include Rudzikas *et al*. [457] and Xu *et al*. [458].

Nanostructures exploit the effects of wavelength-specific light absorption and scattering and have been shown to be successful in the coloration of PV devices and modules. Perharz *et al*. [441] demonstrated the potential of this technique by applying metallic nanoparticles (NP) structures based on silver (Ag). The authors deposited thin Ag films on a commercial monocrystalline surface using DC sputtering, followed by an annealing process at 300°C, thus creating a coating based on Ag NPs. The second row of Fig. 29 presents scanning electron microscopy (SEM) images of Ag NPs deposited on the surface of the pyramidal-textured solar cell with sizes ranging from 50 to 150 nm. These NPs create plasmonic scattering that produces a reflectance peak at 500 nm. This shift in reflectance changes the perceived color from blue to green.

Similarly, Neder *et al*. [459] demonstrated that green colors could be produced by using c-Si nanocylinders that scatter light at a wavelength value around 540 nm. Other colors have also been proven by Uleman *et al*. [460] with the design of semitransparent meta-grating based on silicon nanowires. The layout allowed control of light scattering over a wide range of angles by modulating the pitch of the structures, the final design provided a red, matte appearance that emulates roof materials. Zhou *et al.* [461] also studied the aesthetic potential of using a PMMA matrix that contains NPs based on $Si\text{-}SiO_2$ core shells. In general, the reported relative efficiency losses of nanostructural approaches ranged from 2% [462] to 13% [460]

The use of metal-based nanostructures has the disadvantage of inducing absorptive losses that hinder the electrical output of the PV module; however, alternative dielectric-based structures could reduce this problem. The main advantage of this approach is its unique ability to modulate light in a wavelength-dependent manner using a single layer. In this respect, the fundamental principles of obtaining colors using these structures is well known [463], as is their application in PV devices [59]. However, to date, only single-module demonstrators or small-area devices have been showcased. The technique is still in its infancy when it comes to mass production, with no clear method that could be translated into a large area, reliable, and cost-effective

industrial application. However, some recent approaches, such as that presented by Das Gupta *et al.* [464], offer promising results in terms of versatility and potential scalability.

11.2b. Semitransparent PV Modules

For integration layouts that require transparency, such as glass facades, skylights, and canopies, thin-film-based PV modules have reached a significant level of maturity at the industrial level. The same approaches discussed for opaque PV modules can be applied to provide color to semitransparent modules. As stated in the previous section, the challenge is to provide the transmitted spectra required according to the application. For indoor office lighting, semitransparency and color must comply with health and safety requirements [415]. In applications such as agrivoltaic systems, the quality and nature of the incoming light spectra can affect the quality and growth of the produce [465]. This means that the design of the product must consider both color transmittance and color reflectance. Kim *et al*. [466] demonstrate that nanostructures made with SiO_2 and TiO_2 in hexagonal patterns can create colorful CIGS solar cells. Yoo *et al*. [467] presented coloring concepts for CIGS solar modules based on a triple-layer photonic crystal made with SiO_2 and TiO_2. The authors focused on semitransparent modules and presented designs for a blue, yellow, and red PV module for window applications.

Amorphous silicon (a-Si:H) is an extremely versatile technology with respect to customized modules with different levels of transparency. Lee *et al*. [468] created semitransparent colored solar cells based on thin films of a-Si:H and cuprite Cu_2O. Myong and Jeon [469] discuss ways to produce colored and semitransparent glass-to-glass (GTG) PV modules based on a-Si:H solar cells, including the use of colored materials for encapsulation and transparent contacts. Given the transparency achievable in solar cell fabrication, the colored layer is placed on the back side of the active area, thus avoiding optical losses. Neugebohrn *et al.* [470] focused on the use of oxide–metal oxide stacks made of aluminum-doped zinc oxide ZnO:Al and silver in $Cu(In,Ga)Se_2$ solar cells. Adjusting the physical properties of this stack changed the color produced.

Products based on this solar cell technology have an outstanding level of maturity and development. Onyx Solar [471] is one of the largest BIPV manufacturers in the world, with a significant portfolio of projects, many of which are based on semitransparent and even colored a-Si:H PV glass. Their main drawback, compared with potential new alternatives (semitransparent c-Si-based products, perovskite approaches), is their lower PCE, which, depending on their level of transparency, can range between 4% and 10%.

11.3. Advances Required to Meet Future Challenges

In general, a wide range of coloring techniques have reached industrial-scale technological readiness. For example, products based on microscopic ink patterns and interference structures are now readily available with all the necessary conditions to evolve into a terawatt-level market. Nanophotonic structures, in contrast, still need significant technical development to reach this same status, but their advantage of wavelength modulation with only one applied layer represents a promising approach for industrial applications. Other approaches using add-on layers (here called *intermezzo*) use established industrial processes and have the potential for rapid implementation. In general, the aesthetic potential and versatility of all these combined techniques offer unlimited design options to architects and customers.

Furthermore, color PV products can be produced with considerable electrical efficiency. Colors based on interference structures can induce relative losses well below 10%. Methods using nanophotonic structures have reported relative losses close to 10%. Other approaches, such as microscopic ink patterns and added color layers, result in higher losses. However, with c-Si modules reaching higher efficiencies, there is still the possibility of producing modules with all the techniques mentioned above with electrical efficiencies close to or above 20%.

However, some barriers remain. Pelle *et al*. [435] has highlighted the need for more comprehensive and accurate models for color BIPV modules. The main challenge is that the modeling needed usually requires detailed optical characterization of all the layers within the module. Any change in the layout or properties of these materials can produce a change in the behavior of the final product. For interference structures, modeling textured surfaces usually requires a complex combination of ray tracing techniques [256,472–474] and models based on the transfer matrix method [450,475]. A change in the textured pattern implies a reconfiguration of the model input. In addition, useful optimization algorithms that could reduce unwanted optical losses, such as the needle technique [476], are not yet available when working on texture surfaces with roughness in micrometers. For the case of ceramic inks, the transmittance of each of the materials and dyes used must be characterized to estimate their induced optical loss. Comprehensive CAD tools that address these aspects could reduce the time and costs required to develop new products.

More modeling efforts are needed to include the impact that any coloring technique can have on the operating temperature of a PV module. The published performance loss is usually estimated under laboratory conditions, where temperature effects are not taken into account. This may lead to an underestimation not only of the power output of a color PV module but also of its potential lifetime, both extremely important parameters in life cycle and LCOE analysis.

It is also important that researches and industry agree on a standard way of assessing color matching and color stability, particularly for applications in which these aspects are critical, such as heritage buildings or seamless integration into open environments. Some works utilize the CIEDE2000 color difference standard ΔE_{00}, which is defined in the HCL color space, whereas others use the CIE76 color difference standard ΔE_{76}, based on CIELAB. There are important differences between these two approaches, especially in terms of perceptual uniformity. Standardizing these approaches, as well as the limiting values of perceived color differences according to different hues, is essential to guarantee excellence in the final product. In this sense, Borja Block *et al*. [477] proposes the use of an innovative large area colorimeter that allows to accurately characterize the color of BIPV products.

Data sheets for color BIPV products should be more oriented toward the building sector. The performance of a given BIPV product will depend on the layout of the installation. Information about expected performance in different orientations and integration layouts could be beneficial to their marketing. For example, a company that offers substantial information for a preliminary feasibility study is Onyx Solar [478]. Based on their experience, they developed a tool that allows potential users to estimate the environmental and economic benefit, per meter squared, of the implementation of any of their solutions. This can be assessed for two different module technologies (c-Si and a-Si:H) for four different types of orientation. These initiatives are key in generating better engagement with end users.

12. CONCLUSION

C. Becker and K. Jäger

In this article, we have presented a selection of optical research topics that we currently, as of late 2024, consider to be crucial for the further expansion of PV on a terawatt scale. We were guided by the following question.

Where can innovative optical concepts be used to accelerate the further expansion of PV and, thus, the transformation of the energy system?

We started with two sections that summarized the current state of photovoltaics (PV) and classic light management concepts in solar cells. Based on the challenges identified to promote the expansion of PV, we addressed the following optical research topics in the subsequent sections: The development of ecofriendly and earth-abundant optical materials enabling the sustainable production of PV cells on terawatt scale. With the aim of achieving higher power-conversion efficiencies, we selected the topics luminescent processes in the solar cells, the optics of multijunction solar cells and spectral shaping. For an extension of the module lifetime and a maximization of energy yield (EY), we discussed the topics thermal management and accurate EY predictions. Finally, we treated the importance of color and an aesthetic appearance of the modules aiming at a broad social acceptance of PV in the built environment. At the end of each section we identified optical advances that need to be addressed in the coming years.

FUNDING

Slovenian Research and Innovation Agency (ARIS) (P2-0415); U.S. Department of Energy (DE-SC0001293, DE-SC00019140); H2020 European Research Council (947221, 101125948, 101084046); Bundesministerium für Wirtschaft und Klimaschutz ("50Prozent" (03EE1060), "PV-Hide" (03EE1049A), "micro-CPV" (03EE1046A)); Fraunhofer-Gesellschaft (ICON grant "MEEt"); Ministerstvo Školství, Mládeže a Tělovýchovy (LUASK 22202, PVKSC 9F23003); Berlin Mathematics Research Center MATH+ (390685689).

ACKNOWLEDGMENTS

This article was conceptualized during the 4th International Workshop on Optics for Solar Energy, which was held in Berlin, Germany, on 9 and 10 October 2023. This workshop was financially supported by the Helmholtz-Zentrum Berlin für Materialien and Energie GmbH, Germany. The authors thank Dr. Osbel Almora Rodríguez from Universitat Rovira i Virgili (URV), Tarragona, Spain, for providing the data of Fig. 19. O.H. received funding from the European Research Council (ERC) under the grant PHASE (No. 101125948). U.A. acknowledges the support from Simon Zeder and the Setfos development team at Fluxim. H.S. thanks Dr. Takashi Koida and Dr. Takuya Matsui of AIST for fruitful discussion and collaboration. E.Y. and Z.O. have benefited from many insights and suggestions by the solar cell authority, Dick Swanson. The work of B.E. and E.A.L. is part of the Dutch Research Council (NWO) and was performed at the research institute AMOLF. B.E. received funding from the ERC under the European Union's Horizon 2020 research and innovation programme under grant agreement No. 947221. K.J., S.B., P.M., and C.B. performed their work at the Berlin Joint Lab for Optical Simulations for Energy Research (BerOSE) of Helmholtz-Zentrum Berlin für Materialien und Energie, Zuse Institute Berlin, and Freie Universität Berlin.

DISCLOSURES

U.A.: Fluxim AG (E); S.B.: JCMwave GmbH (I,E); J.M. (P); P.M.: JCMwave GmbH (E); A.P.R. (P). The authors declare no conflicts of interest.

DATA AVAILABILITY

The data presented in Fig. 12 are available from W.F. (wilfried.favre@cea.fr) on reasonable request. Further, no data were generated or analyzed in the presented research.

REFERENCES

1. Global Solar Council, "Global Solar Council announces 2 terawatt milestone achieved for solar," (2024). https://www.globalsolarcouncil.org/news/global-solar-council-announces-2-terawatt-milestone-achieved-for-solar/.
2. N. M. Haegel, P. Verlinden, M. Victoria, *et al.*, "Photovoltaics at multi-terawatt scale: waiting is not an option," Science **380**, 39–42 (2023).
3. M. Fischer, M. Woodhouse, and P. Baliozian, "International technology roadmap for photovoltaics (ITRPV)—2023 results," Tech. Rep. (VDMA, 2024).
4. M. Fischer, M. Woodhouse, P. Baliozian, *et al.*, "International technology roadmap for photovoltaics—2022 results," Tech. Rep. (VDMA, 2023).
5. A. H. M. Smets, K. Jäger, O. Isabella, *et al.*, *Solar Energy: The Physics and Engineering of Photovoltaic Conversion Technologies and Systems* (UIT Cambridge, 2016).
6. J. W. Blakers, A. Wang, A. M. Milne, *et al.*, "22.8% efficient silicon solar cell," Appl. Phys. Lett. **55**, 1363–1365 (1989).
7. F. Feldmann, M. Bivour, C. Reichel, *et al.*, "Passivated rear contacts for high-efficiency n-type Si solar cells providing high interface passivation quality and excellent transport characteristics," Sol. Energy Mater. Sol. Cells **120**, 270–274 (2014).
8. H. Lin, M. Yang, X. Ru, *et al.*, "Silicon heterojunction solar cells with up to 26.81% efficiency achieved by electrically optimized nanocrystalline-silicon hole contact layers," Nat. Energy **8**, 789–799 (2023).
9. R. Kopecek, F. Buchholz, V. D. Mihailetchi, *et al.*, "Interdigitated back contact technology as final evolution for industrial crystalline single-junction silicon solar cells," Solar **3**, 1–14 (2023).
10. K. K. Markose, A. Antony, and M. K. Jayaray, "Solar cell technologies: an overview," in *Energy Harvesting and Storage — Fundamentals and Materials*, M. K. Jayaraj, A. Antony, and P. P. Subha, eds. (Springer, 2022), pp. 1–59.
11. M. A. Green, "The Passivated Emitter and Rear Cell (PERC): from conception to mass production," Sol. Energy Mater. Sol. Cells **143**, 190–197 (2015).
12. E. Bellini, "Jolywood claims 26.7% efficiency for n-type TOPCon solar cell," *PV Magazine* (2023). https://www.pv-magazine.com/2023/04/12/jolywood-claims-26-7-efficiency-for-n-type-topcon-solar-cell/.
13. E. V. Kerschaver and G. Beaucarne, "Back-contact solar cells: a review," Prog. Photovoltaics **14**, 107–123 (2006).
14. Longi, "LONGi sets a new world record of 27.3% for the efficiency of silicon heterojunction back-contact (HBC) solar cells," (2024). https://www.longi.com/en/news/heterojunction-back-contact-battery/.
15. M. Green, E. D. Dunlop, M. Yoshita, *et al.*, "Solar cell efficiency tables (Version 65)," Prog. Photovoltaics **33**, 3–15 (2025).

16. V. Raj, T. Haggren, W. W. Wong, *et al.*, "Topical review: pathways toward cost-effective single-junction III–V solar cells," J. Phys. D: Appl. Phys. **55**, 143002 (2022).
17. J. Li, A. Aierken, Y. Liu, *et al.*, "A brief review of high efficiency III–V solar cells for space application," Front. Phys. **8**, 631925 (2021).
18. H. Helmers, O. Höhn, D. Lackner, *et al.*, "Advancing solar energy conversion efficiency to 47.6% and exploring the spectral versatility of III–V photonic power converters," in *Physics, Simulation, and Photonic Engineering of Photovoltaic Devices XIII*, A. Freundlich, K. Hinzer, S. Collin, and I. R. Sellers, eds. (SPIE, 2024), p. 36.
19. H. Yao and J. Hou, "Recent advances in single-junction organic solar cells," Angew. Chem., Int. Ed. **61**, e202209021 (2022).
20. L. Zhu, M. Zhang, J. Xu, *et al.*, "Single-junction organic solar cells with over 19% efficiency enabled by a refined double-fibril network morphology," Nat. Mater. **21**, 656–663 (2022).
21. C. V. M. Vijila, A. Antony, and M. K. Jayaraj, "Perovskite solar cells: concepts and prospects," in *Energy Harvesting and Storage — Fundamentals and Materials*, M. K. Jayaraj, A. Antony, and P. P. Subha, eds. (Springer, 2022), pp. 97–133.
22. W. Shockley and H. J. Queisser, "Detailed balance limit of efficiency of *p-n* junction solar cells," J. Appl. Phys. **32**, 510–519 (1961).
23. P. Verlinden, "Future challenges for photovoltaic manufacturing at the terawatt level," J. Renewable Sustainable Energy **12**, 053505 (2020).
24. D. Bogdanov, M. Ram, A. Aghahosseini, *et al.*, "Low-cost renewable electricity as the key driver of the global energy transition towards sustainability," Energy **227**, 120467 (2021).
25. H. Dittmar, T. Garabetian, R. Fki, *et al.*, "Towards sustainable and massive deployment of photovoltaics: the nexus of socio-economic and technological challenges," Tech. Rep. (ETIP PV, 2023).
26. A. Urbina, "Sustainability of photovoltaic technologies in future net-zero emissions scenarios," Prog. Photovoltaics **31**, 1255–1269 (2022).
27. M. Libra, D. Mrazek, I. Tyukhov, *et al.*, "Reduced real lifetime of PV panels — economic consequences," Sol. Energy **259**, 229–234 (2023).
28. R. Saive, "Light trapping in thin silicon solar cells: a review on fundamentals and technologies," Prog. Photovoltaics **29**, 1125–1137 (2021).
29. M. Schmid, "Review on light management by nanostructures in chalcopyrite solar cells," Semicond. Sci. Technol. **32**, 043003 (2017).
30. M. A. Green, "Crystalline silicon solar cells," in *Series on Photoconversion of Solar Energy*, Chap. 4 (Imperial College Press, 2014), pp. 87–137.
31. J. Lindmayer and J. Allison, "The violet cell: an improved silicon solar cell," Sol. Cells **29**, 151–166 (1990).
32. R. S. Bonilla, B. Hoex, P. Hamer, *et al.*, "Dielectric surface passivation for silicon solar cells: a review," Phys. Status Solidi A **214**, 1 (2017).
33. A. Deinega, I. Valuev, B. Potapkin, *et al.*, "Minimizing light reflection from dielectric textured surfaces," J. Opt. Soc. Am. A **28**, 770 (2011).
34. E. Yablonovitch, "Statistical ray optics," J. Opt. Soc. Am. **72**, 899 (1982).
35. J. Haynos, J. Allison, R. Arndt, *et al.*, "The COMSAT nonreflective silicon solar cell: a second generation improved cell," in *Int. Conf. on Photovoltaic Power Generation* (1974), p. 487
36. J. Zhao, A. Wang, P. Altermatt, *et al.*, "Twenty-four percent efficient silicon solar cells with double layer antireflection coatings and reduced resistance loss," Appl. Phys. Lett. **66**, 3636–3638 (1995).

37. A. Ingenito, O. Isabella, and M. Zeman, "Nano-cones on micro-pyramids: modulated surface textures for maximal spectral response and high-efficiency solar cells," Prog. Photovoltaics **23**, 1649–1659 (2015).
38. Z. Yu, A. Raman, and S. Fan, "Fundamental limit of nanophotonic light trapping in solar cells," Proc. Natl. Acad. Sci. U. S. A. **107**, 17491–17496 (2010).
39. S. Bhattacharya and S. John, "Designing high-efficiency thin silicon solar cells using parabolic-pore photonic crystals," Phys. Rev. Appl. **9**, 044009 (2018).
40. B. Bläsi, M. Hanser, K. Jäger, *et al.*, "Light trapping gratings for solar cells: an analytical period optimization approach," Opt. Express **30**, 24762 (2022).
41. C. Battaglia, C.-M. Hsu, K. Söderström, *et al.*, "Light trapping in solar cells: can periodic beat random?" ACS Nano **6**, 2790–2797 (2012).
42. R. Cariou, J. Benick, F. Feldmann, *et al.*, "III–V-on-silicon solar cells reaching 33% photoconversion efficiency in two-terminal configuration," Nat. Energy **3**, 326–333 (2018).
43. P. Schygulla, R. Müller, O. Höhn, *et al.*, "Wafer-bonded two-terminal III–V//Si triple-junction solar cell with power conversion efficiency of 36.1% at AM1.5g," Prog. Photovoltaics **1**, 3769 (2024).
44. E. R. Martins, J. Li, Y. Liu, *et al.*, "Deterministic quasi-random nanostructures for photon control," Nat. Commun. **4**, 2665 (2013).
45. J. Xavier, J. Probst, F. Back, *et al.*, "Quasicrystalline-structured light harvesting nanophotonic silicon films on nanoimprinted glass for ultra-thin photovoltaics," Opt. Mater. Express **4**, 2290 (2014).
46. M.-C. van Lare and A. Polman, "Optimized scattering power spectral density of photovoltaic light-trapping patterns," ACS Photonics **2**, 822–831 (2015).
47. H. Hauser, K. Mühlbach, O. Höhn, *et al.*, "Tailored disorder: a self-organized photonic contact for light trapping in silicon-based tandem solar cells," Opt. Express **28**, 10909 (2020).
48. P. M. Piechulla, B. Fuhrmann, E. Slivina, *et al.*, "Tailored light scattering through hyperuniform disorder in self-organized arrays of high-index nanodisks," Adv. Opt. Mater. **9**, 2100186 (2021).
49. N. Tavakoli, R. Spalding, A. Lambertz, *et al.*, "Over 65% sunlight absorption in a 1 μm Si slab with hyperuniform texture," ACS Photonics **9**, 1206–1217 (2022).
50. D. Derkacs, S. Lim, P. Matheu, *et al.*, "Improved performance of amorphous silicon solar cells via scattering from surface plasmon polaritons in nearby metallic nanoparticles," Appl. Phys. Lett. **89**, 93103 (2006).
51. S. Pillai, K. R. Catchpole, T. Trupke, *et al.*, "Surface plasmon enhanced silicon solar cells," J. Appl. Phys. **101**, 093105 (2007).
52. K. Catchpole and A. Polman, "Plasmonic solar cells," Opt. Express **16**, 21793–21800 (2008).
53. H. A. Atwater and A. Polman, "Plasmonics for improved photovoltaic devices," Nat. Mater. **9**, 205–213 (2010).
54. M. Ihara, M. Kanno, and S. Inoue, "Photoabsorption-enhanced dye-sensitized solar cell by using localized surface plasmon of silver nanoparticles modified with polymer," Phys. E **42**, 2867–2871 (2010).
55. V. E. Ferry, M. A. Verschuuren, M. C. v. Lare, *et al.*, "Optimized spatial correlations for broadband light trapping nanopatterns in high efficiency ultrathin film a-Si:H solar cells," Nano Lett. **11**, 4239–4245 (2011).
56. R. A. Pala, J. S. Q. Liu, E. S. Barnard, *et al.*, "Optimization of non-periodic plasmonic light-trapping layers for thin-film solar cells," Nat. Commun. **4**, 2095 (2013).
57. H. Tan, R. Santbergen, A. H. M. Smets, *et al.*, "Plasmonic light trapping in thin-film silicon solar cells with improved self-assembled silver nanoparticles," Nano Lett. **12**, 4070–4076 (2012).

58. C. Pahud, O. Isabella, A. Naqavi, *et al.*, "Plasmonic silicon solar cells: impact of material quality and geometry," Opt. Express **21**, A786 (2013).
59. M. Schmid, P. Andrae, and P. Manley, "Plasmonic and photonic scattering and near fields of nanoparticles," Nanoscale Res. Lett. **9**, 50 (2014).
60. A. Basch, F. J. Beck, T. Söderström, *et al.*, "Combined plasmonic and dielectric rear reflectors for enhanced photocurrent in solar cells," Appl. Phys. Lett. **100**, 243903 (2012).
61. P. Spinelli, M. Verschuuren, and A. Polman, "Broadband omnidirectional antireflection coating based on subwavelength surface Mie resonators," Nat. Commun. **3**, 692–696 (2012).
62. J. Grandidier, D. M. Callahan, J. N. Munday, *et al.*, "Light absorption enhancement in thin-film solar cells using whispering gallery modes in dielectric nanospheres," Adv. Mater. **23**, 1272–1276 (2011).
63. C. van Lare, G. Yin, A. Polman, *et al.*, "Light coupling and trapping in ultrathin Cu(In,Ga)Se_2 solar cells using dielectric scattering patterns," ACS Nano **9**, 9603–9613 (2015).
64. M. Morales-Masis, S. De Wolf, R. Woods-Robinson, *et al.*, "Transparent electrodes for efficient optoelectronics," Adv. Electron. Mater. **3**, 1600529 (2017).
65. M. Morales-Masis, E. Rucavado, R. Monnard, *et al.*, "Highly conductive and broadband transparent Zr-Doped In_2O_3 as front electrode for solar cells," IEEE J. Photovoltaics **8**, 1202–1207 (2018).
66. T. Koida, H. Fujiwara, and M. Kondo, "Hydrogen-doped In_2O_3 as high-mobility transparent conductive oxide," Jpn. J. Appl. Phys. **46**, L685 (2007).
67. O. Kluth, B. Rech, L. Houben, *et al.*, "Texture etched ZnO:Al coated glass substrates for silicon based thin film solar cells," Thin Solid Films **351**, 247–253 (1999).
68. S. Fay, J. Steinhauser, N. Oliveira, *et al.*, "Opto-electronic properties of rough LP-CVD ZnO:B for use as TCO in thin-film silicon solar cells," Thin Solid Films **515**, 8558–8561 (2007).
69. Z. C. Holman, M. Filipic, A. Descoeudres, *et al.*, "Infrared light management in high-efficiency silicon heterojunction and rear-passivated solar cells," J. Appl. Phys. **113**, 013107 (2013).
70. A. Cruz, D. Erfurt, P. Wagner, *et al.*, "Optoelectrical analysis of TCO+Silicon oxide double layers at the front and rear side of silicon heterojunction solar cells," Sol. Energy Mater. Sol. Cells **236**, 111493 (2022).
71. H. Wang, H. A. Dewi, T. M. Koh, *et al.*, "Bifacial, color-tunable semitransparent perovskite solar cells for building-integrated photovoltaics," ACS Appl. Mater. Interfaces **12**, 484–493 (2020).
72. Y. Li, S. W. Tabernig, G. Yin, *et al.*, "Beyond light-trapping benefits: the effect of SiO_2 nanoparticles in bifacial semitransparent ultrathin Cu(In,Ga)Se_2 solar cells," Sol. RRL **6**, 2200695 (2022).
73. L. M. Einhaus, G. C. Heres, J. Westerhof, *et al.*, "Free-space diffused light collimation and concentration," ACS Photonics **10**, 508–517 (2023).
74. E. Bellini, "Light redirecting film to improve heterojunction solar module performance," *PV Magazine* (2023). https://www.pv-magazine.com/2023/03/17/light-redirecting-film-to-improve-heterojunction-solar-module-performance/.
75. C. Algora and I. Rey-Stolle eds., *Handbook of Concentrator Photovoltaic Technology* (Wiley, 2016).
76. S. A. Halasah, D. Pearlmutter, and D. Feuermann, "Field installation versus local integration of photovoltaic systems and their effect on energy evaluation metrics," Energy Policy **52**, 462–471 (2013).

77. N. Jost, T. Gu, J. Hu, *et al.*, "Integrated micro-scale concentrating photovoltaics: a scalable path toward high-efficiency, low-cost solar power," Sol. RRL **7**, 2300363 (2023).
78. M. Wiesenfarth, D. Iankov, J. F. Martínez, *et al.*, "Technical boundaries of micro-CPV module components: how small is enough?" in *AIP Conf. Proc.*, Vol. 2550 (2022), p. 030008.
79. C. Domínguez, N. Jost, S. Askins, *et al.*, "A review of the promises and challenges of micro-concentrator photovoltaics," in *AIP Conf. Proc.*, Vol. 1881 (2017), p. 080003.
80. T. Gu, D. Li, L. Li, *et al.*, "Wafer-level integrated micro-concentrating photovoltaics," in *Light, Energy and the Environment, PV* (Optica Publishing Group, 2016), p. PTh3A.1.
81. E. Kaiser, M. Wiesenfarth, P. Schöttl, *et al.*, "Two-step nested opto-electrical Monte-Carlo approach to analyze the impact of manufacturing tolerances on Micro-CPV module performance," in *Proceedings of the 19th International Conference on Concentrator Photovoltaic Systems (CPV-19),* (2024).
82. K. Sato, K. Ito, S. Hata, *et al.*, "Self-alignment of microparts using liquid surface tension—behavior of micropart and alignment characteristics," Precis. Eng. **27**, 42–50 (2003).
83. M. Mastrangeli, Q. Zhou, V. Sariola, *et al.*, "Surface tension-driven self-alignment," Soft Matter **13**, 304–327 (2017).
84. V. Vareilles, E. Kaiser, P. Voarino, *et al.*, "Experimental and simulative correlations of the influence of solder volume and receptor size on the capillary self-alignment of micro solar cells," J. Microelectromech. Syst. **33**, 290–295 (2024).
85. E. Kaiser, M. Wiesenfarth, V. Vareilles, *et al.*, "Forced motion activated self-alignment of micro-CPV solar cells," IEEE J. Photovoltaics **14**, 288–295 (2024).
86. M. Paire, L. Lombez, N. Péré-Laperne, *et al.*, "Microscale solar cells for high concentration on polycrystalline Cu(In,Ga)Se_2 thin films," Appl. Phys. Lett. **98**, 264102 (2011).
87. B. Reinhold, M. Schmid, D. Greiner, *et al.*, "Monolithically interconnected lamellar Cu(In,Ga)Se_2 micro solar cells under full white light concentration," Prog. Photovoltaics **23**, 1929–1939 (2015).
88. B. Heidmann, S. Andree, S. Levcenkoe, *et al.*, "Fabrication of regularly arranged chalcopyrite micro solar cells via femtosecond laser-induced forward transfer for concentrator application," ACS Applied Energy Materials **1**, 27–31 (2017).
89. B. Heidmann, F. Ringleb, K. Eylers, *et al.*, "Local growth of $CuInSe_2$ micro solar cells for concentrator application," Mater. Today Energy **6**, 238–247 (2017).
90. A. Lewandowska and A. Matuszak-Flejszman, "Eco-design as a normative element of Environmental Management Systems—the context of the revised ISO 14001:2015," Int. J. Life Cycle Assess. **19**, 1794–1798 (2014).
91. F. Vallet, B. Eynard, D. Millet, *et al.*, "Using eco-design tools: an overview of experts' practices," Design Stud. **34**, 345–377 (2013).
92. R. Frischknecht, P. Stolz, G. Heath, *et al.*, "Methodology guidelines on life cycle assessment of photovoltaic 2020," Tech. Rep. (IEA PVPS, 2020).
93. M. Grohol and C. Veeh, *Study on the Critical Raw Materials for the EU 2023 – Final Report* (Publications Office of the European Union, 2023).
94. N. U. P. I. Irena, "Constructing a ranking of critical materials for the global energy transition," Tech. Rep. (International Renewable Energy Agency, 2024).
95. Y. Zhang, M. Kim, L. Wang, *et al.*, "Design considerations for multi-terawatt scale manufacturing of existing and future photovoltaic technologies: challenges and opportunities related to silver, indium and bismuth consumption," Energy Environ. Sci. **14**, 5587–5610 (2021).

96. B. Hallam, M. Kim, Y. Zhang, *et al.*, "The silver learning curve for photovoltaics and projected silver demand for net-zero emissions by 2050," Prog. Photovoltaics **31**, 598–606 (2023).
97. IEA, *Net Zero Roadmap: a Global Pathway to Keep the 1.5°C Goal in Reach* (IEA, 2023), https://www.iea.org/reports/net-zero-roadmap-a-global-pathway-to-keep-the-15-0c-goal-in-reach.
98. M. Taguchi, A. Yano, S. Tohoda, *et al.*, "24.7% record efficiency HIT solar cell on thin silicon wafer," IEEE J. Photovoltaics **4**, 96–99 (2014).
99. D. Adachi, J. L. Hernández, and K. Yamamoto, "Impact of carrier recombination on fill factor for large area heterojunction crystalline silicon solar cell with 25.1% efficiency," Appl. Phys. Lett. **107**, 233506 (2015).
100. X. Ru, M. Qu, J. Wang, *et al.*, "25.11% efficiency silicon heterojunction solar cell with low deposition rate intrinsic amorphous silicon buffer layers," Sol. Energy Mater. Sol. Cells **215**, 110643 (2020).
101. S. Herasimenka, W. Dauksher, M. Boccard, *et al.*, "ITO/SiO_x:H stacks for silicon heterojunction solar cells," Sol. Energy Mater. Sol. Cells **158**, 98–101 (2016).
102. M. Boccard, V. Paratte, E. Rucavado, *et al.*, *Paths for Maximal Light Incoupling and Excellent Electrical Performances in Silicon Heterojunction Solar Cells* (IEEE, 2019), pp. 2541–2545.
103. A. Cruz, E.-C. Wang, A. Morales-Vilches, *et al.*, "Effect of front TCO on the performance of rear-junction silicon heterojunction solar cells: insights from simulations and experiments," Sol. Energy Mater. Sol. Cells **195**, 339–345 (2019).
104. W. Liu, L. Zhang, X. Yang, *et al.*, "Damp-heat-stable, high-efficiency, industrial-size silicon heterojunction solar cells," Joule **4**, 913–927 (2020).
105. G. Du, Y. Bai, J. Huang, *et al.*, "Surface passivation of ITO on heterojunction solar cells with enhanced cell performance and module reliability," ECS J. Solid State Sci. Technol. **10**, 035008 (2021).
106. C. Han, R. Santbergen, M. Van Duffelen, *et al.*, "Towards bifacial silicon heterojunction solar cells with reduced TCO use," Prog. Photovoltaics **30**, 750–762 (2022).
107. U. Heitmann, L. Tutsch, A. De Rose, *et al.*, "Reduction of ITO by a low-cost sprayed TiO_x capping layer for SHJ solar cells," in *8th World Conference on Photovoltaic Energy Conversion* (2022), pp. 59–62.
108. C. Yu, Q. Zou, Q. Wang, *et al.*, "Silicon solar cell with undoped tin oxide transparent electrode," Nat. Energy **8**, 1119–1125 (2023).
109. P. Schmid, W. Wolke, H. Nagel, *et al.*, "Reducing indium consumption in silicon hetero junction solar cells with TCO stack systems of ITO and AZO," IEEE J. Photovoltaics **13**, 646–655 (2023).
110. Q. Tang, W. Duan, A. Lambertz, *et al.*, "> 85% indium reduction for high-efficiency silicon heterojunction solar cells with aluminum-doped zinc oxide contacts," Sol. Energy Mater. Sol. Cells **251**, 112120 (2023).
111. Y. Zhao, P. Procel, C. Han, *et al.*, "Strategies for realizing high-efficiency silicon heterojunction solar cells," Sol. Energy Mater. Sol. Cells **258**, 112413 (2023).
112. G. Dong, J. Li, Y. Zhao, *et al.*, "Highly efficient silicon heterojunction solar cells with ZnO:Al transparent electrode and transition metal doped indium oxide interfacial layer," Prog. Photovoltaics **31**, 931–938 (2023).
113. T. Gageot, J. Veirman, F. Jay, *et al.*, "Feasibility test of drastic indium cut down in SHJ solar cells and modules using ultra-thin ITO layers," Sol. Energy Mater. Sol. Cells **261**, 112512 (2023).
114. A. Cruz, F. Ruske, A. Eljarrat, *et al.*, "Influence of silicon layers on the growth of ITO and AZO in silicon heterojunction solar cells," IEEE J. Photovoltaics **10**, 703–709 (2020).

115. H. Li, W. Duan, A. Lambertz, *et al.*, "Influence of room temperature sputtered Al-doped zinc oxide on passivation quality in silicon heterojunction solar cells," IEEE J. Photovoltaics **9**, 1485–1491 (2019).
116. D. Meza, A. Cruz, A. Morales-Vilches, *et al.*, "Aluminum-doped zinc oxide as front electrode for rear emitter silicon heterojunction solar cells with high efficiency," Appl. Sci. **9**, 862 (2019).
117. A. Morales-Vilches, A. Cruz, S. Pingel, *et al.*, "ITO-free silicon heterojunction solar cells with ZnO:Al/SiO_2 front electrodes reaching a conversion efficiency of 23%," IEEE J. Photovoltaics **9**, 34–39 (2019).
118. Z. Wu, W. Duan, A. Lambertz, *et al.*, "Low-resistivity p-type a-Si:H/AZO hole contact in high-efficiency silicon heterojunction solar cells," Appl. Surf. Sci. **542**, 148749 (2021).
119. Longi, "LONGi achieves new world record for indium-free HJT cell efficiency" (2022), https://www.longi.com/en/news/indium-free-hjt/.
120. T. Koida, T. Matsui, and H. Sai, "Amorphous SnO_2 as earth-abundant stable transparent conductive oxide and its application to Si heterojunction solar cells," Sol. RRL **7**, 2300381 (2023).
121. S. Li, M. Pomaska, A. Lambertz, *et al.*, "Transparent-conductive-oxide-free front contacts for high-efficiency silicon heterojunction solar cells," Joule **5**, 1535–1547 (2021).
122. J. He, G. Wang, Y. Qiu, *et al.*, "Enabling transparent-conductive-oxide free efficient heterojunction solar cells by flexibly using dopant-free contact," Adv. Funct. Mater. **32**, 2205901 (2022).
123. H. Sai and T. Matsui, "Toward TCO-free silicon heterojunction solar cells: effect of TCO layers in electrical transport and stability," Sol. RRL **7**, 2300290 (2023).
124. K. Masuko, M. Shigematsu, T. Hashiguchi, *et al.*, "Achievement of more than 25% conversion efficiency with crystalline silicon heterojunction solar cell," IEEE J. Photovoltaics **4**, 1433–1435 (2014).
125. K. Yoshikawa, W. Yoshida, T. Irie, *et al.*, "Exceeding conversion efficiency of 26% by heterojunction interdigitated back contact solar cell with thin film Si technology," Sol. Energy Mater. Sol. Cells **173**, 37–42 (2017).
126. T. Minami, "Substitution of transparent conducting oxide thin films for indium tin oxide transparent electrode applications," Thin Solid Films **516**, 1314–1321 (2008).
127. J. Cashmore, M. Apolloni, A. Braga, *et al.*, "Record 12.34% stabilized conversion efficiency in a large area thin-film silicon tandem (MICROMORPH^{TM}) module," Prog. Photovoltaics **23**, 1441–1447 (2015).
128. T. Kato, "Cu(In,Ga)$(Se,S)_2$ solar cell research in Solar Frontier: progress and current status," Jpn. J. Appl. Phys. **56**, 04CA02 (2017).
129. M. Kambe, M. Fukawa, N. Taneda, *et al.*, "Improvement of a-Si solar cell properties by using SnO_2:F TCO films coated with an ultra-thin TiO_2 layer prepared by APCVD," Sol. Energy Mater. Sol. Cells **90**, 3014–3020 (2006).
130. N. Paudel and Y. Yan, "Fabrication and characterization of high-efficiency CdTe-based thin-film solar cells on commercial SnO_2:F-coated soda-lime glass substrates," Thin Solid Films **549**, 30–35 (2013).
131. M. Weidner, J. Jia, Y. Shigesato, *et al.*, "Comparative study of sputter-deposited SnO_2 films doped with antimony or tantalum," Phys. Status Solidi B **253**, 923–928 (2016).
132. J. Wang, C. Meng, H. Liu, *et al.*, "Application of indium tin oxide/aluminum-doped zinc oxide transparent conductive oxide stack films in silicon heterojunction solar cells," ACS Appl. Energy Mater. **4**, 13586–13592 (2021).

133. J.-P. Niemelä, B. Macco, L. Barraud, *et al.*, "Rear-emitter silicon heterojunction solar cells with atomic layer deposited ZnO:Al serving as an alternative transparent conducting oxide to In_2O_3:Sn," Sol. Energy Mater. Sol. Cells **200**, 109953 (2019).
134. F. Jay, T. Gageot, G. Pinoit, *et al.*, "Reduction in indium usage for silicon heterojunction solar cells in a short-term industrial perspective," Sol. RRL **7**, 2200598 (2022).
135. B. Stannowski, A. Cruz, D. Erfurt, *et al.*, "Approaches for SHJ cells with low or no indium content," in *12th International Conference on Crystalline Silicon Photovoltaics* (2022).
136. A. Steinmetz, M. Bivour, S. Pingel, *et al.*, "Reduction of resource critical materials in the SHJ production," in *5th International Workshop on SHJ Solar Cells 2022* (Institute Nationale de Énergie Solaire (INES), 2022).
137. D. Adachi, T. Terashita, T. Uto, *et al.*, "Effects of SiO_x barrier layer prepared by plasma-enhanced chemical vapor deposition on improvement of long-term reliability and production cost for Cu-plated amorphous Si/crystalline Si heterojunction solar cells," Sol. Energy Mater. Sol. Cells **163**, 204–209 (2017).
138. J. Haschke, G. Christmann, C. Messmer, *et al.*, "Lateral transport in silicon solar cells," J. Appl. Phys. **127**, 114501 (2020).
139. S. Tepner and A. Lorenz, "Printing technologies for silicon solar cell metallization: a comprehensive review," Prog. Photovoltaics **31**, 557–590 (2023).
140. S. Dubois, B. Paviet-Salomon, J. Chen, *et al.*, "n-type silicon solar cells," in *n-Type Crystalline Silicon Photovoltaics: Technology, Applications and Economics*, D. Munoz and R. Kopecek, eds. (Institution of Engineering and Technology, 2022), pp. 69–170.
141. D. Ourinson, A. Brand, A. Lorenz, *et al.*, "Paste-based silver reduction for iTOPCon rear side metallization," Sol. Energy Mater. Sol. Cells **266**, 112646 (2024).
142. Y. Zeng, C.-W. Peng, W. Hong, *et al.*, "Review on metallization approaches for high-efficiency silicon heterojunction solar cells," Trans. Tianjin Univ. **28**, 358–373 (2022).
143. Y. Li, X. Ru, M. Yang, *et al.*, "Flexible silicon solar cells with high power-to-weight ratios," Nature **626**, 105–110 (2024).
144. S. Kluska, R. Haberstoh, B. Grübel, *et al.*, "Enabling savings in silver consumption and poly-Si thickness by integration of plated Ni/Cu/Ag contacts for bifacial TOPCon solar cells," Sol. Energy Mater. Sol. Cells **246**, 111889 (2022).
145. C. Yu, K. Gao, C.-W. Peng, *et al.*, "Industrial-scale deposition of nanocrystalline silicon oxide for 26.4%-efficient silicon heterojunction solar cells with copper electrodes," Nat. Energy **8**, 1375–1385 (2023).
146. J. Yu, Y. Bai, J. Li, *et al.*, "Process challenges of high-performance silicon heterojunction solar cells with copper electrodes," Sol. Energy Mater. Sol. Cells **250**, 112057 (2023).
147. A. Tomasi, B. Paviet-Salomon, D. Lachenal, *et al.*, "Photolithography-free interdigitated back-contacted silicon heterojunction solar cells with efficiency >21%," in *2014 IEEE 40th Photovoltaic Specialist Conference (PVSC)* (IEEE, 2014), pp. 3644–3648.
148. V. Ganapati, M. A. Steiner, and E. Yablonovitch, "The voltage boost enabled by luminescence extraction in solar cells," IEEE J. Photovoltaics **6**, 801–809 (2016).
149. M. Scalora, J. P. Dowling, C. M. Bowden, *et al.*, "The photonic band edge optical diode," J. Appl. Phys. **76**, 2023–2026 (1994).
150. D.-W. Wang, H.-T. Zhou, M.-J. Guo, *et al.*, "Optical diode made from a moving photonic crystal," Phys. Rev. Lett. **110**, 093901 (2013).

151. M. J. Kerr, A. Cuevas, and P. Campbell, "Limiting efficiency of crystalline silicon solar cells due to Coulomb-enhanced Auger recombination," Prog. Photovoltaics **11**, 97–104 (2003).
152. P. Würfel and U. Würfel, *Physics of Solar Cells: From Basic Principles to Advanced Concepts*, 3rd ed. (Wiley-VCH, 2016).
153. N. Mrkyvkova, V. Held, P. Nadazdy, *et al.*, "Combined in situ photoluminescence and X-ray scattering reveals defect formation in lead-halide perovskite films," J. Phys. Chem. Lett. **12**, 10156–10162 (2021).
154. V. Held, N. Mrkyvkova, P. Nadazdy, *et al.*, "Evolution of structure and optoelectronic properties during halide perovskite vapor deposition," J. Phys. Chem. Lett. **13**, 11905–11912 (2022).
155. Q. Guesnay, F. Sahli, K. Artuk, *et al.*, "Pizza oven processing of organohalide perovskites (POPOP): a simple, versatile and efficient vapor deposition method," Adv. Energy Mater. **14**, 2303423 (2024).
156. U. Rau, U. W. Paetzold, and T. Kirchartz, "Thermodynamics of light management in photovoltaic devices," Phys. Rev. B **90**, 035211 (2014).
157. R. T. Ross, "Some thermodynamics of photochemical systems," J. Chem. Phys. **46**, 4590–4593 (1967).
158. O. D. Miller, E. Yablonovitch, and S. R. Kurtz, "Strong internal and external luminescence as solar cells approach the Shockley–Queisser limit," IEEE J. Photovoltaics **2**, 303–311 (2012).
159. A. Fell, T. Niewelt, B. Steinhauser, *et al.*, "Radiative recombination in silicon photovoltaics: modeling the influence of charge carrier densities and photon recycling," Sol. Energy Mater. Sol. Cells **230**, 111198 (2021).
160. A. Martí, J. L. Balenzategui, and R. F. Reyna, "Photon recycling and Shockley's diode equation," J. Appl. Phys. **82**, 4067–4075 (1997).
161. L. M. Pazos-Outón, M. Szumilo, R. Lamboll, *et al.*, "Photon recycling in lead iodide perovskite solar cells," Science **351**, 1430–1433 (2016).
162. L. M. Pazos-Outón, T. P. Xiao, and E. Yablonovitch, "Fundamental efficiency limit of lead iodide perovskite solar cells," J. Phys. Chem. Lett. **9**, 1703–1711 (2018).
163. V. Ganapati, C.-S. Ho, and E. Yablonovitch, "Air gaps as intermediate selective reflectors to reach theoretical efficiency limits of multibandgap solar cells," IEEE J. Photovoltaics **5**, 410–417 (2015).
164. D. Derkacs, D. T. Bilir, and V. A. Sabnis, "Luminescent coupling in GaAs/GaInNAsSb multijunction solar cells," IEEE J. Photovoltaics **3**, 520–527 (2012).
165. E. Lopez, O. Höhn, M. Schauerte, *et al.*, "Experimental coupling process efficiency and benefits of back surface reflectors in photovoltaic multi-junction photonic power converters," Prog. Photovoltaics **29**, 461–470 (2021).
166. A. R. Bowman, F. Lang, Y.-H. Chiang, *et al.*, "Relaxed current matching requirements in highly luminescent perovskite tandem solar cells and their fundamental efficiency limits," ACS Energy Lett. **6**, 612–620 (2021).
167. X. Sheng, M. H. Yun, C. Zhang, *et al.*, "Device architectures for enhanced photon recycling in thin-film multijunction solar cells," Adv. Energy Mater. **5**, 1400919 (2015).
168. M. A. Steiner and J. F. Geisz, "Non-linear luminescent coupling in series-connected multijunction solar cells," Appl. Phys. Lett. **100**, 251106 (2012).
169. K. Jäger, P. Tillmann, E. A. Katz, *et al.*, "Perovskite/silicon tandem solar cells: effect of luminescent coupling and bifaciality," Sol. RRL **5**, 2000628 (2021).
170. D. J. Friedman, J. F. Geisz, and M. A. Steiner, "Analysis of multijunction solar cell current–voltage characteristics in the presence of luminescent coupling," IEEE J. Photovoltaics **3**, 1429–1436 (2013).

171. D. J. Friedman, J. F. Geisz, and M. A. Steiner, "Effect of luminescent coupling on the optimal design of multijunction solar cells," IEEE J. Photovoltaics **4**, 986–990 (2014).
172. T. Kirchartz, F. Staub, and U. Rau, "Impact of photon recycling on the open-circuit voltage of metal halide perovskite solar cells," ACS Energy Lett. **1**, 731–739 (2016).
173. R. R. Chance, A. Prock, and R. Silbey, "Lifetime of an emitting molecule near a partially reflecting surface," J. Chem. Phys. **60**, 2744–2748 (1974).
174. W. Lukosz, "Theory of optical-environment-dependent spontaneous-emission rates for emitters in thin layers," Phys. Rev. B **22**, 3030–3038 (1980).
175. J. A. E. Wasey and W. L. Barnes, "Efficiency of spontaneous emission from planar microcavities," J. Mod. Opt. **47**, 725–741 (2000).
176. H. Greiner and O. J. F. Martin, "Numerical modeling of light emission and propagation in organic LEDs using the Green's tensor," in *Organic Light-Emitting Materials and Devices VII*, Vol. 5214 Z. H. Kafafi and P. A. Lane, eds., International Society for Optics and Photonics (SPIE, 2004), pp. 248–259.
177. C. Cho and N. C. Greenham, "Computational study of dipole radiation in re-absorbing perovskite semiconductors for optoelectronics," Adv. Sci. **8**, 2003559 (2021).
178. U. Aeberhard, S. J. Zeder, and B. Ruhstaller, "Impact of photon recycling on the light extraction from metal halide perovskite light emitting diodes," Opt. Quant. Electron. **54**, 617 (2022).
179. S. J. Zeder, U. Aeberhard, B. Ruhstaller, *et al.*, *18 – Metal Halide Perovskites for Generation, Manipulation and Detection of Light*, J. P. Martinez-Pastor, P. P. Boix, and G. Xing, eds., Photonic Materials and Applications (Elsevier, 2023), pp. 507–545.
180. M. G. Abebe, A. Abass, G. Gomard, *et al.*, "Rigorous wave-optical treatment of photon recycling in thermodynamics of photovoltaics: perovskite thin-film solar cells," Phys. Rev. B **98**, 075141 (2018).
181. W. van Roosbroeck and W. Shockley, "Photon-radiative recombination of electrons and holes in germanium," Phys. Rev. **94**, 1558–1560 (1954).
182. U. Aeberhard, S. Zeder, and B. Ruhstaller, "Reconciliation of dipole emission with detailed balance rates for the simulation of luminescence and photon recycling in perovskite solar cells," Opt. Express **29**, 14773–14788 (2021).
183. S. Zeder, B. Ruhstaller, and U. Aeberhard, "Assessment of photon recycling in perovskite solar cells by fully coupled optoelectronic simulation," Phys. Rev. Appl. **17**, 014023 (2022).
184. U. Aeberhard, S. J. Zeder, and B. Ruhstaller, "Effects of photon recycling and luminescent coupling in all-perovskite tandem solar cells assessed by full opto-electronic simulation," Sol. RRL **8**, 2400264 (2024).
185. S. J. Zeder, B. Blülle, B. Ruhstaller, *et al.*, "Optical multiscale model for quantification of photon recycling including incoherent light scattering," Opt. Express **32**, 34154–34171 (2024).
186. Y. Kashima, N. Maeda, E. Matsuura, *et al.*, "High external quantum efficiency (10%) AlGaN-based deep-ultraviolet light-emitting diodes achieved by using highly reflective photonic crystal on p-AlGaN contact layer," Appl. Phys. Express **11**, 012101 (2017).
187. Y. Zheng, Y. Zhang, J. Zhang, *et al.*, "Effects of meshed p-type contact structure on the light extraction effect for deep ultraviolet flip-chip light-emitting diodes," Nanoscale Res. Lett. **14**, 149 (2019).
188. L. Zschiedrich, H. J. Greiner, S. Burger, *et al.*, "Numerical analysis of nanostructures for enhanced light extraction from OLEDs," Proc. SPIE **8641**, 86410B (2013).

189. S. Nanz, R. Schmager, M. G. Abebe, *et al.*, "Photon recycling in nanopatterned perovskite thin-films for photovoltaic applications," APL Photonics **4**, 076104 (2019).
190. C. H. Henry, "Limiting efficiencies of ideal single and multiple energy gap terrestrial solar cells," J. Appl. Phys. **51**, 4494–4500 (1980).
191. E. Yablonovitch, "Light emission in photonic crystal micro-cavities," in *NATO ASI Series*, Vol. 340 in NATO Science, Series B, C. Weisbuch and E. Burstein, eds. (Springer, 1995), pp. 635–646.
192. ASTM Standard G173-03, *Standard Tables for Reference Solar Spectral Irradiances: Direct Normal and Hemispherical on 37° Tilted Surface, ASTM G173-03(2020)* (ASTM International, 2020).
193. M. A. Green, J. Zhao, A. Wang, *et al.*, "Efficient silicon light-emitting diodes," Nature **412**, 805–808 (2001).
194. E. S. Rittner, "Improved theory of the silicon p-n junction solar cell," J. Energy **1**, 9–17 (1977).
195. J. Brandhorst and W. Henry, "Summary of silicon high efficiency solar cell workshop," in *Solar Cell High Efficiency and Radiation Damage*, Vol. 2097 of *NASA Conference Publication* (1979), p.113.
196. R. Swanson, "Silicon photovoltaic cells in thermophotovoltaic energy conversion," in *1978 International Electron Devices Meeting* (IRE, 1978).
197. R. Swanson, S. Beckwith, R. Crane, *et al.*, "Point-contact silicon solar cells," IEEE Trans. Electron Devices **31**, 661 (1984).
198. H. Kroemer, "A proposed class of hetero-junction injection lasers," Proc. IEEE **51**, 1782–1783 (1963).
199. H. Kroemer, "Nobel lecture: quasielectric fields and band offsets: teaching electrons new tricks," Rev. Mod. Phys. **73**, 783–793 (2001).
200. K. Jäger and S. Albrecht, "Perovskite-based tandem solar cells," in *Hybrid Perovskite Solar Cells*, H. Fujiwara, ed., Chap. 17 (John Wiley & Sons, Ltd., 2021), pp. 463–508.
201. A. De Vos and H. Pauwels, "On the thermodynamic limit of photovoltaic energy conversion," Appl. Phys. **25**, 119–125 (1981).
202. O. Almora, D. Baran, G. C. Bazan, *et al.*, "Device performance of emerging photovoltaic materials (Version 3)," Adv. Energy Mater. **13**, 2203313 (2023).
203. A. Richter, M. Hermle, and S. W. Glunz, "Reassessment of the limiting efficiency for crystalline silicon solar cells," IEEE J. Photovoltaics **3**, 1184–1191 (2013).
204. S. Schäfer and R. Brendel, "Accurate calculation of the absorptance enhances efficiency limit of crystalline silicon solar cells with lambertian light trapping," IEEE J. Photovoltaics **8**, 1156–1158 (2018).
205. I. Schnitzer, E. Yablonovitch, C. Caneau, *et al.*, "Ultrahigh spontaneous emission quantum efficiency, 99.7% internally and 72% externally, from AlGaAs/GaAs/AlGaAs double heterostructures," Appl. Phys. Lett. **62**, 131–133 (1993).
206. V. Badescu and P. T. Landsberg, "Influence of photon recycling on solar cell efficiencies," Semicond. Sci. Technol. **12**, 1491–1497 (1997).
207. A. W. Walker, O. Hohn, D. N. Micha, *et al.*, "Impact of photon recycling on GaAs solar cell designs," IEEE J. Photovoltaics **5**, 1636–1645 (2015).
208. M. A. Steiner, J. F. Geisz, I. Garcia, *et al.*, "Effects of internal luminescence and internal optics on V_{oc} and J_{sc} of III–V solar cells," IEEE J. Photovoltaics **3**, 1437–1442 (2013).
209. J. Buencuerpo, M. A. Steiner, and A. C. Tamboli, "Optically-thick 300 nm GaAs solar cells using adjacent photonic crystals," Opt. Express **28**, 13845 (2020).
210. I. Massiot, A. Cattoni, and S. Collin, "Progress and prospects for ultrathin solar cells," Nat. Energy **5**, 959–972 (2020).

211. B. Frouin, A. Cattoni, H.-L. Chen, *et al.*, "A path toward 25%-efficient ultrathin GaAs solar cells," in *Physics, Simulation, and Photonic Engineering of Photovoltaic Devices X*, A. Freundlich, K. Hinzer, and S. Collin, eds. (SPIE, 2021), p. 2.
212. H.-L. Chen, A. Cattoni, R. De Lépinau, *et al.*, "A 19.9%-efficient ultrathin solar cell based on a 205-nm-thick GaAs absorber and a silver nanostructured back mirror," Nat. Energy **4**, 761–767 (2019).
213. G. Yin, M. W. Knight, M.-C. van Lare, *et al.*, "Optoelectronic enhancement of ultrathin $CuIn_{1-x}Ga_xSe_2$ solar cells by nanophotonic contacts," Adv. Opt. Mater. **5**, 1600637 (2017).
214. S. Ishizuka, J. Nishinaga, K. Beppu, *et al.*, "Physical and chemical aspects at the interface and in the bulk of $CuInSe_2$ -based thin-film photovoltaics," Phys. Chem. Chem. Phys. **24**, 1262–1285 (2022).
215. J. Keller, P. Pearson, N. Shariati Nilsson, *et al.*, "Performance limitations of wide-gap (Ag,Cu)(In,Ga)Se_2 thin-film solar cells," Sol. RRL **5**, 2100403 (2021).
216. M. A. Contreras, L. M. Mansfield, B. Egaas, *et al.*, "Wide bandgap Cu(In,Ga)Se_2 solar cells with improved energy conversion efficiency," Prog. Photovoltaics **20**, 843–850 (2012).
217. W. N. Shafarman and L. Stolt, "Cu(InGa)Se_2 solar cells," in *Handbook of Photovoltaic Science and Engineering*, A. Luque and S. Hegedus, eds., Chap. 13 (Wiley, 2003), pp. 546–599.
218. R. E. Brandt, J. R. Poindexter, P. Gorai, *et al.*, "Searching for 'defect-tolerant,' photovoltaic materials: combined theoretical and experimental screening," Chem. Mater. **29**, 4667–4674 (2017).
219. C. M. Sutter-Fella, Y. Li, M. Amani, *et al.*, "High photoluminescence quantum yield in band gap tunable bromide containing mixed halide perovskites," Nano Lett. **16**, 800–806 (2016).
220. K. Schötz, A. M. Askar, W. Peng, *et al.*, "Double peak emission in lead halide perovskites by self-absorption," J. Mater. Chem. C **8**, 2289–2300 (2020).
221. E. T. Hoke, D. J. Slotcavage, E. R. Dohner, *et al.*, "Reversible photo-induced trap formation in mixed-halide hybrid perovskites for photovoltaics," Chem. Sci. **6**, 613–617 (2015).
222. R. D. J. Oliver, P. Caprioglio, F. Peña-Camargo, *et al.*, "Understanding and suppressing non-radiative losses in methylammonium-free wide-bandgap perovskite solar cells," Energy Environ. Sci. **15**, 714–726 (2022).
223. Y. Wang, I. Ahmad, T. Leung, *et al.*, "Encapsulation and stability testing of perovskite solar cells for real life applications," ACS Mater. Au **2**, 215–236 (2022).
224. H. Zai, Y. Ma, Q. Chen, *et al.*, "Ion migration in halide perovskite solar cells: mechanism, characterization, impact and suppression," J. Energy Chem. **63**, 528–549 (2021).
225. Z. Xu, H. Bristow, M. Babics, *et al.*, "Reverse-bias resilience of monolithic perovskite/silicon tandem solar cells," Joule **7**, 1992–2002 (2023).
226. S. Essig, C. Allebé, T. Remo, *et al.*, "Raising the one-Sun conversion efficiency of III–V/Si solar cells to 32.8% for two junctions and 35.9% for three junctions," Nat. Energy **2**, 17144 (2017).
227. M. P. Lumb, A. L. Dobbin, D. B. Bushnell, *et al.*, "Comparing the energy yield of (III–V) multi-junction cells with different numbers of sub-cells," AIP Conf. Proc. **1277**, 299–302 (2010).
228. I. Mathews, S. Lei, and R. Frizzell, "Predicted annual energy yield of III–V/c-Si tandem solar cells: modelling the effect of changing spectrum on current-matching," Opt. Express **28**, 7829 (2020).

229. S. Heckelmann, D. Lackner, C. Karcher, *et al.*, "Investigations on $Al_xGa_{1-x}As$ solar cells grown by MOVPE," IEEE J. Photovoltaics **5**, 446–453 (2015).
230. M. Feifel, J. Ohlmann, J. Benick, *et al.*, "Direct growth of III–V/silicon triple-junction solar cells with 19.7% efficiency," IEEE J. Photovoltaics **8**, 1590–1595 (2018).
231. U. Heitmann, J. Bartsch, S. Kluska, *et al.*, "Pathways and potentials for III–V on Si tandem solar cells realized using a ZnO-based transparent conductive adhesive," IEEE J. Photovoltaics **11**, 85–92 (2021).
232. P.-L. Nguyen, J. Buencuerpo, P. Baranek, *et al.*, "Glued III–V on Si tandem solar cells using hybrid transparent conductive layers," in *2022 IEEE 49th Photovoltaics Specialists Conference (PVSC)* (IEEE, 2022), pp. 625.
233. A. Cordaro, R. Müller, S. W. Tabernig, *et al.*, "Nanopatterned back-reflector with engineered near-field/far-field light scattering for enhanced light trapping in silicon-based multijunction solar cells," ACS Photonics **10**, 4061–4070 (2023).
234. G. M. Wilson, M. Al-Jassim, W. K. Metzger, *et al.*, "The 2020 photovoltaic technologies roadmap," J. Phys. D: Appl. Phys. **53**, 493001 (2020).
235. W. Guter, F. Dunzer, L. Ebel, *et al.*, "Space solar cells – 3G30 and next generation radiation hard products," in *E3S Web Conf.*, Vol. 16 (2017), p. 03005.
236. R. M. France, J. F. Geisz, I. García, *et al.*, "Design flexibility of ultrahigh efficiency four-junction inverted metamorphic solar cells," IEEE J. Photovoltaics **6**, 578–583 (2016).
237. M. Klitzke, J. Schön, R. H. Van Leest, *et al.*, "Ultra-lightweight and flexible inverted metamorphic four junction solar cells for space applications," EPJ Photovolt. **13**, 25 (2022).
238. B. M. Kayes, L. Zhang, R. Twist, *et al.*, "Flexible thin-film tandem solar cells with > 30% efficiency," IEEE J. Photovoltaics **4**, 729–733 (2014).
239. K. Sasaki, T. Agui, K. Nakaido, *et al.*, "Development of InGaP/GaAs/InGaAs inverted triple junction concentrator solar cells," AIP Conf. Proc. **1556**, 22–25 (2013).
240. R. M. France, J. F. Geisz, T. Song, *et al.*, "Triple-junction solar cells with 39.5% terrestrial and 34.2% space efficiency enabled by thick quantum well superlattices," Joule **8**, 1121–2235 (2022).
241. J. F. Geisz, R. M. France, K. L. Schulte, *et al.*, "Six-junction III–V solar cells with 47.1% conversion efficiency under 143 Suns concentration," Nat. Energy **5**, 326–335 (2020).
242. P. Schroth, R. Löckenhoff, D. Fuhrmann, *et al.*, "AZUR's new 5C46 CPV cell: final design for optimized outdoor performance," AIP Conf. Proc. **2550**, 020008 (2022).
243. Longi, "34.6%! Record-breaker LONGi once again sets a new world efficiency for silicon-perovskite tandem solar cells," https://www.longi.com/en/news/2024-snec-silicon-perovskite-tandem-solar-cells-new-world-efficiency/ (2024).
244. J. Liu, Y. He, L. Ding, *et al.*, "Perovskite/silicon tandem solar cells with bilayer interface passivation," Nature **635**, 596–603 (2024).
245. B. Chen, Z. J. Yu, S. Manzoor, *et al.*, "Blade-coated perovskites on textured silicon for 26%-efficient monolithic perovskite/silicon tandem solar cells," Joule **4**, 850–864 (2020).
246. Y. Hou, E. Aydin, M. De Bastiani, *et al.*, "Efficient tandem solar cells with solution-processed perovskite on textured crystalline silicon," Science **367**, 1135–1140 (2020).
247. A. Harter, S. Mariotti, L. Korte, *et al.*, "Double-sided nano-textured surfaces for industry compatible high-performance silicon heterojunction and perovskite/silicon tandem solar cells," Prog. Photovoltaics **31**, 813–823 (2023).

248. M. De Bastiani, R. Jalmood, J. Liu, *et al.*, "Monolithic perovskite/silicon tandems with >28% efficiency: role of silicon-surface texture on perovskite properties," Adv. Funct. Mater. **33**, 2205557 (2023).
249. P. Tockhorn, J. Sutter, A. Cruz, *et al.*, "Nano-optical designs for high-efficiency monolithic perovskite–silicon tandem solar cells," Nat. Nanotechnol. **17**, 1214–1221 (2022).
250. Z. Ying, Z. Yang, J. Zheng, *et al.*, "Monolithic perovskite/black-silicon tandems based on tunnel oxide passivated contacts," Joule **6**, 2644–2661 (2022).
251. F. Sahli, J. Werner, B. A. Kamino, *et al.*, "Fully textured monolithic perovskite/silicon tandem solar cells with 25.2% power conversion efficiency," Nat. Mater. **17**, 820–826 (2018).
252. M. Roß, S. Severin, M. B. Stutz, *et al.*, "Co-evaporated formamidinium lead iodide based perovskites with 1000 h constant stability for fully textured monolithic perovskite/silicon tandem solar cells," Adv. Energy Mater. **11**, 2101460 (2021).
253. A. Onno, N. Rodkey, A. Asgharzadeh, *et al.*, "Predicted power output of silicon-based bifacial tandem photovoltaic systems," Joule **4**, 580–596 (2020).
254. J. Lehr, M. Langenhorst, R. Schmager, *et al.*, "Energy yield of bifacial textured perovskite/silicon tandem photovoltaic modules," Sol. Energy Mater. Sol. Cells **208**, 110367 (2020).
255. M. De Bastiani, A. Mirabelli, Y. Hou, *et al.*, "Efficient bifacial monolithic perovskite/silicon tandem solar cells via bandgap engineering," Nat. Energy **6**, 167–175 (2021).
256. P. Tillmann, K. Jäger, A. Karsenti, *et al.*, "Model-chain validation for estimating the energy yield of bifacial perovskite/silicon tandem solar cells," Sol. RRL **6**, 2200079 (2022).
257. H. Hao, S.-T. Zhang, K. Wang, *et al.*, "Energy yield prediction of bifacial perovskite/silicon tandem photovoltaic modules," Sol. RRL **7**, 2300218 (2023).
258. K. Ganesh and R. Padmanabhan, "Analysis of perovskite-silicon tandem solar cells using a semi-analytical model," in *2022 IEEE 22nd International Conference on Nanotechnology (NANO)* (IEEE, 2022), pp. 496–499.
259. A. Pusch, P. Pearce, and N. J. Ekins-Daukes, "Analytical expressions for the efficiency limits of radiatively coupled tandem solar cells," IEEE J. Photovoltaics **9**, 679–687 (2019).
260. R. Mishima, W. Yoshida, H. Ishibashi, *et al.*, "Luminescence coupling in 28.4%-efficient tandem solar cell utilizing 20.8%-efficient perovskite minimodule stacked on silicon cell," Appl. Phys. Lett. **123**, 263510 (2023).
261. V. Neder, S. W. Tabernig, and A. Polman, "Detailed-balance efficiency limits of two-terminal perovskite/silicon tandem solar cells with planar and Lambertian spectral splitters," J. Photonics Energy **12**, 015502 (2022).
262. M. Jošt, E. Köhnen, A. Al-Ashouri, *et al.*, "Perovskite/CIGS tandem solar cells: from certified 24.2% toward 30% and beyond," ACS Energy Lett. **7**, 1298–1307 (2022).
263. M. A. Ruiz-Preciado, F. Gota, P. Fassl, *et al.*, "Monolithic two-terminal perovskite/CIS tandem solar cells with efficiency approaching 25%," ACS Energy Lett. **7**, 2273–2281 (2022).
264. T. Feeney, I. M. Hossain, S. Gharibzadeh, *et al.*, "Four-terminal perovskite/copper indium gallium selenide tandem solar cells: unveiling the path to >27% in power conversion efficiency," Sol. RRL **6**, 2200662 (2022).
265. X. Liu, J. Zhang, L. Tang, *et al.*, "Over 28% efficiency perovskite/Cu(InGa)Se_2 tandem solar cells: highly efficient sub-cells and their bandgap matching," Energy Environ. Sci. **16**, 5029–5042 (2023).

266. M. Schmid, R. Caballero, R. Klenk, *et al.*, "Experimental verification of optically optimized $CuGaSe_2$ top cell for improving chalcopyrite tandems," EPJ Photovoltaics **1**, 10601 (2010).
267. K. Kim, S. K. Ahn, J. H. Choi, *et al.*, "Highly efficient Ag-alloyed Cu(In,Ga)Se_2 solar cells with wide bandgaps and their application to chalcopyrite-based tandem solar cells," Nano Energy **48**, 345–352 (2018).
268. X. Wu, B. Li, Z. Zhu, *et al.*, "Designs from single junctions, heterojunctions to multijunctions for high-performance perovskite solar cells," Chem. Soc. Rev. **50**, 13090–13128 (2021).
269. Q.-Q. Chu, Z. Sun, J. Hah, *et al.*, "Progress, challenges, and further trends of all perovskites tandem solar cells: a comprehensive review," Mater. Today **67**, 399–423 (2023).
270. J. Werner, G. Dubuis, A. Walter, *et al.*, "Sputtered rear electrode with broadband transparency for perovskite solar cells," Sol. Energy Mater. Sol. Cells **141**, 407–413 (2015).
271. B. Chen, Z. Yu, A. Onno, *et al.*, "Bifacial all-perovskite tandem solar cells," Sci. Adv. **8**, eadd0377 (2022).
272. Z. Yu, J. Wang, B. Chen, *et al.*, "Solution-processed ternary tin (II) alloy as hole-transport layer of Sn–Pb perovskite solar cells for enhanced efficiency and stability," Adv. Mater. **34**, 2205769 (2022).
273. M. Moradbeigi and M. Razaghi, "Investigation of optical and electrical properties of novel 4T all perovskite tandem solar cell," Sci. Rep. **12**, 6733 (2022).
274. K. Jáger, A. Tejada, S. Berwig, *et al.*, "Optical simulations of nanotextured all-perovskite tandem solar cells," Adv. Theory Simul. **1**, 2400724 (2024).
275. K. Jáger, J. Sutter, M. Hammerschmidt, *et al.*, "Prospects of light management in perovskite/silicon tandem solar cells," Nanophotonics **10**, 1991–2000 (2021).
276. F. Gota, S. X. X. An, H. Hu, *et al.*, "Energy yield modeling of bifacial all-perovskite two-terminal tandem photovoltaics," Adv. Opt. Mater. **11**, 2201691 (2023).
277. H. Li, Y. Wang, H. Gao, *et al.*, "Revealing the output power potential of bifacial monolithic all-perovskite tandem solar cells," eLight **2**, 21 (2022).
278. Y. Gao, R. Lin, K. Xiao, *et al.*, "Performance optimization of monolithic all-perovskite tandem solar cells under standard and real-world solar spectra," Joule **6**, 1944–1963 (2022).
279. M. Hanna and A. Nozik, "Solar conversion efficiency of photovoltaic and photoelectrolysis cells with carrier multiplication absorbers," J. Appl. Phys. **100**, 74510 (2006).
280. A. Shalav, B. Richards, and M. Green, "Luminescent layers for enhanced silicon solar cell performance: up-conversion," Sol. Energy Mater. Sol. Cells **91**, 829–842 (2007).
281. H. Hovel, R. Hodgson, and J. Woodall, "The effect of fluorescent wavelength shifting on solar cell spectral response," Sol. Energy Mater. **2**, 19–29 (1979).
282. A. Sinha, K. Hurst, S. Ulicna, *et al.*, "Assessing UV-Induced degradation in bifacial modules of different cell technologies," in *2021 IEEE 48th Photovoltaic Specialists Conference (PVSC)* (IEEE, 2021), pp. 0767–0770.
283. M. Smith and J. Michl, "Singlet fission," Chem. Rev. **110**, 6891–6936 (2010).
284. M. Wilson, A. Rao, B. Ehrler, *et al.*, "Singlet exciton fission in polycrystalline pentacene: from photophysics toward devices," Acc. Chem. Res. **46**, 1330–1338 (2013).
285. R. Alfano, S. Shapiro, and M. Pope, "Fission rate of singlet excitons in a tetracene crystal measured with picosecond laser pulses," Opt. Commun. **9**, 388–391 (1973).

286. S. Eaton, L. Shoer, S. Karlen, *et al.*, "Singlet exciton fission in polycrystalline thin films of a slip-stacked perylenediimide," J. Am. Chem. Soc. **135**, 14701–14712 (2013).
287. M. Smith and J. Michl, "Recent advances in singlet fission," Annu. Rev. Phys. Chem. **64**, 361–386 (2013).
288. M. Einzinger, T. Wu, J. Kompalla, *et al.*, "Sensitization of silicon by singlet exciton fission in tetracene," Nature **571**, 90–94 (2019).
289. B. Daiber, S. Maiti, S. M. Ferro, *et al.*, "Change in tetracene polymorphism facilitates triplet transfer in singlet fission-sensitized silicon solar cells," J. Phys. Chem. Lett. **11**, 8703–8709 (2020).
290. N. Nagaya, K. Lee, C. F. Perkinson, *et al.*, "Exciton fission enhanced silicon solar cell," arXiv (2024).
291. D. Dexter, "Two ideas on energy transfer phenomena: ion-pair effects involving the OH stretching mode, and sensitization of photovoltaic cells," J. Lumin. **18-19**, 779–784 (1979).
292. B. Daiber, K. Van Den Hoven, M. Futscher, *et al.*, "Realistic efficiency limits for singlet-fission silicon solar cells," ACS Energy Lett. **6**, 2800–2808 (2021).
293. M. Futscher, A. Rao, and B. Ehrler, "The potential of singlet fission photon multipliers as an alternative to silicon-based tandem solar cells," ACS Energy Lett. **3**, 2587–2592 (2018).
294. M. Tabachnyk, B. Ehrler, S. Gélinas, *et al.*, "Resonant energy transfer of triplet excitons from pentacene to PbSe nanocrystals," Nat. Mater. **13**, 1033–1038 (2014).
295. N. Thompson, M. Wilson, D. Congreve, *et al.*, "Energy harvesting of non-emissive triplet excitons in tetracene by emissive PbS nanocrystals," Nat. Mater. **13**, 1039–1043 (2014).
296. T. Veeken, B. Daiber, H. Agrawal, *et al.*, "Directional quantum dot emission by soft-stamping on silicon Mie resonators," Nanoscale Adv. **4**, 1088–1097 (2022).
297. Y. Jiang, M. Nielsen, A. Baldacchino, *et al.*, "Singlet fission and tandem solar cells reduce thermal degradation and enhance lifespan," Prog. Photovoltaics **29**, 899–906 (2021).
298. X. Li, S. Duan, H. Liu, *et al.*, "Mechanism for the extremely efficient sensitization of Yb^{3+}luminescence in $CsPbCl_3$ nanocrystals," J. Phys. Chem. Lett. **10**, 487–492 (2019).
299. D. Kroupa, J. Roh, T. Milstein, *et al.*, "Quantum-cutting ytterbium-doped $CsPb(Cl_{1-x}B_x)_3$ perovskite thin films with photoluminescence quantum yields over 190%," ACS Energy Lett. **3**, 2390–2395 (2018).
300. T. Milstein, D. Kroupa, and D. Gamelin, "Picosecond quantum cutting generates photoluminescence quantum yields over 100% in ytterbium-doped $CsPbCl_3$ nanocrystals," Nano Lett. **18**, 3792–3799 (2018).
301. T. Schulze and T. Schmidt, "Photochemical upconversion: present status and prospects for its application to solar energy conversion," Energy Environ. Sci. **8**, 103–125 (2015).
302. E. Gholizadeh, "Photochemical upconversion of near-infrared light from below the silicon bandgap," Nat. Photonics **14**, 585–590 (2020).
303. S. Wen, J. Zhou, K. Zheng, *et al.*, "Advances in highly doped upconversion nanoparticles," Nat. Commun. **9**, 2415 (2018).
304. M. Bettinelli, L. Carlos, and X. Liu, "Lanthanide-doped upconversion nanoparticles," Phys. Today **68**, 38–44 (2015).
305. N. Sun, Y. Ding, D. Sagar, *et al.*, "Photon upconversion towards applications in energy conversion and bioimaging," Prog. Surf. Sci. **92**, 281–316 (2017).

306. R. Martín-Rodríguez, S. Fischer, A. Ivaturi, *et al.*, "Highly efficient IR to NIR upconversion in Gd_2O_2>S: Er^{3+} for photovoltaic applications," Chem. Mater. **25**, 1912–1921 (2013).
307. W. Zou, C. Visser, J. Maduro, *et al.*, "Broadband dye-sensitized upconversion of near-infrared light," Nat. Photonics **6**, 560–564 (2012).
308. F. Zhao, D. Yin, C. Wu, *et al.*, "Huge enhancement of upconversion luminescence by dye/Nd^{3+} sensitization of quenching-shield sandwich structured upconversion nanocrystals under 808 nm excitation," Dalton Trans. **46**, 16180–16189 (2017).
309. D. Garfield, N. Borys, S. Hamed, *et al.*, "Enrichment of molecular antenna triplets amplifies upconverting nanoparticle emission," Nat. Photonics **12**, 402–407 (2018).
310. W. Weber and J. Lambe, "Luminescent greenhouse collector for solar radiation," Appl. Opt. **15**, 2299 (1976).
311. A. Goetzberger and W. Greube, "Solar energy conversion with fluorescent collectors," Appl. Phys. **14**, 123–139 (1977).
312. C. Traverse, R. Pandey, M. Barr, *et al.*, "Emergence of highly transparent photovoltaics for distributed applications," Nat. Energy **2**, 849–860 (2017).
313. F. Meinardi, S. Ehrenberg, L. Dhamo, *et al.*, "Highly efficient luminescent solar concentrators based on earth-abundant indirect-bandgap silicon quantum dots," Nat. Photonics **11**, 177–185 (2017).
314. F. Meinardi, F. Bruni, and S. Brovelli, "Luminescent solar concentrators for building-integrated photovoltaics," Nat. Rev. Mater. **2**, 17072 (2017).
315. G. Smestad, H. Ries, R. Winston, *et al.*, "The thermodynamic limits of light concentrators," Sol. Energy Mater. **21**, 99–111 (1990).
316. Z. Krumer, W. G. van Sark, R. E. Schropp, *et al.*, "Compensation of self-absorption losses in luminescent solar concentrators by increasing luminophore concentration," Sol. Energy Mater. Sol. Cells **167**, 133–139 (2017).
317. B. Vishwanathan, A. Reinders, D. de Boer, *et al.*, "A comparison of performance of flat and bent photovoltaic luminescent solar concentrators," Sol. Energy **112**, 120–127 (2015).
318. O. Kate, K. Hooning, and E. Van Der Kolk, "Quantifying self-absorption losses in luminescent solar concentrators," Appl. Opt. **53**, 5238–5245 (2014).
319. N. D. Bronstein, Y. Yao, L. Xu, *et al.*, "Quantum dot luminescent concentrator cavity exhibiting 30-fold concentration," ACS Photonics **2**, 1576–1583 (2015).
320. C. Li, W. Chen, D. Wu, *et al.*, "Large stokes shift and high efficiency luminescent solar concentrator incorporated with $CuInS_2$/ZnS quantum dots," Sci. Rep. **5**, 17777 (2015).
321. T. K. Baikie, B. Daiber, E. Kensington, *et al.*, "Revealing the potential of luminescent solar concentrators in real-world environments," Joule **8**, 799–816 (2024).
322. C. Erickson, M. Crane, T. Milstein, *et al.*, "Photoluminescence saturation in quantum-cutting Yb^{3+}-doped $CsPb(Cl_{1-x}Br_x)_3$ perovskite nanocrystals: implications for solar downconversion," J. Phys. Chem. C **123**, 12474–12484 (2019).
323. D. Zhou, R. Sun, W. Xu, *et al.*, "Impact of host composition, codoping, or tridoping on quantum-cutting emission of ytterbium in halide perovskite quantum dots and solar cell applications," Nano Lett. **19**, 6904–6913 (2019).
324. D. Du, J. Darkwa, and G. Kokogiannakis, "Thermal management systems for photovoltaics (PV) installations: a critical review," Sol. Energy **97**, 238–254 (2013).
325. P. Dwivedi, K. Sudhakar, A. Soni, *et al.*, "Advanced cooling techniques of P.V. modules: a state of art," Case Stud.Therm. Eng. **21**, 100674 (2020).

326. L. Xu, W. Liu, H. Liu, *et al.*, "Heat generation and mitigation in silicon solar cells and modules," Joule **5**, 631–645 (2021).
327. M. M. Hossain and M. Gu, "Radiative cooling: principles, progress, and potentials," Adv. Sci. **3**, 1500360 (2016).
328. C. Granqvist and A. Hjortsberg, "Radiative cooling to low temperatures: general considerations and application to selectively emitting SiO films," J. Appl. Phys. **52**, 4205–4220 (1981).
329. A. P. Raman, M. A. Anoma, L. Zhu, *et al.*, "Passive radiative cooling below ambient air temperature under direct sunlight," Nature **515**, 540–544 (2014).
330. L. Zhu, A. Raman, K. X. Wang, *et al.*, "Radiative cooling of solar cells," Optica **1**, 32–38 (2014).
331. L. Zhu, A. Raman, and S. Fan, "Color-preserving daytime radiative cooling," Appl. Phys. Lett. **103**, 223902 (2013).
332. L. Zhu, A. P. Raman, and S. Fan, "Radiative cooling of solar absorbers using a visibly transparent photonic crystal thermal blackbody," Proc. Natl. Acad. Sci. U. S. A. **112**, 12282–12287 (2015).
333. B. Zhao, M. Hu, X. Ao, *et al.*, "Performance analysis of enhanced radiative cooling of solar cells based on a commercial silicon photovoltaic module," Sol. Energy **176**, 248–255 (2018).
334. Y. An, C. Sheng, and X. Li, "Radiative cooling of solar cells: opto-electro-thermal physics and modeling," Nanoscale **11**, 17073–17083 (2019).
335. W. Li, Y. Shi, K. Chen, *et al.*, "A comprehensive photonic approach for solar cell cooling," ACS Photonics **4**, 774–782 (2017).
336. D. Sato and N. Yamada, "Review of photovoltaic module cooling methods and performance evaluation of the radiative cooling method," Renewable Sustainable Energy Rev. **104**, 151–166 (2019).
337. X. Sun, T. J. Silverman, Z. Zhou, *et al.*, "Optics-based approach to thermal management of photovoltaics: selective-spectral and radiative cooling," IEEE J. Photovoltaics **7**, 566–574 (2017).
338. G. Perrakis, A. C. Tasolamprou, G. Kenanakis, *et al.*, "Passive radiative cooling and other photonic approaches for the temperature control of photovoltaics: a comparative study for crystalline silicon-based architectures," Opt. Express **28**, 18548–18565 (2020).
339. Z. Zhou, Z. Wang, and P. Bermel, "Radiative cooling for low-bandgap photovoltaics under concentrated sunlight," Opt. Express **27**, A404–A418 (2019).
340. Z. Wang, D. Kortge, J. Zhu, *et al.*, "Lightweight, passive radiative cooling to enhance concentrating photovoltaics," Joule **4**, 2702–2717 (2020).
341. I. M. Slauch, M. G. Deceglie, T. J. Silverman, *et al.*, "Spectrally selective mirrors with combined optical and thermal benefit for photovoltaic module thermal management," ACS Photonics **5**, 1528–1538 (2018).
342. I. M. Slauch, M. G. Deceglie, T. J. Silverman, *et al.*, "Optical approaches for passive thermal management in c-Si photovoltaic modules," Cell Rep. Phys. Sci. **2**, 100430 (2021).
343. B. M. Cote, I. M. Slauch, M. G. Deceglie, *et al.*, "Light management in bifacial photovoltaics with spectrally selective mirrors," ACS Appl. Energy Mater. **4**, 5397–5402 (2021).
344. P. Shukla, J. Skea, R. Slade, *et al.*, eds. *Climate Change 2022 - Mitigation of Climate Change: Working Group III Contribution to the Sixth Assessment Report of the Intergovernmental Panel on Climate Change* (Cambridge University Press, 2023).
345. D. J. Sailor, J. Anand, and R. R. King, "Photovoltaics in the built environment: a critical review," Energy Build. **253**, 111479 (2021).

346. G. A. Barron-Gafford, R. L. Minor, N. A. Allen, *et al.*, "The photovoltaic heat island effect: larger solar power plants increase local temperatures," Sci. Rep. **6**, 35070 (2016).
347. Z. Li, S. Ahmed, and T. Ma, "Investigating the effect of radiative cooling on the operating temperature of photovoltaic modules," Sol. RRL **5**, 2000735 (2021).
348. F. Gota, M. Langenhorst, R. Schmager, *et al.*, "Energy yield advantages of three-terminal perovskite-silicon tandem photovoltaics," Joule **4**, 2387–2403 (2020).
349. Š. Tomšič, M. Jošt, K. Brecl, *et al.*, "Energy yield modeling for optimization and analysis of perovskite-silicon tandem solar cells under realistic outdoor conditions," Adv. Theory Simul. **6**, 2200931 (2023).
350. R. Schmager, M. Langenhorst, J. Lehr, *et al.*, "Methodology of energy yield modelling of perovskite-based multi-junction photovoltaics," Opt. Express **27**, A507 (2019).
351. Y. Kato, H. Katayama, T. Kobayashi, *et al.*, "Global prediction of the energy yields for hybrid perovskite/Si tandem and Si heterojunction single solar modules," Prog. Photovoltaics **30**, 1198–1218 (2022).
352. M. Sengupta, A. Habte, P. Gotseff, *et al.*, "A physics-based GOES satellite product for use in NREL's national solar radiation database," Tech. Rep. NREL/CP-5D00-62237 (National Renewable Energy Laboratory, NREL) (2014).
353. M. Sengupta, A. Weekley, A. Habte, *et al.*, "Validation of the National Solar Radiation Database (NSRDB) (2005–2012)," *31st European Photovoltaic Solar Energy Conference and Exhibition* (2015), pp. 1710–1716.
354. C. Gueymard, "SMARTS2, a simple model of the atmospheric radiative transfer of sunshine: algorithms and performance assessment," Tech. Rep. FSEC-PF-270-95 (Florida Solar Energy Center, 1995).
355. C. A. Gueymard, "Parameterized transmittance model for direct beam and circumsolar spectral irradiance," Sol. Energy **71**, 325–346 (2001).
356. R. Ross, "Accuracy of solar-flare observations," J. Atmos. Terr. Phys. **7**, 344–345 (1976).
357. J. Duffie and W. Beckman, *Solar Engineering of Thermal Processes* (Wiley, 2013).
358. M. De Bastiani, E. Van Kerschaver, Q. Jeangros, *et al.*, "Toward stable monolithic perovskite/silicon tandem photovoltaics: a six-month outdoor performance study in a hot and humid climate," ACS Energy Lett. **6**, 2944–2951 (2021).
359. M. Jošt, B. Lipovšek, B. Glažar, *et al.*, "Perovskite solar cells go outdoors: field testing and temperature effects on energy yield," Adv. Energy Mater. **10**, 2000454 (2020).
360. E. Köhnen, M. Jošt, A. B. Morales-Vilches, *et al.*, "Highly efficient monolithic perovskite silicon tandem solar cells: analyzing the influence of current mismatch on device performance," Sustainable Energy Fuels **3**, 1995–2005 (2019).
361. E. Aydin, T. G. Allen, M. De Bastiani, *et al.*, "Interplay between temperature and bandgap energies on the outdoor performance of perovskite/silicon tandem solar cells," Nat. Energy **5**, 851–859 (2020).
362. J. Ascencio-Vásquez, K. Brecl, and M. Topic, "Methodology of Köppen-Geiger-photovoltaic climate classification and implications to worldwide mapping of PV system performance," Sol. Energy **191**, 672–685 (2019).
363. N. Tucher, O. Höhn, J. Murthy, *et al.*, "Energy yield analysis of textured perovskite silicon tandem solar cells and modules," Opt. Express **27**, A1419 (2019).
364. F. Gota, R. Schmager, A. Farag, *et al.*, "Energy yield modelling of textured perovskite/silicon tandem photovoltaics with thick perovskite top cells," Opt. Express **30**, 14172 (2022).
365. A. Knight and L. Herz, "Preventing phase segregation in mixed-halide perovskites: a perspective," Energy Environ. Sci. **13**, 2024–2046 (2020).

366. M. Hörantner and H. Snaith, "Predicting and optimising the energy yield of perovskite-on-silicon tandem solar cells under real world conditions," Energy Environ. Sci. **10**, 1983–1993 (2017).
367. S. Pal, A. Reinders, and R. Saive, "Simulation of bifacial and monofacial silicon solar cell short-circuit current density under measured spectro-angular solar irradiance," IEEE J. Photovoltaics **10**, 1803–1815 (2020).
368. S. S. Pal, "Tracing the light: designing reflectors for bifacial photovoltaic yield enhancement under outdoor irradiance," Ph.D. thesis (University of Twente, 2022).
369. M. R. Khan, A. Hanna, X. Sun, *et al.*, "Vertical bifacial solar farms: physics, design, and global optimization," Appl. Energy **206**, 240–248 (2017).
370. C. Valdivia, C. Li, A. Russell, *et al.*, "Bifacial photovoltaic module energy yield calculation and analysis," in *2017 IEEE 44th Photovoltaic Specialist Conference (PVSC)* (IEEE, 2017), pp. 1094–1099.
371. S. Pelaez, C. Deline, P. Greenberg, *et al.*, "Model and validation of single-axis tracking with bifacial PV," IEEE J. Photovoltaics **9**, 715–721 (2019).
372. S. Pelaez, C. Deline, S. Macalpine, *et al.*, "Comparison of bifacial solar irradiance model predictions with field validation," IEEE J. Photovoltaics **9**, 82–88 (2019).
373. A. Russell, C. Valdivia, C. Bohemier, *et al.*, "DUET: a novel energy yield model with 3-D shading for bifacial photovoltaic systems," IEEE J. Photovoltaics **12**, 1576–1585 (2022).
374. E. Tonita, C. Valdivia, A. Russell, *et al.*, "A general illumination method to predict bifacial photovoltaic system performance," Joule **7**, 5–12 (2023).
375. E. Tonita, A. Russell, C. Valdivia, *et al.*, "Optimal ground coverage ratios for tracked, fixed-tilt, and vertical photovoltaic systems for latitudes up to 75°N," Sol. Energy **258**, 8–15 (2023).
376. M. Brennan, A. Abramase, R. Andrews, *et al.*, "Effects of spectral albedo on solar photovoltaic devices," Sol. Energy Mater. Sol. Cells **124**, 111–116 (2014).
377. R. Andrews and J. Pearce, "The effect of spectral albedo on amorphous silicon and crystalline silicon solar photovoltaic device performance," Sol. Energy **91**, 233–241 (2013).
378. T. Russell, R. Saive, A. Augusto, *et al.*, "The influence of spectral albedo on bifacial solar cells: a theoretical and experimental study," IEEE J. Photovoltaics **7**, 1611–1618 (2017).
379. N. Lindsay, Q. Libois, J. Badosa, *et al.*, "Errors in PV power modelling due to the lack of spectral and angular details of solar irradiance inputs," Sol. Energy **197**, 266–278 (2020).
380. S. Ovaitt, M. Brown, C. Deline, *et al.*, "Spectral rear irradiance testing and modeling for degradation and performance of solar fields," in *2022 IEEE 49th Photovoltaics Specialists Conference (PVSC)* (IEEE, pp. 2022), pp. 992–994.
381. S. Pal, F. Van Loenhout, J. Westerhof, *et al.*, "Understanding and benchmarking ground reflectors for bifacial photovoltaic yield enhancement," IEEE J. Photovoltaics **14**, 160–169 (2024).
382. M. Ernst, G. E. Conechado, and C.-A. Asselineau, "Accelerating the simulation of annual bifacial illumination of real photovoltaic systems with ray tracing," iScience **25**, 103698 (2022).
383. J. Forster, G. Tsutzkiridze, C. Herr, *et al.*, "Photovoltaic noise barriers as energy generating infrastructure: functional overview about five solutions," in *40th European Photovoltaic Solar Energy Conference and Exhibition* (WIP-Munich, 2023), pp. 001–006.
384. S. Bundo, S. Pal, M. Ernst, *et al.*, "Spectro-angular analysis of roadside-integrated bifacial solar power systems with reflecting sound barriers," J. Phys. Photonics **6**, 025006 (2024).

385. M. Heinrich and J. Forster, "Road infrastructure integrated photovoltaics - equipping noise barriers or road canopies with solar," in *Green Week Event of the Government of Navarra* (Brussels, 2022).
386. M. Junedi, N. Ludin, N. Hamid, *et al.*, "Environmental and economic performance assessment of integrated conventional solar photovoltaic and agrophotovoltaic systems," Renew. Sustain. Energy Rev. **168**, 112799 (2022).
387. W. Kim, J. Nam, G. Gim, *et al.*, "Investigation on the effect of abnormal climate in high value added crops utilizing agrophotovoltaic structures," Curr. Photovoltaics Res. **9**, 45–50 (2021).
388. D. Ketzer, N. Weinberger, C. Rösch, *et al.*, "Land use conflicts between biomass and power production – citizens' participation in the technology development of agrophotovoltaics," J. Responsible Innov. **7**, 193–216 (2020).
389. A. Weselek, A. Ehmann, S. Zikeli, *et al.*, "Agrophotovoltaic systems: applications, challenges, and opportunities. A review," Agron. Sustain. Dev. **39**, 35 (2019).
390. C. Meyer, "Agro PV - Next2Sun's vertical installations," in *6th bifiPV Workshop* (2019).
391. M. A. A. Mamun, P. Dargusch, D. Wadley, *et al.*, "A review of research on agrivoltaic systems," Renew. Sustain. Energy Rev. **161**, 112351 (2022).
392. S. Guo, T. M. Walsh, and M. Peters, "Vertically mounted bifacial photovoltaic modules: a global analysis," Energy **61**, 447–454 (2013).
393. A. Rikhof, "Modelling the yield of building integrated photovoltaic systems employing free space luminescent solar concentrators," Master's thesis (University of Twente, 2023).
394. J. Reagan and S. Kurtz, "Energetic comparison of vertical bifacial to tilted monofacial solar," IEEE J. Photovoltaics **12**, 1334–1340 (2022).
395. W. Tress, K. Domanski, B. Carlsen, *et al.*, "Performance of perovskite solar cells under simulated temperature-illumination real-world operating conditions," Nat. Energy **4**, 568–574 (2019).
396. Architecture2030.org, "Why the built environment," (2023). [Accessed 15 May 2024], https://www.architecture2030.org/why-the-built-environment/why-buildings/.
397. Energy Agency International, "Technology and innovation pathways for zero-carbon-ready buildings by 2030," Tech. Rep. (IEA, 2022).
398. E. Ohene, A. P. Chan, and A. Darko, "Review of global research advances towards net-zero emissions buildings," Energy Build. **266**, 112142 (2022).
399. A. Ahmed, T. Ge, J. Peng, *et al.*, "Assessment of the renewable energy generation towards net-zero energy buildings: a review," Energy Build. **256**, 111755 (2022).
400. M. K. Basher, M. Nur-E-Alam, M. M. Rahman, *et al.*, "Aesthetically appealing building integrated photovoltaic systems for net-zero energy buildings. Current status, challenges, and future developments—a review," Buildings **13**, 863 (2023).
401. Grand View Research, "Building-integrated photovoltaics market size, share & trends analysis report by technology (crystalline silicon, thin film), by application (roof, glass, wall, facade), by end-use, by region, and segment forecasts, 2023–2030," Tech. Rep. (Grand View Research, 2023).
402. C. Ballif, L.-E. Perret-Aebi, S. Lufkin, *et al.*, "Integrated thinking for photovoltaics in buildings," Nat. Energy **3**, 438–442 (2018).
403. S. A. Awuku, A. Bennadji, F. Muhammad-Sukki, *et al.*, "Myth or gold? The power of aesthetics in the adoption of building integrated photovoltaics (BIPVs)," Energy Nexus **4**, 100021 (2021).
404. J. S. Kumar, "The psychology of colour influences consumers' buying behaviour – a diagnostic study," Ushus J. Bus. Manage. **16**, 1–13 (2017).

405. S. L. Hille, H. C. Curtius, and R. Wüstenhagen, "Red is the new blue. The role of color, building integration and country of origin in homeowners preferences for residential photovoltaics," Energy Build. **162**, 21–31 (2018).
406. E. Lucchi, J. Adami, and A. E. Stawinoga, "Social acceptance of photovoltaic systems in heritage buildings and landscapes: exploring barriers, benefits, drivers, and challenges for technical stakeholders in northern Italy," Sustainable Energy Technol. Assess. **60**, 103544 (2023).
407. C. S. Polo Lopez, E. Lucchi, and G. Franco, "Acceptance of building integrated photovoltaic (BIPV) in heritage buildings and landscapes: potentials, barrier and assessment criteria," in *REHABEND 2020 Congress* (2020), p. 553.
408. N. Sánchez-Pantoja, R. Vidal, and M. C. Pastor, "Aesthetic impact of solar energy systems," Renew. Sustain. Energy Rev. **98**, 227–238 (2018).
409. P. Bonomo, G. Eder, N. M. Chivelet, *et al.*, "Categorization of BIPV applications," Tech. rep. (IEA PVPS, 2021).
410. N. Martín-Chivelet, K. Kapsis, H. R. Wilson, *et al.*, "Building-Integrated Photovoltaic (BIPV) products and systems: a review of energy-related behavior," Energy Build. **262**, 111998 (2022).
411. G. Peharz and A. Ulm, "Quantifying the influence of colors on the performance of c-Si photovoltaic devices," Renewable Energy **129**, 299–308 (2018).
412. F. Rosa, "Building-integrated photovoltaics (BIPV) in historical buildings: opportunities and constraints," Energies **13**, 3628 (2020).
413. A. Morlier, B. Lim, S. Blankemeyer, *et al.*, "Photovoltaic modules with the look and feel of a stone façade for building integration," Sol. RRL **6**, 2100356 (2022).
414. T. Rose and A. Wollert, "The dark side of photovoltaic — 3D simulation of glare assessing risk and discomfort," Environ. Impact Asses. **52**, 24–30 (2015).
415. A. Ghosh, S. Sundaram, and T. K. Mallick, "Colour properties and glazing factors evaluation of multicrystalline based semi-transparent photovoltaic-vacuum glazing for BIPV application," Renewable Energy **131**, 730–736 (2019).
416. H. Gholami, H. N. Røstvik, and D. Müller-Eie, "Holistic economic analysis of building integrated photovoltaics (BIPV) system: case studies evaluation," Energy Build. **203**, 109461 (2019).
417. H. Gholami and H. N. Røstvik, "Economic analysis of BIPV systems as a building envelope material for building skins in Europe," Energy **204**, 117931 (2020).
418. R. Zimmerman, A. Panda, and V. Bulović, "Techno-economic assessment and deployment strategies for vertically-mounted photovoltaic panels," Appl. Energy **276**, 115149 (2020).
419. T. Smith and J. Guild, "The C.I.E colorimetric standards and their use," Trans. Opt. Soc., London **33**, 73–134 (1931).
420. R. Granit, *Sensory Mechanisms of the Retina* (Hafner, 1963).
421. D. B. Judd, D. L. MacAdam, G. Wyszecki, *et al.*, "Spectral distribution of typical daylight as a function of correlated color temperature," J. Opt. Soc. Am. **54**, 1031 (1964).
422. A. Gilchrist and J. Nobbs, "Colorimetry, theory," in *Encyclopedia of Spectroscopy and Spectrometry*, J. C. Lindon, G. E. Tranter, and D. W. Koppenaal, eds. (Elsevier, 2017), pp. 328–333.
423. G. Sharma, W. Wu, and E. N. Dalal, "The CIEDE2000 color-difference formula: implementation notes, supplementary test data, and mathematical observations," Color Res. Appl. **30**, 21–30 (2004).
424. J. Halme and P. Mäkinen, "Theoretical efficiency limits of ideal coloured opaque photovoltaics," Energy Environ. Sci. **12**, 1274–1285 (2019).
425. A. M. Shirazi, Z. S. Zomorodian, and M. Tahsildoost, "Techno-economic BIPV evaluation method in urban areas," Renewable Energy **143**, 1235–1246 (2019).

426. C. Zomer, I. Custódio, A. Antoniolli, *et al.*, "Performance assessment of partially shaded building-integrated photovoltaic (BIPV) systems in a positive-energy solar energy laboratory building: architecture perspectives," Sol. Energy **211**, 879–896 (2020).
427. A. Calcabrini, R. Weegink, P. Manganiello, *et al.*, "Simulation study of the electrical yield of various PV module topologies in partially shaded urban scenarios," Sol. Energy **225**, 726–733 (2021).
428. P. Kozlovas, S. Gudzius, J. Ciurlionis, *et al.*, "Assessment of technical and economic potential of urban rooftop solar photovoltaic systems in Lithuania," Energies **16**, 5410 (2023).
429. Y. Zhou, D. Wilmink, M. Zeman, *et al.*, "A geographic information system-based large scale visibility assessment tool for multi-criteria photovoltaic planning on urban building roofs," Renewable Sustainable Energy Rev. **188**, 113885 (2023).
430. J. C. Ortiz Lizcano, S. Villa, Y. Zhou, *et al.*, "Optimal design of multilayer optical color filters for building-integrated photovoltaic (BIPV) applications," Sol. RRL **7**, 2300256 (2023).
431. I. Kaaya, M. Koehl, A. P. Mehilli, *et al.*, "Modeling outdoor service lifetime prediction of PV modules: effects of combined climatic stressors on PV module power degradation," IEEE J. Photovoltaics **9**, 1105–1112 (2019).
432. H. Meddeb, M. Götz-Köhler, N. Neugebohrn, *et al.*, "Tunable photovoltaics: adapting solar cell technologies to versatile applications," Adv. Energy Mater. **12**, 2200713 (2022).
433. P. Sehati, I. Malmros, S. Karlsson, *et al.*, "Aesthetically pleasing PV modules for the built environment," Tech. Rep. RISE Rapport 2019: 08 (RISE Research Institutes of Sweden, 2019).
434. Z. Li, T. Ma, H. Yang, *et al.*, "Transparent and colored solar photovoltaics for building integration," Sol. RRL **5**, 2000614 (2021).
435. M. Pelle, F. Causone, L. Maturi, *et al.*, "Opaque coloured building integrated photovoltaic (BIPV): a Review of models and simulation frameworks for performance optimisation," Energies **16**, 1991 (2023).
436. C. Kutter, B. Bläsi, H. Wilson, *et al.*, "Decorated building-integrated photovoltaic modules: power loss, color appearance and cost analysis," in *35th European Photovoltaic Solar Energy Conference and Exhibition* (2018), pp. 1488–1492.
437. F. Lisco, G. Cattaneo, A. Virtuani, *et al.*, "Design and testing of a demonstrative BIPV façade manufactured with novel glass-free colored lightweight PV modules," in *2023 International Conference on Clean Electrical Power, ICCEP 2023* (Institute of Electrical and Electronics Engineers Inc., 2023), pp. 657–662.
438. T. Gewohn, M. R. Vogt, B. Lim, *et al.*, "Postproduction coloring of photovoltaic modules with imprinted textiles," IEEE J. Photovoltaics **11**, 138–143 (2021).
439. Kameleon Solar, "Portfolio," (2024). [Accessed 15 May 2024], https://kameleonsolar.com/portfolio/.
440. B. Bläsi, T. Kroyer, T. Kuhn, *et al.*, "The morphocolor concept for colored photovoltaic modules," IEEE J. Photovoltaics **11**, 1305–1311 (2021).
441. G. Peharz, K. Berger, B. Kubicek, *et al.*, "Application of plasmonic coloring for making building integrated PV modules comprising of green solar cells," Renewable Energy **109**, 542–550 (2017).
442. T. Masuda, Y. Kudo, and D. Banerjee, "Visually attractive and high-power-retention solar modules by coloring with automotive paints," Coatings **8**, 282 (2018).
443. M. K. Basher, M. Nur-E-Alam, M. M. Rahman, *et al.*, "Design, development, and characterization of highly efficient colored photovoltaic module for sustainable buildings applications," Sustainability **14**, 4278 (2022).

444. W. G. Shin, J. Y. Shin, H. M. Hwang, *et al.*, "Power generation prediction of building-integrated photovoltaic system with colored modules using machine learning," Energies **15**, 2589 (2022).
445. B. Riedel, P. Messaoudi, Y. B. Assoa, *et al.*, "Color coated glazing for next generation BIPV: performance vs aesthetics," EPJ Photovoltaics **12**, 11 (2021).
446. O. Isabella, "Light management in thin-film silicon solar cells," Ph.D. thesis (Delft University of Technology, 2013).
447. H. A. Macleod, *Thin-Film Optical Filters*, 5th ed. (Taylor & Francis Group, 2015).
448. A. Soman and A. Antony, "Colored solar cells with spectrally selective photonic crystal reflectors for application in building integrated photovoltaics," Sol. Energy **181**, 1–8 (2019).
449. A. Røyset, T. Kolås, Ø. Nordseth, *et al.*, "Optical interference coatings for coloured building integrated photovoltaic modules: predicting and optimising visual properties and efficiency," Energy Build. **298**, 113517 (2023).
450. A. Wessels, A. Callies, B. Bläsi, *et al.*, "Modeling the optical properties of morpho-inspired thin-film interference filters on structured surfaces," Opt. Express **30**, 14586 (2022).
451. A. Ingenito, J. C. O. Lizcano, S. L. Luxembourg, *et al.*, "Optimized back reflectors for rear diffused c-Si solar cells," Energy Procedia **55**, 94–100 (2014).
452. LOF Solar, "Commercial Projects," (2024). [Accessed 15 May 2024], http://www.lofsolar.com/LofsolarPerformance/category/17.
453. Soluxa, "Our Projects," (2024). [Accessed 15 May 2024], https://www.soluxa.solar/facade/.
454. Kromatix, "References," (2024). [Accessed 15 May 2024], https://kromatix.com/references.
455. Megasol, "SolarColor morpho," (2024). [Accessed 15 May 2024], https://solarcolor.ch/morpho/.
456. N. Jolissaint, R. Hanbali, J. C. Hadorn, *et al.*, "Colored solar façades for buildings," Energy Procedia **122**, 175–180 (2017).
457. M. Rudzikas, J. Donėlienė, E. Bužavaitė-Vertelienė, *et al.*, "Design and investigation of 1D photonic crystal based structures for BIPV cell colorization by sol-gel dipping technology," Sol. Energy **250**, 285–294 (2023).
458. Z. Xu, T. Matsui, K. Matsubara, *et al.*, "Tunable and angle-insensitive structural coloring of solar cell modules for high performance building-integrated photovoltaic application," Sol. Energy Mater. Sol. Cells **247**, 111952 (2022).
459. V. Neder, S. L. Luxembourg, and A. Polman, "Efficient colored silicon solar modules using integrated resonant dielectric nanoscatterers," Appl. Phys. Lett. **111**, 073902 (2017).
460. F. Uleman, V. Neder, A. Cordaro, *et al.*, "Resonant metagratings for spectral and angular control of light for colored rooftop photovoltaics," ACS Appl. Energy Mater. **3**, 3150–3156 (2020).
461. Y. Zhou, C. Jia, K. Lu, *et al.*, "Energy-efficient colorful silicon photovoltaic modules driven by transparent-colored radiative cooling," Sol. Energy Mater. Sol. Cells **259**, 112459 (2023).
462. Z. Li, T. Ma, S. Li, *et al.*, "High-efficiency, mass-producible, and colored solar photovoltaics enabled by self-assembled photonic glass," ACS Nano **16**, 11473–11482 (2022).
463. Y. Wu, Y. Chen, Q. Song, *et al.*, "Dynamic structural colors based on all-dielectric Mie resonators," Adv. Opt. Mater. **9**, 2002126 (2021).
464. T. Das Gupta, L. Martin-Monier, W. Yan, *et al.*, "Self-assembly of nanostructured glass metasurfaces via templated fluid instabilities," Nat. Nanotechnol. **14**, 320–327 (2019).

465. E. J. Stallknecht, C. K. Herrera, C. Yang, *et al.*, "Designing plant–transparent agrivoltaics," Sci. Rep. **13**, 1903 (2023).
466. W. J. Kim, D. H. Cho, S. H. Hong, *et al.*, "Implementation of various colors in Cu(In,Ga)Se_2 thin-film solar cells by diffractive nanostructures," Sol. Energy Mater. Sol. Cells **257**, 112392 (2023).
467. G. Y. Yoo, J. S. Jeong, S. Lee, *et al.*, "Multiple-color-generating Cu(In,Ga)$(S,Se)_2$ thin-film solar cells via dichroic film incorporation for power-generating window applications," ACS Appl. Mater. Interfaces **9**, 14817–14826 (2017).
468. S. H. Lee, S. J. Yun, M. Shin, *et al.*, "Cu_2O thin films as the color-adjusting layer in semi-transparent a-Si:H solar cells," Sol. Energy Mater. Sol. Cells **117**, 519–525 (2013).
469. S. Yeop Myong and S. Won Jeon, "Design of esthetic color for thin-film silicon semi-transparent photovoltaic modules," Sol. Energy Mater. Sol. Cells **143**, 442–449 (2015).
470. N. Neugebohrn, K. Gehrke, K. Brucke, *et al.*, "Multifunctional metal oxide electrodes: colour for thin film solar cells," Thin Solid Films **685**, 131–135 (2019).
471. Onyx Solar, "Projects," (2024). [Accessed 15 May 2024], https://onyxsolar.com/projects.
472. R. Santbergen, T. Meguro, T. Suezaki, *et al.*, "GenPro4 optical model for solar cell simulation and its application to multijunction solar cells," IEEE J. Photovoltaics **7**, 919–926 (2017).
473. H. Holst, "Development and application of a modular ray tracing framework to multi-scale simulations in photovoltaics," Ph.D. thesis (Gottfried Wilhelm Leibniz Universitat Hannover, 2015).
474. N. Tucher, J. Eisenlohr, H. Gebrewold, *et al.*, "Optical simulation of photovoltaic modules with multiple textured interfaces using the matrix-based formalism OPTOS," Opt. Express **24**, A1083 (2016).
475. A. Wessels, L. Christen, A. Callies, *et al.*, "Modeling of thin-film interference filters on structured substrates: microfacet-based BSDF versus ray tracing," Opt. Express **31**, 20102–20111 (2023).
476. A. V. Tikhonravov, "Needle optimization technique: the history and the future," P. Soc. Photo-opt. Ins. **3133**, 2 (1997).
477. A. Borja Block, J. Escarre Palou, A. Faes, *et al.*, "Accurate color characterization of solar photovoltaic modules for building integration," Sol. Energy **267**, 112227 (2024).
478. Onyx Solar, "Feasibility studies," (2024). [Accessed 15 May 2024], https://onyxsolar.com/feasibility-studies-roi.

Klaus Jäger has been working at Helmholtz-Zentrum Berlin für Materialien und Energie (HZB), Germany, since 2015, where he is deputy head of the department Optics for Solar Energy and vice director of the Joint Lab "BerOSE" between HZB, Zuse Institute Berlin, Germany, and Freie Universität Berlin, Germany. From August to November 2024 he was Gerhard R. Andlinger Visiting Fellow at Princeton University, Princeton, New Jersey, USA. He holds an M.Sc. from ETH Zurich, Switzerland and a Ph.D. from Delft University of Technology, the Netherlands. His main research interests lie in optical simulations for solar cells, employing various approaches such as the finite-element method, the net radiation method, and advanced concepts such as Bayesian optimization algorithms. In addition, he is passionate about science communication

and regularly engages with the general public to discuss the climate crisis and the role of renewable energy.

Urs Aeberhard received his Ph.D. in theoretical solid state physics from ETH Zürich, Switzerland, in 2008. From 2009–2018, he was a postdoc, senior scientist, and group leader at the Institute of Energy and Climate Research — Photovoltaics (IEK-5), Forschungszentrum Jülich, Germany, heading the activities in theory and multiscale simulation. In 2013, he was a visiting research scholar at the National Renewable Energy Lab (NREL) in Golden, Colorado, USA. Since 2018, he has performed applied research and model development as a senior R&D scientist at the company Fluxim based in Winterthur, Switzerland. Since 2019, he has also been a Guest Lecturer for the simulation of PV devices at ETH Zürich.

Esther Alarcon Llado is a professor at the University of Amsterdam, the Netherlands, and leads the 3DPV group at the NWO-I AMOLF in Amsterdam, the Netherlands. She obtained her Ph.D. in Physics from the University of Barcelona, Spain. She spent her postdoctoral time in a*STAR IMRE in Singapore, Lawrence Berkeley National Laboratory, USA, and at the École Polytechnique Fédérale de Lausanne, Switzerland. Her research focuses on developing photonic strategies for sustainable energy conversion and storage.

Benedikt Bläsi received his M.Sc. from the University of Durham, UK, and his Ph.D. in physics from Albert-Ludwigs-University Freiburg, Germany. He has been at Fraunhofer Institute for Solar Energy Systems ISE, Freiburg, Germany, since 1995. From 2005 until 2023 he was head of the group "Microstructured Surfaces." Since 2024 he has been Science Manager Optics for Photovoltaics at ISE. His main research focus is on light management for PV systems, with a special focus on optically functional micro- and nanostructures.

Sven Burger graduated from the University of Hannover, Germany, from where he also received a Ph.D. in Physics. He has been a postdoctoral researcher at the University of Florence, Italy. He leads the Computational Nano Optics research group at Zuse Institute Berlin, Germany, and he is a board member of JCMwave GmbH, Berlin, Germany.

Bruno Ehrler leads the Hybrid Solar Cells group and the Sustainable Energy Materials/LMPV department at the NWO-Institute AMOLF in Amsterdam, the Netherlands. He received his Ph.D. from the University of Cambridge, UK. His research focuses on the next generation of solar PV materials and devices, with a particular interest in ion migration in metal halide perovskites. He also coordinates SolarLab, a national research program supporting the industrialization efforts of SolarNL, an initiative that aims to establish a solar energy industry in the Netherlands.

Wilfried Favre obtained his Ph.D. in Physics from the Université d'Orsay, Paris 11, France, in 2011 for his work on characterization and modeling of heterojunction devices at GeePs Laboratory, CentraleSupelec, Paris, France. He then joined CEA at INES, Le Bourget-du-Lac, France, for a two-year postdoc followed by a permanent position to develop high-efficiency heterojunction solar cells at lab and preindustrial stages (several MW pilot lines at CEA). From 2016 to 2020, he worked on industrial transfer of the silicon heterojunction technology to production lines notably the Enel Green Power one based in Catania, Sicily, Italy. Since 2020, he has been Head of the Heterojunction Solar Cells Laboratory at CEA (with more than 30 personnel) and is still active in silicon-based PV technologies developments. He has co-authored more than 50 communications in journals and international conferences, collected several patents, and supervised Ph.D. students and postdoctoral researchers.

Antonín Fejfar heads the Laboratory of Nanostructures and Nanometers, which is part of the CzechNanoLab large research infrastructure in Prague, Czech Republic. His research interest are thin films of nanostructured semiconductors, in particular for PV and photonics. He has led multiple grant projects, including international (H2020 project NextBase, FP7 project PolySiMode, FP5 project aSiNet, Barrande, DAAD etc.). He has been a visiting professor at Kyoto University, Japan, and visiting researcher at Ecole Polytechnique at Palaiseau, France. He is a member of the Science Council of the Czech Academy of Sciences, which he chaired from April 2017 to March 2021. He is also a member of the Scientific board of the Technical University of Liberec, Czech Republic, Scientific board of CEITEC Nano and member of the Czech selection committee of the L'Oréal – UNESCO For Women in Science. He represents Czech Republic in the Nanometer Structures Division of International Union for Vacuum Science, Techniques and Applications (IUVSTA). He is one of the principal organizers of the Summer School Series on Physics at Nanoscale.

Tristan Gageot is a physics researcher working at CEA, the French Alternative Energies and Atomic Energy Commission (CEA), Le Bourget-du-Lac, France. He received a Ph.D. in Material Science at the Grenoble Alpes University (UGA), France, in 2024. Since then, he has been working on the PECVD processes for silicon heterojunction solar cells.

Ivan Gordon obtained his Ph.D. from the University of Leuven, Belgium, in February 2002. He started to work in the field of PV in June 2003 at IMEC, Leuven, Belgium. Currently, he is director of the IMOMEC department of IMEC, and vice-director of the Institute of Material Research (IMO) of Hasselt University, Belgium. In addition, he is also part-time professor in Digital Photovoltaics at Delft University of Technology, the Netherlands, and Editor-in-Chief of the international scientific journal *Solar Energy Materials and Solar Cells*. Since January 2016, he is the coordinator of the joint program on Photovoltaics of the European Energy Research Alliance (EERA) and a steering committee member of the European Technology and Innovation Platform Photovoltaics (ETIP-PV).

Henning Helmers studied physics and philosophy in Oldenburg, Germany, and in Lund, Sweden. He received his Ph.D. from University of Oldenburg in 2013. Since 2019, he has co-headed the department "III–V Photovoltaics and Concentrator Technology." His research interests include high efficiency device design for III–V solar cells and photonic power converters, multijunction device architectures, micro-concentrating PV, and power-by-light technology. He is co-chairing SPIE Photonics West 2025: Physics, Simulation, and Photonic Engineering of Photovoltaic Devices XIV.

Oliver Höhn received his Ph.D. in physics in 2015 from Albert-Ludwigs-University, Freiburg, Germany. He joined the Fraunhofer Institute for Solar Energy Systems ISE, Freiburg, Germany, in 2008. There, he has been head of the group "III–V semiconductor technology" since 2022. In December 2023, he received an ERC Consolidator Grant and thus started a group at University Freiburg to work on ultrathin III–V tandem solar cells. His main research interests include III–V multijunction solar cells, optical modeling and realization of micro- and nanostructured surfaces and optical modeling of high-efficiency solar cells.

Olindo Isabella (prof. dr. ir.) graduated in electronic engineering from University of Naples Federico II, Naples, Italy. He holds a Ph.D. (cum laude) on advanced light management applied to thin-film silicon solar cells from Delft University of Technology, the Netherlands. He was a visiting researcher at AIST, Tsukuba, Japan, working on plasma conditions for stable thin-film solar cells based on silicon–germanium. Since 2012 his research has focused on crystalline silicon solar cells and related applications up to system level. From materials science, to devices and systems, he has interest in multiscale modeling with several works specialized on PV modules modeling and distributed PV systems in the urban environment. Since 2019 he has lead the Photovoltaic Materials and Devices group at Delft University of Technology and he has been a full professor there since 2021.

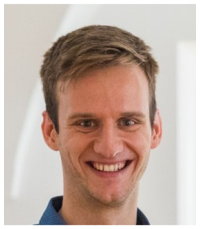

Marko Jošt received his Ph.D. from the University of Ljubljana, Slovenia, and Technical University of Berlin, Germany, in 2017. Between 2017 and 2020, he was employed as a postdoctoral researcher at the Helmholtz-Zentrum Berlin, Germany, developing perovskite-based tandem solar cells. Since 2020, he is employed as an assistant professor at the Faculty of Electrical Engineering, University of Ljubljana. He continues to research perovskite solar cells in the LPVO laboratory, with the aim of improving the stability of long-term operation under realistic external conditions.

Martin Ledinský received his Ph.D. in 2009 from Charles University in Prague, Czech Republic. Following his doctoral studies, he undertook a postdoctoral fellowship at EPFL's Photovoltaics and Thin Film Electronics Laboratory (PV-LAB) in Neuchâtel, Switzerland (2013–2014) and completed a research stay at KAUST, Saudi Arabia (February–April 2018). Since 2018, he has been leading the Thin Films for Photovoltaics group at the Institute of Physics of the Czech Academy of Sciences (FZU) in Prague, Czech Republic. His primary expertise is in the optical characterization of active PV materials and their passivation. In addition, he is dedicated to the popularization of PV and physics in general, regularly giving lectures for audiences ranging from preschool to university students.

Jyotirmoy Mandal is an assistant professor in the Department of Civil and Environmental Engineering at Princeton University, Princeton, New Jersey, USA. His research involves understanding and controlling nano-to-macro-scale radiative heat flows in both natural environments and artificial surfaces, with characterizing and mitigating ambient heat in a warming world as a guiding theme.

Phillip Manley obtained a Masters in Physics from Durham University, UK, in 2012 and a doctorate in Physics at the Free University Berlin, Germany, in 2016. He was employed as a post-doc at the Helmholtz Zentrum Berlin, Germany, from 2017 until 2021. Since then, he has worked as a senior research scientist at JCMwave GmbH, Berlin, Germany. His research focuses on modeling nano structuring for high-efficiency optical devices.

Delfina Muñoz is strategic project manager and senior researcher in the solar energy department at CEA-LITEN, Le Bourget-du-Lac, France. She is an industrial engineer and holds a Ph.D. in photovoltaics from Universidad Politécnica de Cataluña, Barcelona, Spain. She has more than 60 publications and more than 100 conference presentations, mostly in science and materials for PV. She is on the Board of the Chilean ATAMOSTEC project related to reliability of PV in desert areas, on the steering committee of the heterojunction and tandemPV workshops, and topic organizer of WCPC, PVSEC, and IEEE conferences. Since 2019, she has been on the steering committee of the European Technology and Innovation Platform Photovoltaics (ETIP-PV). She still combines project activity with the laboratory research, directing Ph.D. students, and developing the next generation of PV technology.

Zunaid Omair is currently a product engineer at Lam Research, Fremont, California, USA, where he focuses on new hardware concepts for high-aspect-ratio dielectric etch. He obtained his M.Sc. (2020) and Ph.D. (2021) from the University of California, Berkeley, California, USA, and performed postdoctoral research at Stanford University (2021–2022), Stanford, California, USA. He has previously worked on designing coherent and incoherent imaging systems for extreme-UV lithography, optical design, and imaging system development.

Juan Camilo Ortiz Lizcano received a B.Sc. degree in mechanical engineering at the Universidad Industrial de Santander, Colombia, and worked as an engineer in the field of natural gas compression. Afterwards, he decided to continue his studies at Delft University of Technology, the Netherlands, where he obtained an M.Sc. degree in Sustainable Energy Technology. In mid-2017, he started his Ph.D. studies in performance modeling of innovative concepts for integrating PV systems into the urban environment at Delft University of Technology. Currently, he works as a researcher on the design and technical implementation of PV systems to energize The Green Village.

Ulrich W. Paetzold is a Professor at the Karlsruhe Institute of Technology (KIT), Germany, where he leads the research division "Next Generation Photovoltaics" at the Institute of Microstructure Technology and the Light Technology Institute. He was a doctoral student at Forschungszentrum Jülich, Germany, and received his Ph.D. in physics from RWTH Aachen University, Aachen, Germany, in 2013, then continued as a postdoc at imec in Leuven, Belgium. In 2016, he joined the Karlsruhe Institute of Technology (KIT) and started to build-up his research group. His team's research is focused on the fabrication, upscaling, characterization, and understanding of device physics of perovskite PV and perovskite-based tandem PV. In 2023, Ulrich W. Paetzold was awarded the prestigious ERC Consolidator Grand by the European Union. In the next five years, his ambition is to advance the stability and scalability of perovskite-based (tandem) PV.

Aaswath P. Raman is an Associate Professor of Materials Science and Engineering at the University of California, Los Angeles, California, USA. His research interests include radiative cooling, nanophotonics, and energy systems more generally. He is known for first demonstrating daytime radiative cooling in 2014, as well as radiative cooling's use for solar cells in subsequent work. He received his Ph.D. in Applied Physics from Stanford University in 2013, and has received early career awards from the Materials Research Society, DARPA, NSF, and MIT Technology Review. He is also co-founder and chief scientific officer of a startup commercializing daytime radiative cooling technology, SkyCool Systems.

Hitoshi Sai is a Principal Senior Researcher at Renewable Energy Research Center in National Institute of Advanced Industrial Science and Technology (AIST), Japan, and a visiting professor at Tsukuba University. He received a Ph.D. in Mechanical Engineering from Tohoku University, Sendai, Japan, in 2004. He joined Toyota Technological Institute, Nagoya, Japan, in 2004 as a JSPS post-doctoral fellow for PV device research. In 2007, he joined AIST. Since then, he has worked on developing thin-film silicon, crystalline silicon solar cells, and tandem cells, with a great interest in light management.

Rebecca Saive is a Professor of Applied Physics at the University of Twente, the Netherlands. Her research focuses on advanced light management techniques for PV systems, such as photonic metamaterials for enhanced light collection and effectively transparent front contacts. Her work bridges fundamental physics and applied technology, from computational modeling to prototyping. Furthermore, her group develops novel micromanufacturing techniques and advances optoelectronic scanning probe microscopy. She earned her Ph.D. from the University of Heidelberg, Germany, and completed postdoctoral research at the California Institute of Technology, Pasadena, California, USA. She co-founded a successful startup in the semiconductor sector and was named one of the Innovators Under 35 Europe and Global by MIT Technology Review in recognition of her contributions to solar energy.

Martina Schmid is a Professor of Experimental Physics and Head of the MultioptiX group at the University of Duisburg-Essen, Germany, since 2017. Previously, she was a Junior Professor at the Freie University Berlin (FUB), Germany, and Head of a Helmholtz Young Investigator Group at the Helmholtz-Zentrum Berlin für Materialien und Energie, Germany (since 2012/2013). She pursued postdoctoral research at the California Institute of Technology, Pasadena, California, USA, and the University of Ljubljana, Slovenia. During her Ph.D., which she obtained from FUB in 2010, she also spent a research stay at the University of New South Wales, Australia. Her major research interest is resource-efficient energy conversion including multioptical concepts for tailored light guiding and concentration.

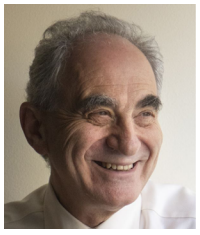

Eli Yablonovitch is Professor in the Graduate School, Electrical Engineering and Computer Sciences Department, University of California, Berkeley, California, USA. He introduced the idea that strained semiconductor lasers could have superior performance due to reduced effective mass (holes). With almost every human interaction with the internet, optical telecommunication occurs by strained semiconductor lasers. In his PV research, he introduced the $4n^2$ ("Yablonovitch limit") light-trapping factor, in worldwide use for almost all commercial solar panels. His mantra "a great solar cell also needs to be a great LED", holds the world record for solar cell efficiency, 29.1% at 1 Sun. He was elected to NAE, NAS, NAI, AmAcArSci, and, as a Foreign Member, the UK Royal Society.

Christiane Becker is head of the Optics for Solar Energy department at Helmholtz Zentrum Berlin für Materialien und Energie (HZB), Germany, and Professor at Hochschule für Technik und Wirtschaft Berlin, Germany. Before, she was a Young Investigator Group Leader at HZB (since 2013) and a guest scientist at University of Lund, NanoLund, Sweden, in 2017. She received her Ph.D. from Karlsruhe Institute of Technology, Germany, in 2006. Her current research interests are the optics of perovskite multijunction solar cells, concepts to improve the aesthetic appearance of solar modules, and EY calculations.